A NOVEL METHOD FOR MAJOR HARMONIC SOURCES IDENTIFICATION IN HIGH VOLTAGE TRANSMISSION SYSTEMS

by

SHUN LIANG

Presented to the Faculty of the Graduate School of

The University of Texas at Arlington in Partial Fulfillment

of the Requirements

for the Degree of

DOCTOR OF PHILOSOPHY

THE UNIVERSITY OF TEXAS AT ARLINGTON

December 2009

ACKNOWLEDGEMENTS

Sincere appreciation is expressed to Dr. Wei-Jen Lee, Dr. Raymond R. Shoults, Dr. William E. Dillon, Dr. Babak Fahimi, and Dr. Rasool Kenarangui for their guidance as members of my graduate committee.

I would like to express particular gratitude to my supervising professor, Dr. Wei-Jen Lee for his guidance and unceasing encouragement. In spite of his busy schedule, Dr. Lee finds time to help and support his students. It was indeed a pleasure and an honor to have worked with him. His dedication to power systems education has to be greatly admired.

I would also want to express appreciation to all members of Energy Systems Research Center (ESRC), the University of Texas at Arlington, for all their valuable assistances, discussions, and enjoyable association. Their careful review, helpful suggestions and discussions in this dissertation are sincerely appreciated.

Finally, the deepest gratitude is reserved for my wife for her love and continuous support. My parents were also a primary source of inspiration during my education. I am very grateful for my family member‘s love, encouragement and support.

September 28, 2009

ABSTRACT

A NOVEL METHOD FOR MAJOR HARMONIC SOURCES IDENTIFICATION IN HIGH VOLTAGE TRANSMISSION SYSTEMS

Shun Liang, PhD

The University of Texas at Arlington, 2009

Supervising Professor: Wei-Jen Lee

Due to the proliferation of high-voltage power electronics devices and nonlinear loads connected to power systems, the penetration of produced harmonics into power transmission networks to pollute power quality of power systems has been a new concern.

Recently, an electric utility company in Texas has observed that harmonic levels may exceed the recommended levels of IEEE Std. 519-1992 at some points in the 138 kV, 161 kV, and 345 kV transmission systems. In order to meet the requirement of the IEEE recommended practice and maintain the power quality of electricity delivered to consumers, identification of major harmonic sources to mitigate harmonic problems by using proper countermeasure is one of the most important tasks of electric utility companies.

In this research work, before applying any harmonic sources identification algorithms, the accuracy of the harmonic component measurement equipments used in this transmission network is verified. The verification effort mainly focuses on two types of Coupling Capacitor Voltage Transformers (CCVTs). Frequency response simulations were conducted to obtain the harmonic measurement adjustment values for these two types of CCVTs. The field tests were carried out to verify the validity of the simulation results.

After the harmonic measurement accuracy is verified, the harmonic characteristics observed in the example transmission system are presented. Because of the harmonic characteristics, it was found that traditional methods for identifying harmonic sources can not be applied effectively in the sample high voltage transmission system due to limited measurement locations. Besides, unbalanced harmonic voltages and harmonic resonance also increase the complexity to the harmonic sources identification problems.

To overcome these difficulties, this dissertation develops a novel two-step method to identify major harmonic sources in high voltage transmission networks using harmonic phase-sequence components, a sub-transmission network extraction scheme, and a harmonic impedance matrix. Based on the proposed harmonic source identification method, a software package was developed, which is named Harmonic Source Identification Software (HSIS). HSIS performs harmonic source identification for high voltage transmission systems. It reads Microsoft Excel files as prepared input data, and calculates possible harmonic sources. The identified possible harmonic sources are stored in an output file. The detailed information about HSIS is also introduced in this dissertation.

Numerical simulations on the IEEE 300-bus system are performed to examine the effectiveness of the proposed method. The simulation results show that the proposed scheme can effectively identify the major harmonic sources with limited harmonic measurement points even with unbalanced harmonic voltages and measurement noises exist in the studied system.

TABLE OF CONTENTS

LIST OF ILLUSTRATIONS

Figure Page

LIST OF TABLES

CHAPTER 1

INTRODUCTION

1.1 Background of Power Quality and Power System Harmonic Distortion

Power quality can be interpreted as service quality that encompasses three aspects: reliability of power supply, quality of power offered, and provision of information [1]. A more restrictive interpretation, widely used in recent literature, relates to:

- The ability of a power system to supply loads without disturbing or damaging them, a property mainly concerned with voltage quality at points of common coupling;
- The ability of electrical power loads to operate without disturbing or reducing the efficiency of the power system, a property mainly, but not exclusively, concerned with the quality of the current waveform.

In contrast to the term “reliability” [2], which generally covers intervals of minutes, typical power quality issues include short-term events such as voltage sags or dips lasting a few cycles to a few seconds caused by faults on nearby feeders, large loads switching on or off etc., and sub-cycle transients caused by switching power factor correction capacitors, lightning strikes, etc. Power system harmonic and flicker issues also fall into the category of power quality, even though these issues tend to occur over much longer intervals than sags and transients [3].

Among all the power quality related issues, harmonic distortion is one of the most significant power quality problems. In addition to the harmonic sources from low and medium voltage levels, the proliferation of high-voltage power-electronics devices and nonlinear loads connected to power systems has led to concerns regarding harmonics injecting into power transmission networks in recent years. Harmonic distortion is recognized as an important factor,

in the deterioration of power quality, which can shorten the lifetime of equipment and interfere with communication and control systems [4].

In order to ensure power quality within their service territory, the electric utility industry has established a general scheme to identify harmonic sources that have exceeded the acceptable limits. The Institute of Electrical and Electronics Engineers (IEEE) has set up a recommended practice on this issue, IEEE Std. 519-1992 [5], which has been adopted by many electric utility companies. In this recommended practice, there are two main criteria which are used to evaluate the harmonic distortion and its impacts. The first is the limitation of harmonic current that an end user can inject into the power system. The second criterion is the quality of voltage that the electric utility company must supply to customers.

In the development of current distortion limits, there will be some diversity between the harmonic currents injected by different customers. This diversity can take the form of different harmonic components that are injected into system, the phase angle differences of the individual harmonic currents, or the differences in the harmonic injection vs. time profiles. In recognition of this diversity, IEEE Std 519-1992 recommended that the current limits be developed so that the maximum individual frequency harmonic voltage caused by a single customer will not exceed the limits in Table 1.1 for systems that can be characterized by a short-circuit impedance.

Table 1.1 Harmonic Current Distortion Limits

SCR at PCC	Maximum Individual Frequency Voltage Harmonic (%)	Related Assumption
10	2.5 – 3.0	Dedicated system
20	2.0 – 2.5	1-2 large customers
50	1.0 – 1.5	A few relatively large customers
100	0.5 – 1.0	5-20 medium size customers
1000	0.05 – 0.10	Many small customers

Note:
SCR: Short Circuit Ratio
PCC: Point of Common Coupling

The second limitation specified in the IEEE recommended practice is the quality of voltage that utility company must furnish to the customers. The IEEE Std. 519 specifies limits on the individual bus harmonic voltage as well as the Total Harmonic Distortion (THD). The THD index can be calculated by the equation 1.1,

$$V_{THD} = \frac{\sqrt{\sum_{h=2}^{\infty} V_h^2}}{V_1} \tag{1.1}$$

In equation 1.1, V_1 is the fundamental voltage magnitude, and V_h is the voltage of h^{th} harmonic. Table 1.2 lists the harmonic voltage requirement as specified in IEEE Std.519-1992.

Table 1.2 Harmonic Voltage Distortion Limits

Bus Voltage at PCC	Individual Voltage Distortion (%)	Total Voltage Distortion (%)
69 kV and below	3.0	5.0
69.001 kV through 161 kV	1.5	2.5
161.001 kV and above	1.0	1.5

The voltage harmonic limits shown in Table 1-2 should be used as system design values for the “worst case” in normal operation. For shorter periods, for example, during large motor start-ups or unusual conditions, the limits may be exceeded by 50%. The electric utility customers are obligated to comply with the regulations. The utilities have the responsibility to identify the harmonic sources if necessary.

1.2 Motivation

Recently, an electric utility company in Texas observed that harmonic levels may exceed the recommended levels of IEEE Std. 519-1992 at some measurement points on its 138 kV, 161 kV, and 345 kV transmission systems, and observed that at some measurement points. In order to maintain good power quality within its service territory, it is important for this electric utility company to locate the harmonic sources and then correct any harmonic problems found, so that the requirements of IEEE Std. 519-1992 are met.

Based on knowledge and experience of the engineers of this utility company, two field investigations were conducted. The purpose of these investigations was trying to find the possible harmonic sources in this high voltage transmission system. One field investigation was carried out in the west Texas area, where many wind farms were built at that area in recent years. Because some engineers suspected that these wind farms may inject harmonic currents into the transmission system and cause harmonic problem. The other investigation was conducted in the east Texas area, near a high voltage direct current (HVDC) back-to-back system, where some engineers also suspected to be a harmonic source. In this section, the information of these two investigations is described.

1.2.1 West Texas Wind Farm Investigation

In recent years, many wind farms were built in west Texas area. At the same time, the harmonic problem emerged and exceeded the IEEE recommended standard. The utility engineers suspect that the harmonic problem was introduced by these wind farms. In this section, this idea will be evaluated by investigating the relationship between wind farm power output and harmonic levels in its vicinity area.

In the wind farm investigation, all the discussions are based on the data measured from July 13, 2007 to July 27, 2007. During this period, this electric utility company measured the voltage and current output data of three different wind farms in the west Texas area. Using these data, the power output of wind farms can be calculated. Also, the voltage and current harmonic injection information of these wind farms can also be calculated by using Fast Fourier Transform.

In the following discussion, the correlation index is used to indicate the strength and direction of the relationships between wind farm power output and harmonic level. In probability and statistics theory [6], the correlation coefficient indicates the strength and direction of a linear relationship between two random variables. The correlation coefficient is 1 in the case of an increasing linear relationship, -1 in the case of a decreasing linear relationship. Values in

between -1 and 1 indicate the degree of linear dependence between the variables. The closer the correlation coefficient is to either -1 or 1, the stronger the correlation between the variables. If the two variables are totally independent, then the correlation coefficient is 0.

The correlation coefficient $\rho_{X,Y}$ between two random variables X and Y with expected values μ_X and μ_Y and the standard deviations σ_X and σ_Y is defined as:

$$\rho_{X,Y} = \frac{\operatorname{cov}(X,Y)}{\sigma_X \sigma_Y} = \frac{E((X-\mu_X)(Y-\mu_Y))}{\sigma_X \sigma_Y} \tag{1.2}$$

In equation 1.2, E is the expected value operator and *cov* represents covariance.

Since $\mu_X = E(X)$, $\sigma_X^2 = E[(X - E(X))^2] = E(X^2) - E^2(X)$, and likewise for Y, equation 1.2 can be rewritten as

$$\rho_{X,Y} = \frac{E(XY) - E(X)E(Y)}{\sqrt{E(X^2) - E^2(X)}\sqrt{E(Y^2) - E^2(Y)}} \tag{1.3}$$

In this research work, equation 1.3 will be employed to calculate the correlation between the wind farm power output and the harmonic injection level. According to field measurements, the observed dominant harmonics signals in the vicinity of the wind farm example area were the 3-rd, 5-th, and 7-th harmonics, the correlation calculation are only carried out on these three harmonic orders. The correlation calculation results between wind farm output power and harmonic injection level are listed in table 1.3.

Table 1.3 Correlation Index between Wind Farm Output and Harmonic Injection Level

	Wind Farm No.1			Wind Farm No.2			Wind Farm No.3		
	Phase A	Phase B	Phase C	Phase A	Phase B	Phase C	Phase A	Phase B	Phase C
Between wind farm output and 3rd harmonic active power component	-0.1581	0.1988	0.1645	-0.1721	0.2730	0.3052	0.2458	0.5986	0.1057
Between wind farm output and 3rd harmonic voltage magnitude	-0.2984	0.3705	0.4767	0.1391	0.2951	0.2020	-0.0395	0.1660	0.0333
Between wind farm output and 5th harmonic active power component	0.4355	0.4480	0.2815	0.1755	0.2318	-0.0338	0.6454	0.3276	0.4640
Between wind farm output and 5th harmonic voltage magnitude	0.0134	-0.0203	0.0110	-0.2352	-0.2100	-0.2711	-0.0207	0.0047	-0.0380
Between wind farm output and 7th harmonic active power component	-0.0178	-0.1023	-0.0165	-0.0853	-0.1723	-0.1302	0.1324	0.3018	0.1784
Between wind farm output and 7th harmonic voltage magnitude	-0.3908	-0.4149	-0.4009	-0.0132	-0.1153	-0.2217	-0.0008	-0.0085	-0.0273

From Table 1.3, one can see that in the west Texas area, the correlation between wind farm output and harmonic level is relative small. No correlation index is greater than 0.5. If there is a strong relationship between wind farm output and harmonic level, the correlation index should be in the range of 0.7~1. Therefore, there is no clear evidence to link the harmonic problem with these newly built wind farms based on the measurement data of July 2007.

1.2.2 High Voltage Direct Current System Field Investigation

In the east Texas area, there is a High Voltage Direct Current (HVDC) back-to-back transmission system. Engineers suspect that the harmonic problems may be caused by this HVDC system. In order to evaluate this theory, field measurements were taken at the HVDC transmission system. The power transferred by the HVDC system and the harmonic level of a nearby bus were recorded. The recorded information is shown in figure 1.1. From figure 1.1, it can be observed that when the harmonic level is high, the power transferred by HVDC system is low, and when the harmonic level is low, the power transferred by HVDC is high. Therefore, there is no clear evidence to link the harmonic problem with the HVDC system.

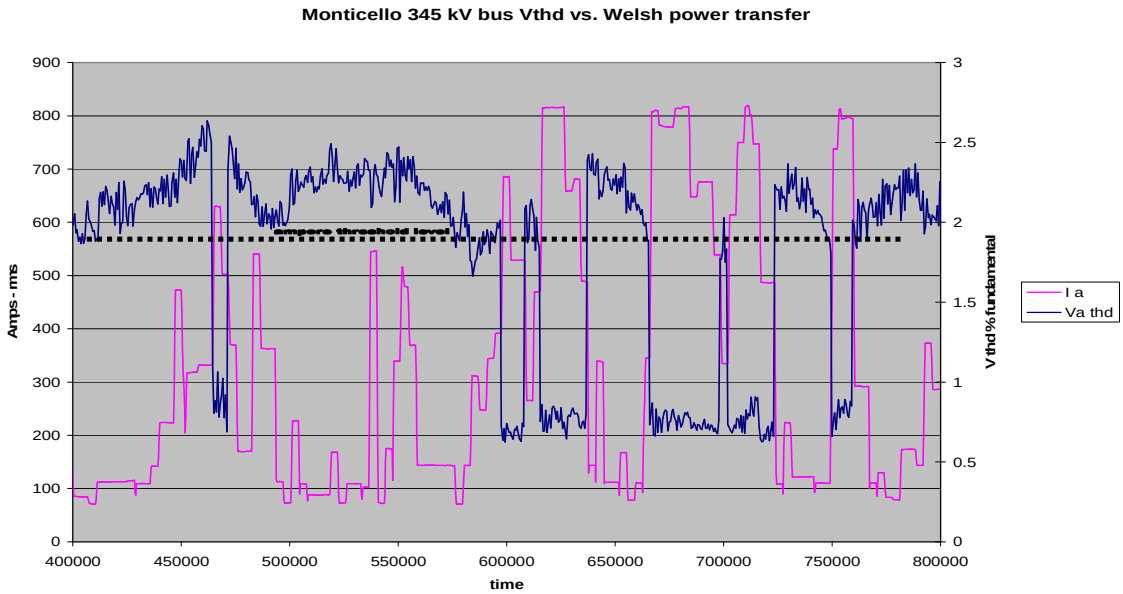

Figure 1.1 345kV bus harmonic V_{THD} level VS. HVDC System Power Transfer
Y-axis units of measurements: Ia – Amps , V_{THD} -- % of fundamental
X-axis units of measurements: time in seconds

1.2.3 Study Motivation

From section 1.2.1 and 1.2.2, one can observe that there is no clear evidence to link the harmonic problems with the newly built wind farms and the HVDC system. Therefore, it is necessary to employ harmonic source identification methods to identify the real harmonic sources in this high voltage transmission system.

1.3 Synopses of Chapters

The material in this dissertation is organized as follows:

Chapter 2 introduces the development of power system harmonic source identification methods. These methods are discussed with details in chapter 2. The last part of chapter 2 explains the limitations of applying previous proposed methods in the high voltage transmission system for the sample case.

Chapter 3 describes the effort to verify the accuracy of harmonic signals measurement instruments. The Coupling Capacitor Voltage Transformer (CCVT) is normally employed to measure voltage in the high voltage transmission system. Because of the internal design of CCVT, it may cause distortions when measuring harmonic signals. The EMTP/ATP software package is employed to study the frequency response of CCVT and provide the necessary adjustment for harmonic measurement. The studied results are verified by field tests in this chapter.

In chapter 4, the characteristics of harmonic signals measured in the Texas electric utility example high voltage transmission system is presented. Based on the harmonic characteristics, a two-step harmonic source identification method is proposed. A triangular method is deployed in the first step to generate the harmonic source suspect buses list. In the next step, the least square error method is employed to refine the suspect list.

In chapter 5, in order to verify the proposed harmonic source identification method, numerical simulations are carried out on the IEEE 300-bus test system. The simulation results have shown that the proposed approach has ability to identify the major harmonic sources in power systems with the existence of unbalanced harmonic sources and measurement noises.

Chapter 6 states the summary and conclusion of this dissertation and discusses the possible topics for further research.

CHAPTER 2

LITERATURE REVIEW OF HARMONIC SOURCE IDENTIFICATION METHODS

2.1 Present Harmonic Sources Identification Methods

Harmonic state estimation (HSE) is one of the most commonly proposed harmonic sources identification approaches in system analysis. The goal of HSE is to locate the possible harmonic sources and to estimate the distribution of harmonic signals by employing state-estimation algorithm. The HSE method was first proposed in [7]. In this paper, Dr. Heydt used least square estimators to identify the location of a harmonic source in a test power system. Line and bus data at several points in the sample network were used with the least square estimator to calculate the injection current spectrum at buses suspected of being harmonic sources. The calculated bus injection current spectrum was used to identify the type of harmonic source by the frequency characteristics of the spectrum.

However, due to the high cost of harmonic measurement equipments, only a limited numbers of harmonic meters are available in most power systems [8]. With only a limited number of harmonic monitoring points, unreliable estimation may result when using a standard least-square estimator [7]. To overcome this difficulty, a neural network based method was proposed in [9] to make an initial estimate. This approach permits measurement of harmonic signal with relatively few permanent harmonic measuring instruments. In [9], Hartana et al. used a trained neutral network to obtain the initial rough estimate of a harmonic source in a power system with a nonlinear load. The initial estimate is then employed as pseudo-measurements for harmonic state estimation to find additional suspect nodes.

When the network is partially observable, a singular value decomposition (SVD) method was proposed in [10]-[11]. In power system harmonic state estimation, in order to have a fully observable system, it is necessary that the number of measurements *m* is greater than or equal

to the number of states n ($m \geq n$) [12]. If $n > m$, then the system is in an underdetermined condition. In [10]-[11], a linear harmonic measurement state variable model in an underdetermined harmonic state estimation problem was established. In this study, the state variables in the observable island were estimated while the other state variables remain unknown.

In [13], a sparsity-maximization method was proposed. This paper proposed a systematic approach to identify and estimate harmonic sources in power system network for the condition where the number of harmonic meters is less than the number of unknown state variables. In this proposed approach, a harmonic state estimator is constructed by considering nodal harmonic injections as state variables. By exploiting the spatial sparsity characteristics of harmonic sources, the estimation problem is formulated as a sparsity maximization problem that can be solved efficiently by linear programming.

In order to minimize meter requirements as well as to avoid ill-conditioned measurement matrix, the optimal meter placement issue for HSE was addressed in [14]-[15]. In [14], a genetic algorithm based technique was proposed to place meters optimally for estimating and identifying the unknown harmonic sources. In [15], the minimum condition number of the measurement matrix is employed as a criterion in conjunction with sequential elimination to reach the near optimal measurement placement. This algorithm can yield a solution for the measurement placement that makes the most of system observable.

An application of HSE to an actual Japanese power system was described in [16]. In this paper, the Harmonic State Estimation method was verified by using field data synchronized with a GPS clock. In other words, the entire harmonic distribution (eight node voltages and 25 branch currents in this study project) of the studied power system was obtained effectively through measured data of eight measurement points.

Other approaches, such as Kalman Filters [17]-[18] and a Cascade Correlation Network method [19] were also proposed for identifying harmonic sources in power systems.

The Kalman filter is an online, recursive and optimal least square estimator suitable for a system described by state variables. The main objective of the Kalman filter is the optimal estimation of the state variables from measurement data corrupted with noise. In [17], the proposed method was based on a Kalman filter estimation model in which each harmonic injection source is treated as a random state variable. Error covariance analysis of harmonic injection by the Kalman filter was used to determine the optimal metering locations in power systems. Based on this optimal arrangement, the Kalman filter was able to estimate and track each harmonic injection in the test power system presented in [17]. In [18], the proposed method used an adaptive Kalman filter, which switched between the Kalman constant model and the Kalman random walk model depending on the state of the system. Its adaptive function allowed for the resetting of the Kalman gain to avoid Kalman filter divergence problems, and the tracking of harmonic sources.

In [19], Whei-Min Lin et al. presented a design of harmonic source detection system with a Cascade Correlation Network (CCN). In this method, at metering buses, the harmonic components of voltages under various loads would form particular patterns in the frequency domain and can be used to create training examples for CCN. The trained CCN can be used to identify the harmonic patterns and harmonic sources.

2.2 Limitations of Present Harmonic Identification Methods

Despite all these efforts, it is still a challenge to identify the major harmonic sources in high voltage transmission network. The reasons are stated as follows.

(1) Observability Issue

In this high voltage transmission network, due to the physical constraints and economic issues, only a very few buses located at some substations are equipped with intelligent electric measurement device (IEMD) that can provide the information of local harmonic voltage and current values. For example, only 15 buses were equipped with IEMD in one sub-system of this transmission system with more than 400 buses. Because of observability issue, HSE method

can not be applied effectively if the harmonic measurement points are less than a critical value for the studied system to be fully observable or even partially observable [12].

(2) Background Noise

In addition to the observability issue, it is common that the harmonic voltages are unbalanced, and the harmonic resonance phenomena do exist in the example transmission system. Both of them make it more difficult to identify the harmonic sources.

Because of the above reasons, the present harmonic sources identification algorithms are not suitable for the example transmission system. A new approach is needed to identification the possible harmonic source in this transmission network.

CHAPTER 3

VERIFICATION OF THE HARMONIC MEASUREMENT ACCURACY

Before applying any harmonic source identification algorithms, the most important task is to verify the accuracy of the harmonic component measurement. In this chapter, the harmonic signal measurement system is described and the measurement error correction efforts are also presented.

3.1 Introduction of Harmonic Measurement System

In the Texas example system, as conventional substation monitoring equipments had previously been installed, the existing instruments were used to take the harmonic measurements. The harmonic measuring system is shown in figure 3.1. In figure 3.1, the main measurement instrument is the intelligent electric measurement device (IEMD), which is installed at strategic substations of the high voltage power transmission system. IEMD can measure fault waveforms of voltages/currents, voltage dips, harmonics, and calculate fault locations. The harmonic current waveform is measured through a Current Transformer (CT). If the bus voltage is below 345-kV, for example 138-kV or 161-kV, a Potential Transformer (PT) is used to measure the voltage waveform. For the 345kV system, the voltage waveform is measured through the Coupling Capacitor Voltage Transformer (CCVT). A Fast Fourier Transform (FFT) algorithm is applied to analyze both the fundamental and harmonic components of voltage and current signals that pass through CCVT/PT or CT, the analog filter, and the analog/digital converter.

Due to the frequency response and the available bandwidth of the measurement devices, measurement errors may exist when measuring different order of harmonic components. Unlike the PT and CT, the CCVT may cause errors or distortions when measuring the harmonic signals [20]-[23]. Therefore, one may misjudge the system performance by using

the measured harmonic voltage information directly from the secondary side of the CCVT. It is necessary to provide adjustments for the measured data by studying the frequency response of the CCVT to obtain true picture of the harmonic voltage signal contents in the primary circuit.

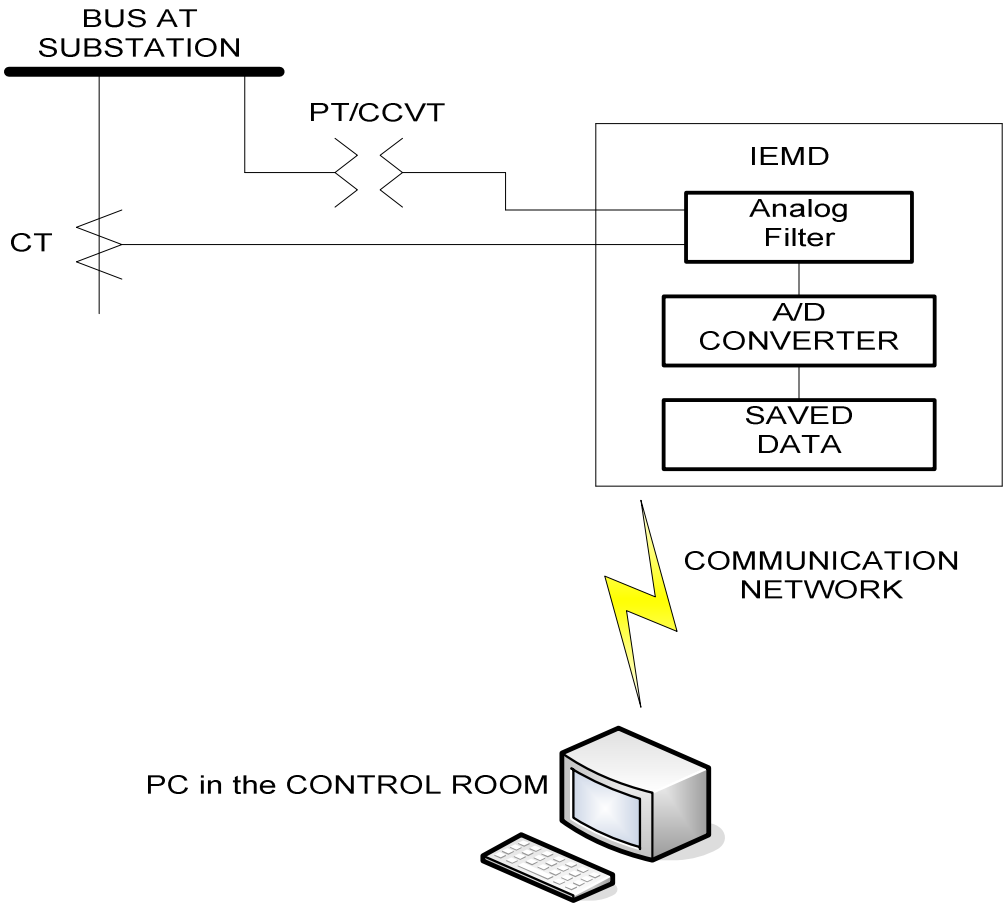

Figure 3.1 Harmonic Measurement Systems at Substations

3.2 Basic Principles of CCVT

The circuit diagram of a CCVT is shown in figure 3.2, and the generic model is shown in figure 3.3 [21]. As one can see from figure 3.2 and figure 3.3, the main components of a CCVT are:

- Capacitor Voltage Divider
- Compensation Reactor (CR)

- Step Down Transformer (SDT)
- Gap Protection Circuit (GPC)
- Ferroresonance Suppression Circuit (FSC)

In order to avoid insulation problems in a wound voltage transformer (VT) at high voltage levels, a step down ratio is achieved by using a capacitive voltage divider prior to applying the voltage to the step down transformer. In the capacitive voltage divider, two capacitors C_1 and C_2 brings the primary voltage down to $V*C_1/(C_1+C_2)$, where V is the source voltage. This divided voltage is then applied to the Step-Down Transformer (SDT), and the output of the SDT is connected to the burden. In many designs, the tuning reactor is in the ground line rather than the high voltage lead of the SDT. However, this does not affect the analysis and simulation results. The function of the tuning reactor is to minimize the equivalent source impedance at 60-Hz (fundamental power system frequency), by tuning it to the capacitance $C_1//C_2$ in order to allow burden to draw necessary current without causing significant voltage drop and thus affecting the accuracy of the measured voltage.

This feature is necessary when the instruments comprising the burden drew significant currents from the CCVT. However, the interaction of the capacitance with the magnetizing inductance L_m of the SDT is responsible for the subsidence transient problem and could lead to ferroresonance under particular excitation conditions.

One of the early techniques used to avoid ferroresonance was to add sufficient damping to the burden. Nowadays, most manufactures add a ferroresonance suppression circuit (FSC) to CCVT. The ferroresonance suppression circuit has low impedance around the subsidence transient frequency, which will increase damping at this frequency.

The gap protection circuit serves as an over voltage protection circuit. In some designs, the burden side may also be equipped with an over voltage protection gap with the connection of a loading resistor as part of the ferroresonance suppressing circuit.

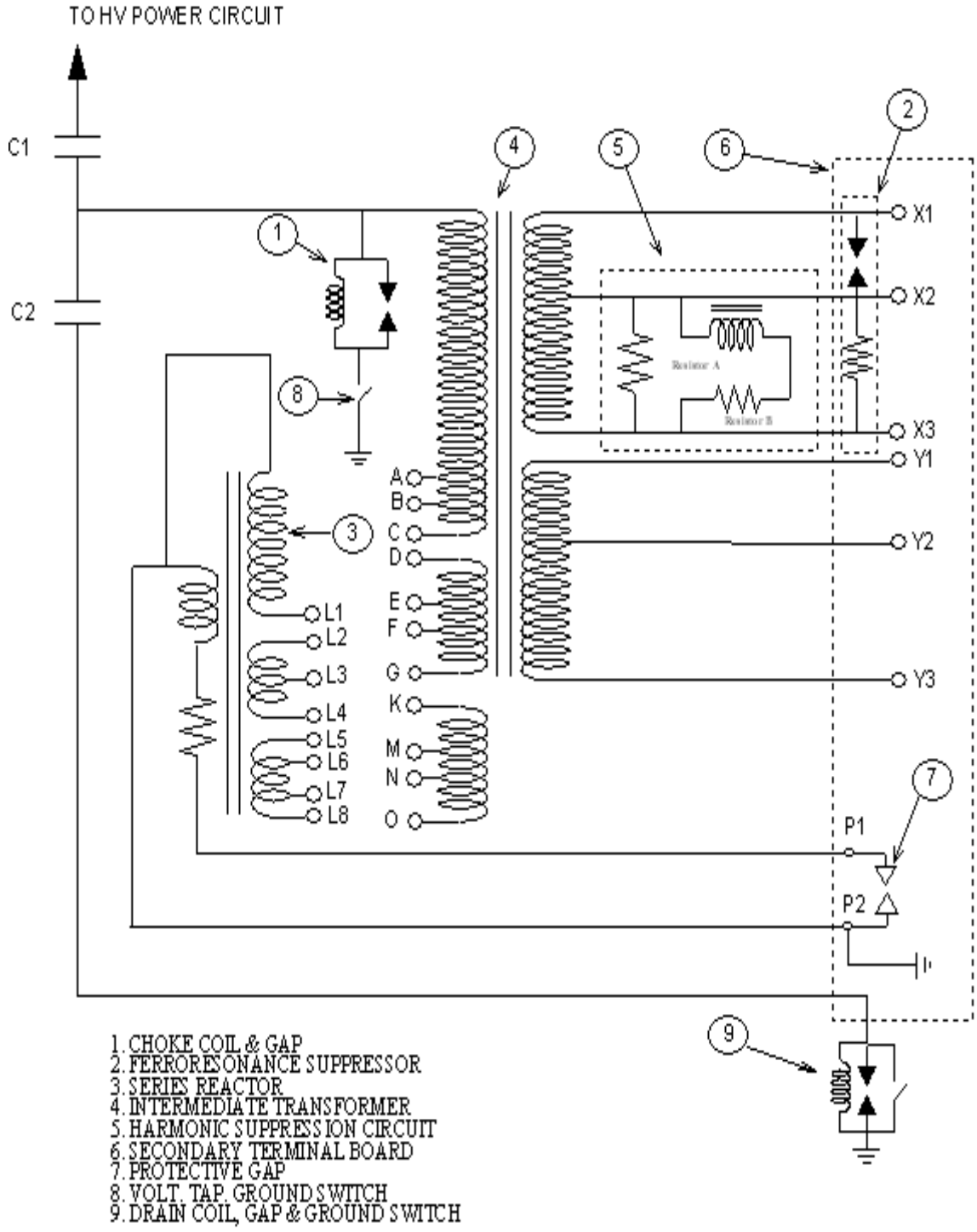

Figure 3.2 Circuit Diagram of a CCVT

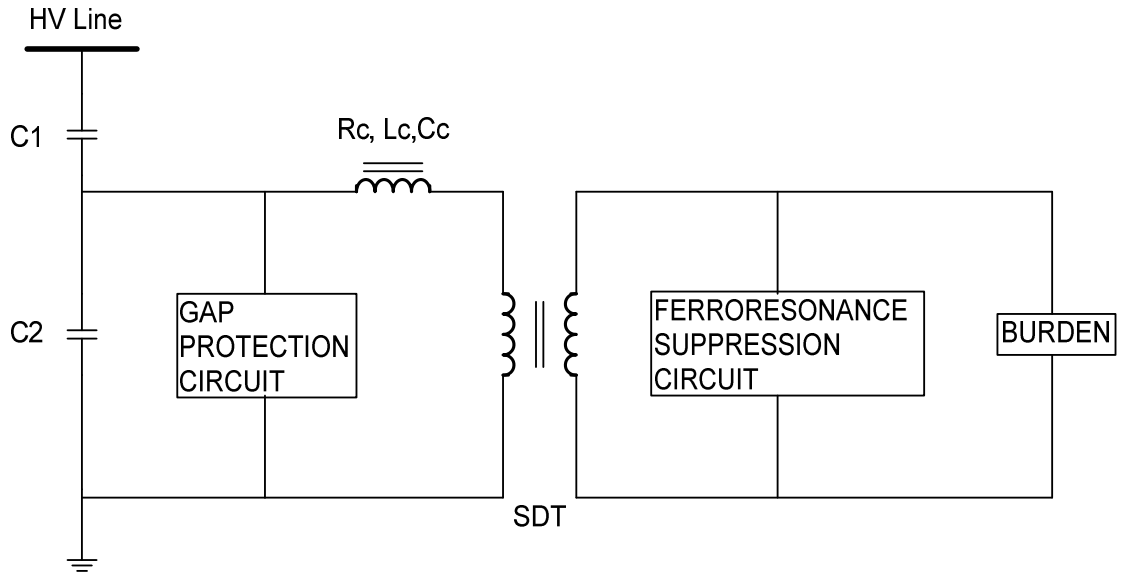

Figure 3.3 Generic CCVT Model

3.3 Digital Simulation Results

Frequency-domain studies were conducted on two types of 345kV CCVTs. Since there is no Phase Measurement Unit (PMU) to synchronize phase measurement in the substations of the example transmission network, this study is focuses on harmonic magnitude measurement.

In this digital simulation, most of parameters are given by the manufactures. Several parameters are given in a range, and some parameters are unknown. The default values from published papers [24], [25] are used for the unknown parameters. For those parameters which are given in a range, a set of frequency-domain studies are conducted to identify the output sensitivity to the parameter variations of the CCVT system. The simulation results are shown from figure 3.4 to figure 3.7. In these frequency response studies, the input voltages and output voltages are measured at various frequencies. The voltage gain is calculated as

$$\text{Gain (dB)} = 20 \times \log (V_{out} / V_{in}) \quad (3.1)$$

The main difference between the two CCVTs, CCVT 1 and CCVT 2 is that CCVT 1 does not have drain coil, whereas CCVT 2 does have a 10mH drain coil L_d. From the simulation results, it can be observed that the CCVT frequency response is significantly affected by the

drain coil L_d at frequencies above 1000-Hz. For both CCVTs, the values of the primary side stray capacitance (C_t) of the STD and the stray capacitance (C_c) of the series reactor are given in a range. Sensitivity analysis was conducted on these parameters. From the sensitivity analysis simulation results, one can observe that for both types of CCVTs, the effect of the primary side stray capacitance (C_t) of the STD on the CCVT frequency response cannot be ignored at frequencies above 1000-Hz, and the notch frequency illustrated in the frequency response is noticeably affected by the stray capacitance (C_c) of the series reactor.

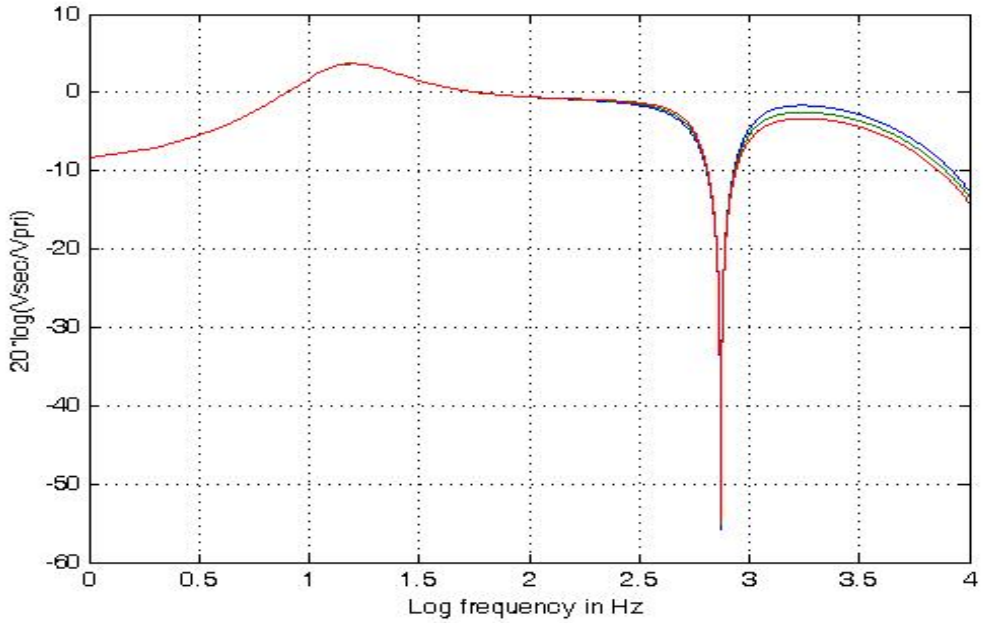

Figure 3.4 Effect of C_t on CCVT 1 frequency response
(Blue: C_t=200pF; Green: C_t=300pF; Red: C_t=400pF)

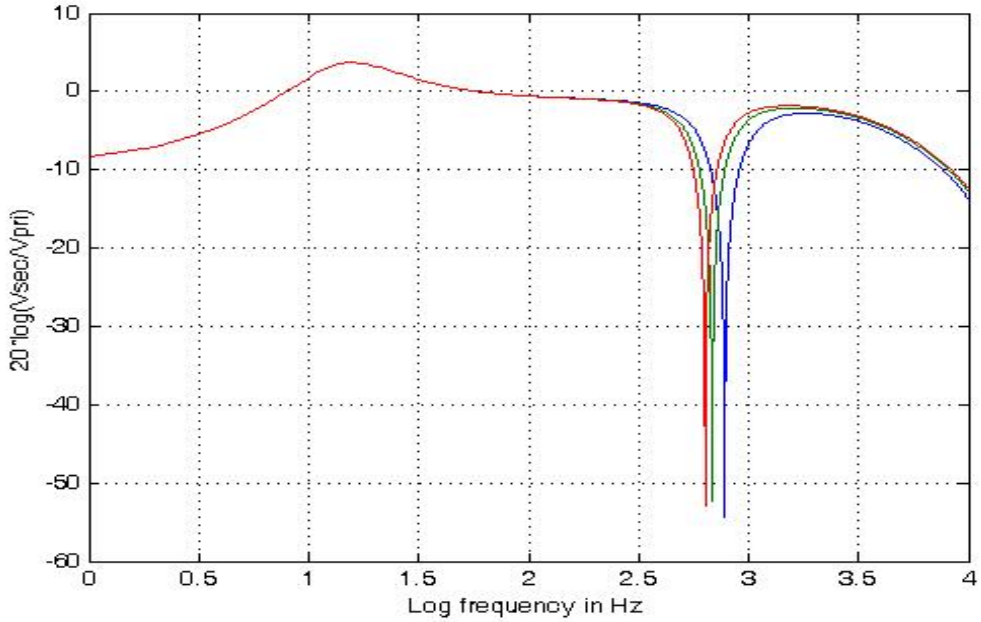

Figure 3.5 Effect of C_c on CCVT 1 frequency response
(Blue: C_c=300pF; Green: C_c=350pF; Red: C_c=400pF)

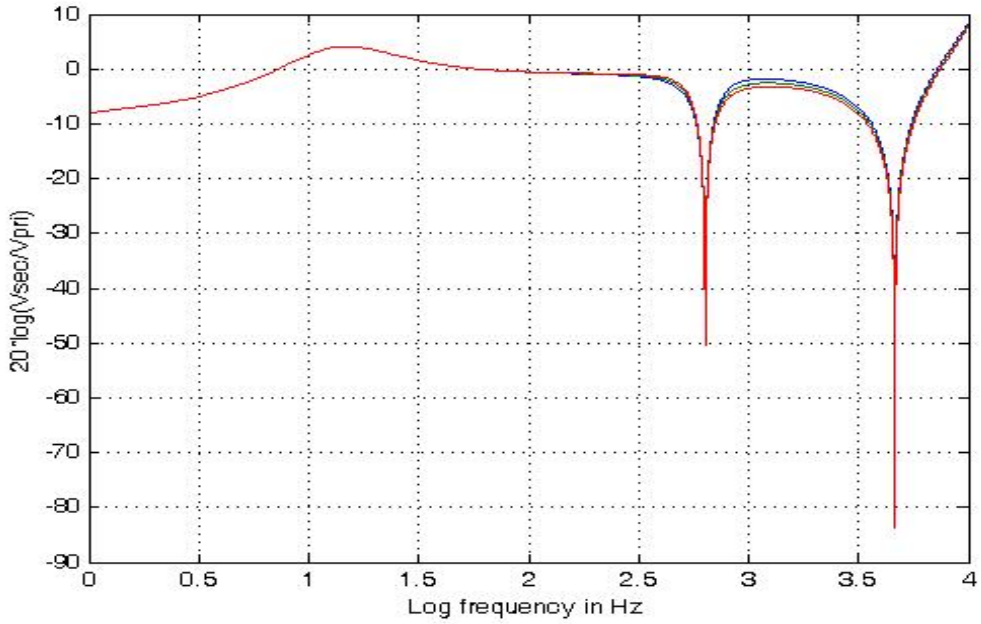

Figure 3.6 Effect of C_t on CCVT 2 frequency response
(Blue: C_t=200pF; Green: C_t=300pF; Red: C_t=400pF)

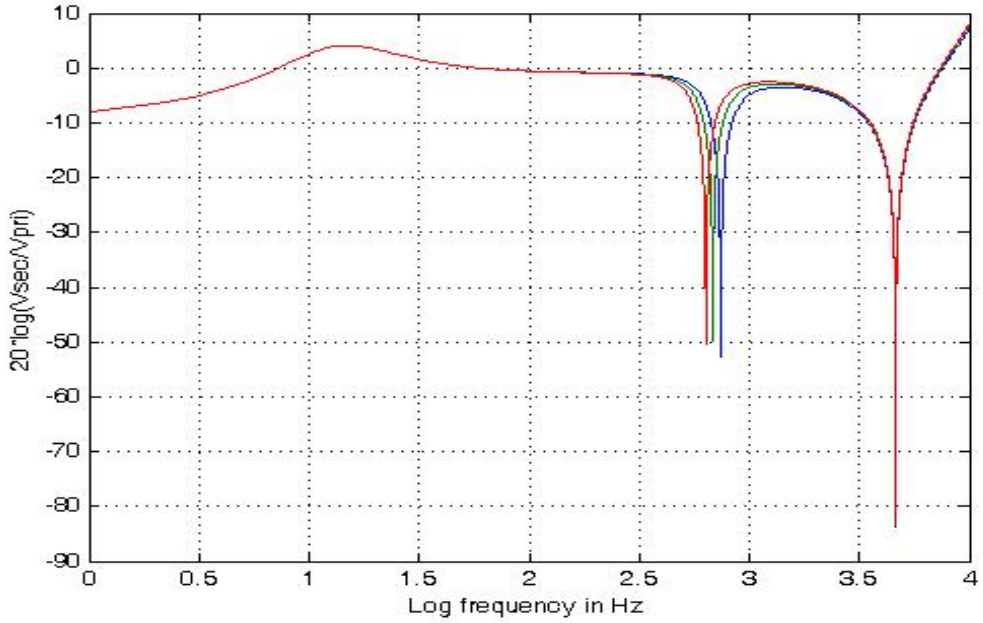

Figure 3.7 Effect of C_c on CCVT 2 frequency response
(Blue: C_c=500pF; Green: C_c=575pF; Red: C_c=650pF)

Using the digital simulation methods presented in this section, the adjustment values for both type 1 CCVT and type 2 CCVT are calculated. For parameters that are given in a range, the average value was employed; for parameters that are unknown, the typical value was employed. The calculated the adjustment values for type 1 CCVT and type 2 CCVT are listed in table 3.1 and table 3.2.

Table 3.1 Adjustment Values for Type 1 CCVT

Harmonic No.	Frequency(Hz)	In (%)	Out (%)
1	60	100	100
2	120	100	102.3
3	180	100	105.7
4	240	100	93.6
5	300	100	85.4
6	360	100	77.9
7	420	100	72.6
8	480	100	53.4
9	540	100	31.3
10	600	100	24.2
11	660	100	15.1
12	720	100	26.2
13	780	100	35.7
14	840	100	36.4
15	900	100	38.7
16	960	100	41.6
17	1020	100	42.4
18	1080	100	43.7
19	1140	100	42.5
20	1200	100	41.6
21	1260	100	37.2
22	1320	100	36.1
23	1380	100	34.2
24	1440	100	33.7
25	1500	100	35.2
26	1560	100	37.2
27	1620	100	32.1
28	1680	100	33.9
29	1740	100	31.2
30	1800	100	29.1
31	1860	100	28.7

Table 3.2 Adjustment Values for Type 2 CCVT

Harmonic No.	Frequency(Hz)	In (%)	Out (%)
1	60	100	100
2	120	100	101.9
3	180	100	104.6
4	240	100	95.4
5	300	100	86.5
6	360	100	78.2
7	420	100	75.3
8	480	100	67.2
9	540	100	45.2
10	600	100	34.2
11	660	100	23.3
12	720	100	32.1
13	780	100	38.1
14	840	100	41.2
15	900	100	43.9
16	960	100	45.7
17	1020	100	46.2
18	1080	100	44.3
19	1140	100	38.2
20	1200	100	36.2
21	1260	100	37.1
22	1320	100	42.1
23	1380	100	37.2
24	1440	100	36.2
25	1500	100	36.7
26	1560	100	35.9
27	1620	100	32.7
28	1680	100	33.2
29	1740	100	34.2
30	1800	100	31.1
31	1860	100	29.1

3.4 Field Tests

In order to validate the digital simulation results, field tests were carried out at two substations in the example transmission network. In substation 1, a potential transformer was used to measure the harmonic voltage component on a 138kV bus, and a type 1 CCVT was employed to measure the harmonic voltage component of a nearby 345kV bus. In substation 2, a potential transformer was used to measure the harmonic voltage component of a 161kV bus, and a type 2 CCVT was employed to measure the harmonic voltage component at a nearby 345kV bus. Since in both case, the MV bus and HV bus are located in the same substation, the harmonic components should be identical.

The measured harmonic voltage components up to 31-st harmonic from PT and the measured values from the CCVT after adjustment are listed in table 3.3 and table 3.4. In both table 3.3 and table 3.3, the harmonic voltage values are listed as the percent of the fundamental values. The absolute values and the percent values of the differences between the two measurements are also listed. The difference in percent values are calculated by using equation 3.2. Where in equation 3.2, D is difference between two measurements; M_p is the measurement from the PT, and M_c is the measurement from the CCVT.

$$D = \lfloor (M_P - M_C) / M_p \rfloor \times 100 \tag{3.2}$$

From table 3.3 and table 3.4, one can observe that after adjustment, the measurement results from the PT and CCVT are very close. This indicates that the CCVT frequency study results are acceptable for harmonic measurement adjustment. Still, it should be mentioned that:

1) At the frequency near the 11-th harmonic, the differences increase. This is because there is a notch near the 11-th harmonic frequency (660-Hz). Since the notch frequency is affected by the value of the stray capacitance (C_c) of the series reactor, the 11-th harmonic should be used with caution if it is employed to calculate the total harmonic distortion [5],
2) After the 14-th harmonic, the differences tend to increase slightly. This is because at frequencies above 1000-Hz, the effect of the primary side stray capacitance (C_t) of the STD

on the CCVT frequency response cannot be ignored. However, one can also observe that, after the 14-th harmonic, the harmonic voltage levels are very small in percentage (generally speaking, less than 0.1%). The low level of higher order harmonics will have little or no effect in determining whether or not that the harmonic levels exceed IEEE recommend standard [5].

Table 3.3 Comparison between PT and CCVT Measurements at Substation 1

Harmonic Order	PT	Original Measurement Results From CCVT	After Adjustment Results From CCVT	Absolute Difference	Percent Difference
1	100.00	100.0000	100.00	0.0000	0
2	0.1008	0.1056	0.1032	0.0024	-2.38
3	0.1661	0.1669	0.1579	0.0082	3.18
4	0.0477	0.0373	0.0399	0.0078	3.38
5	0.7447	0.6569	0.7692	0.0245	-3.27
6	0.0442	0.1202	0.1543	0.1101	-3.41
7	0.6449	0.4881	0.6723	0.0274	-3.76
8	0.0065	0.1274	0.2385	0.2320	-5.29
9	0.0285	0.0429	0.1371	0.1086	-6.69
10	0.0102	0.0295	0.1219	0.1117	-6.74
11	0.0522	0.0370	0.2448	0.1926	-9.04
12	0.0264	0.0307	0.1173	0.0909	7.19
13	0.0061	0.0020	0.0057	0.0004	6.55
14	0.0026	0.0048	0.0133	0.0107	-5.55
15	0.0179	0.0080	0.0207	0.0028	-4.02
16	0.0235	0.0104	0.0251	0.0016	-6.80
17	0.0149	0.0066	0.0156	0.0007	-6.12
18	0.0169	0.0078	0.0179	0.0010	-7.18
19	0.0231	0.0103	0.0243	0.0012	-5.19
20	0.0216	0.0097	0.0232	0.0016	-6.91
21	0.0314	0.0111	0.0298	0.0016	5.69
22	0.0144	0.0055	0.0153	0.0009	-6.25
23	0.0233	0.0075	0.0219	0.0014	6.00
24	0.0143	0.0045	0.0135	0.0008	5.59
25	0.0332	0.0112	0.0319	0.0013	5.34
26	0.0504	0.0199	0.0534	0.0030	-5.95
27	0.0366	0.0124	0.0387	0.0021	-5.73
28	0.0025	0.0040	0.0118	0.0093	5.61
29	0.0136	0.0045	0.0145	0.0009	-6.61
30	0.0072	0.0024	0.0081	0.0009	-5.19
31	0.0121	0.0038	0.0132	0.0011	-7.31

Table 3.4 Comparison between PT and CCVT Measurements at Substation 2

Harmonic Order	PT	Original Measurement Results From CCVT	After Adjustment Results From CCVT	Absolute Difference	Percent Difference
1	100.00	100.0000	100.00	0.0000	0.00
2	0.0651	0.0649	0.0637	0.0014	2.15
3	0.7268	0.7300	0.6979	0.0289	3.98
4	0.0291	0.0282	0.0296	0.0005	-1.72
5	1.2773	1.1481	1.3273	0.0500	-3.91
6	0.0051	0.0041	0.0053	0.0002	-3.90
7	0.5886	0.4608	0.6119	0.0233	-3.96
8	0.0053	0.0038	0.0057	0.0004	-7.38
9	0.0229	0.0110	0.0244	0.0015	-6.56
10	0.0090	0.0033	0.0097	0.0007	-8.26
11	0.2125	0.0542	0.2325	0.0200	-9.41
12	0.0015	0.0005	0.0016	0.0001	-6.62
13	0.0671	0.0267	0.0701	0.0030	-4.47
14	0.0035	0.0015	0.0037	0.0002	-5.79
15	0.0050	0.0023	0.0052	0.0002	-4.02
16	0.0036	0.0017	0.0038	0.0002	-5.58
17	0.0367	0.0179	0.0387	0.0020	-5.51
18	0.0148	0.0068	0.0154	0.0006	-4.06
19	0.0248	0.0097	0.0253	0.0005	-2.01
20	0.0132	0.0047	0.0131	0.0001	0.76
21	0.0153	0.0056	0.0150	0.0003	1.97
22	0.0100	0.0041	0.0098	0.0002	2.00
23	0.0127	0.0046	0.0124	0.0003	2.37
24	0.0100	0.0035	0.0096	0.0004	3.99
25	0.0068	0.0024	0.0065	0.0003	4.40
26	0.0114	0.0039	0.0109	0.0005	4.73
27	0.0096	0.0030	0.0091	0.0005	5.22
28	0.0074	0.0023	0.0070	0.0004	5.42
29	0.0179	0.0057	0.0167	0.0012	6.70
30	0.0150	0.0044	0.0143	0.0007	4.66
31	0.0066	0.0018	0.0063	0.0003	4.53

CHAPTER 4

PROPOSED ALGORITHMS FOR HARMONIC SOURCE IDENTIFICATION

4.1 Harmonic Characteristics Survey

Before we start the harmonic sources identification process, it is necessary to study the characteristics of the harmonic-distortion signals that were measured from the example high voltage transmission network. In this section, the harmonic measurement information is described and the characteristics of measured harmonic information are discussed.

4.1.1 Harmonic Measurements Information

As mentioned in the first chapter, there is no clear evidence to link the harmonic problem with the newly built wind farms or the HVDC system. In order to find the real harmonic sources, it is necessary to take additional harmonic measurements in the example high voltage transmission system.

Four different sets of harmonic measurements were taken inside of the example transmission network. Please refer to Appendix A for detail information about these harmonic measurements.

4.1.2 Dominant Harmonic Components

According to the field measurement results, the observed major harmonics signals were the 5-th, 7-th, and 11-th harmonics, and the dominant component was the 5-th harmonic signal. It was also found that the level of the 3-rd harmonic signals that commonly existed in the power distribution system was relatively low. Since the 3-rd harmonics can easily be blocked by some Δ-Y transformers, this could be the reason why the level of the 3-rd harmonic in the example high voltage transmission system is relatively low. Furthermore, the variation trends of the 5-th, 7-th, and 11-th harmonic voltages are very much alike, and they are similar to the level-variation patterns of the Total Harmonic Distortion (THD).

4.1.3 Time Variant Harmonic Levels

It was also found that the harmonic levels are different at the different times of the day. Figure 4.1 shows the harmonic voltage level change during a workday when measured from a 345 kV bus. From this figure, it can be observed that, during the midnight, the harmonic level is low, and at the peak hours, the harmonic level is high. This shows that the harmonic voltage levels are similar to system load patterns.

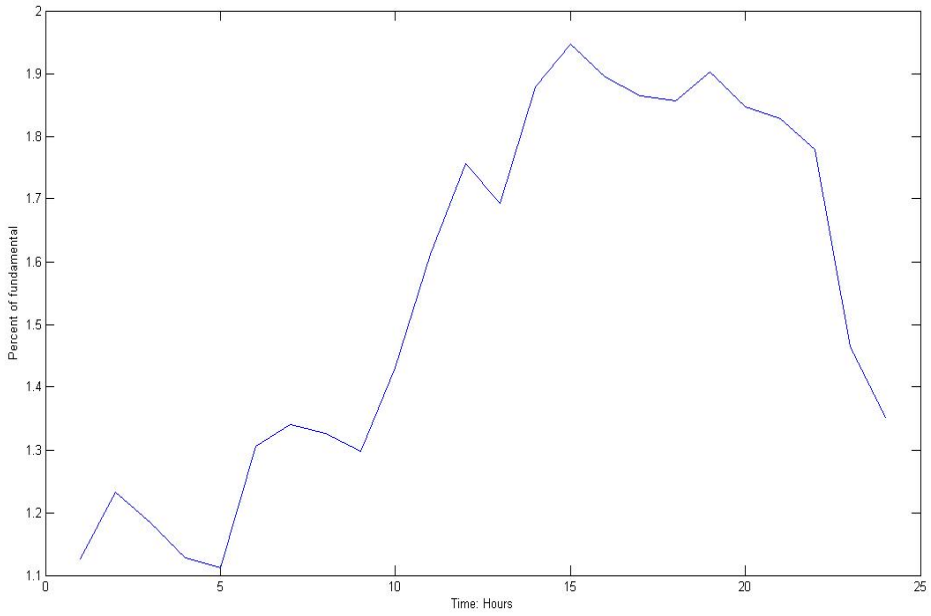

Figure 4.1 THD of Harmonic Voltage on a 345kV Bus during a Workday

4.1.4 Unbalanced Harmonic Signals

It was also observed that the measured harmonic voltages were not balanced at almost every measurement point. Table 4.1 lists measurement results obtained from a 345kV bus of the studied system. It can be clearly seen from table 4.1 that the three-phase harmonic voltages are severely unbalanced.

Table 4.1 Measured Harmonic Voltages at the 345kV Bus of the Studied System

	Peak (Volts)	RMS (Volts)	$V^{(h)}/V^{(1)}$ (%)	Angle (Degree)
5th harmonic of Phase A	2625.40	1856.40	0.9240	4.02
5th harmonic of Phase B	3011.30	2129.30	1.0588	123.65
5th harmonic of Phase C	3918.18	2770.60	1.3715	-110.48
7th harmonic of Phase A	2163.39	1529.76	0.7614	175.18
7th harmonic of Phase B	1653.90	1169.48	0.5815	56.06
7th harmonic of Phase C	2350.00	1661.68	0.8226	-73.34
11th harmonic of Phase A	922.49	652.3	0.3247	110.28
11th harmonic of Phase B	884.45	625.4	0.3113	-111.31
11th harmonic of Phase C	836.08	591.2	0.2943	-15.817

4.1.5 Harmonic Resonance Problems

In some parts of the studied high voltage transmission system, the harmonic resonance problems may be present. Table 4.2 shows an example of possible harmonic resonance problems. In table 4.2, it can be observed that at bus No.3, compared to the 5-th harmonic, the level of 7-th harmonic current is extremely high, while the harmonic voltage level is very low. At bus No.4, compared to the 11-th harmonic, the harmonic current level of the 5-th harmonic is low, and the harmonic voltage level of 5-th is high. At bus No.1, compared to the 5-th harmonic, the current level of the 7-th harmonic is high, while the harmonic voltage level is very low.

Based on above observation and the assumption that there is no measurement error involved in the harmonic measurement, it can be concluded that harmonic resonance played an important role in this phenomenon. In power systems, the presence of capacitors, such as those used for power factor correction, can result in local system resonance, which leads to excessive harmonic current/voltage levels and may possibly cause subsequent damage to the power systems equipment.

Table 4.2 An Example of Harmonic Resonance Problems

	Bus No.1			Bus No.2			Bus No.3			Bus No.4			Bus No.5		
	5-th	7-th	11-th	5-th	7-th	11-th	5-th	7-th	11-th	5-th	7-th	11-th	5-th	7-th	11-th
Phase A Current	4.50	2.49	0.36	2.65	0.49	1.02	0.47	1.41	0.31	1.32	0.14	3.05	0.38	0.90	0.66
Phase A Voltage	0.57	0.02	0.06	1.15	0.10	0.24	1.77	0.34	0.30	1.90	0.26	1.16	1.51	0.47	0.73
Phase B Current	3.50	1.67	0.07	4.02	0.68	1.46	0.30	1.31	0.26	1.09	0.14	3.19	0.35	1.04	0.80
Phase B Voltage	0.46	0.06	0.06	1.15	0.14	0.29	1.29	0.39	0.33	1.92	0.24	1.25	1.60	0.07	0.63
Phase C Current	3.97	1.29	0.52	2.60	0.50	1.06	0.23	1.28	0.48	1.26	0.15	2.98	0.60	0.73	0.62
Phase C Voltage	0.52	0.11	0.08	1.17	0.18	0.26	1.96	0.13	0.28	1.94	0.25	1.17	1.61	0.12	0.54

Note: unit of measurement – percent of fundamental values

Table 4.3 Sequence of the Harmonic Signals

Harmonic Number	Phase A	Phase B	Phase C	Phase Sequence
1	θ_1	θ_1-120	θ_1+120	Positive
2	$\theta_2 \times 2 = 2\theta_2$	$(-120+\theta_2)\times 2 = -240+2\theta_2$ $-240 + 360 = 120$	$(120+\theta_2)\times 2 = 240+2\theta_2$ $240 = -120$	Negative
3	$\theta_3 \times 3 = 3\theta_3$	$(-120+\theta_3)\times 3 = -360+3\theta_3$ $-360=0$	$(120+\theta_3)\times 3 = 360+3\theta_2$ $360=0$	No Rotation
4	$\theta_4 \times 4 = 4\theta_4$	$(-120+\theta_4)\times 4 = -480+4\theta_4$ $-480 + 360 = -120$	$(120+\theta_4)\times 4 = 480+4\theta_2$ $480 - 360 = 120$	Positive
5	$\theta_5 \times 5 = 5\theta_5$	$(-120+\theta_5)\times 5 = -600+5\theta_5$ $-600 + 720 = 120$	$(120+\theta_5)\times 5 = 600+5\theta_5$ $600 - 360 = 240$	Negative
6	$\theta_6 \times 6 = 6\theta_6$	$(-120+\theta_6)\times 6 = -720+6\theta_5$ $-720=0$	$(120+\theta_6)\times 6 = 720+6\theta_6$ $720=0$	No Rotation
7	$\theta_7 \times 7 = 7\theta_7$	$(-120+\theta_7)\times 7 = -840+7\theta_7$ $-840 = -120$	$(120+\theta_7)\times 7 = 840+7\theta_7$ $840 = 120$	Positive
8	$\theta_8 \times 8 = 8\theta_8$	$(-120+\theta_8)\times 8 = -960+8\theta_8$ $-960=120$	$(120+\theta_8)\times 8 = 960+8\theta_8$ $960 = 240$	Negative
9	$\theta_9 \times 9 = 9\theta_9$	$(-120+\theta_9)\times 9 = -1080+9\theta_9$ $-1080=0$	$(120+\theta_8)\times 9 = 1080+9\theta_8$ $1080=0$	No Rotation

4.2 Management of Unbalance Harmonic Voltages

Since the harmonic voltages in the studied transmission system are not balanced, the symmetrical components can be used to deal with the unbalance harmonic voltages.

In a power system, suppose that A_1, B_1, and C_1 represent the fundamental waveform. They are all at the same frequency, but shifted 120^o from each other in terms of phase. Let's call the 3-rd harmonic of each waveform A_3, and B_3, and C_3, respectively. The phase shift between A_3, B_3, and C_3 is not 120 degree (that is the phase shift between A_1, B_1, and C_1), but 3 times that, because the A_3, B_3, and C_3 waveforms alternate three times as fast as A_1, B_1, and C_1. The shift between waveforms is only accurately expressed in terms of phase angle when the same angular velocity is assumed. When relating waveforms of different frequency, the most accurate way to represent phase shift is in terms of time; and the time-shift between A_1, B_1, and C_1 is equivalent to 120 degrees at a frequency three times lower, or 360 degrees at the frequency of A_3, B_3, and C_3. A phase shift of 360 is the same as a phase shift of zero, which is to say no phase shift at all. Thus, A_3, B_3, and C_3 must be in phase with each other. If this mathematical method is extend to include higher numbered harmonics, an interesting pattern will be developed with regard to the rotation or sequence of the harmonic frequencies, which is listed in the table 4.3.

From table 4.3, it can be observed that harmonics such as the 4-th order, and the 7-th order, which "rotate" with the same sequence as the fundamental, are acting like positive sequence components. Harmonics such as the 2-nd order and the 5-th order, which "rotate" in the opposite sequence as the fundamental, are acting like negative sequence components. Because triplen harmonics (3-rd and 9-th shown in this table) don't "rotate" at all, they're in phase with each other and act like zero sequence components.

Because triplen harmonics are acting like zero sequence components, and the zero sequence components can easily be blocked by the Δ-Y transformer, the triplen harmonics will not be employed in the identification process.

As stated in chapter 2, in the example high voltage transmission system, the majority harmonics are 5-th, 7-th and 11-th harmonics. Therefore, in this dissertation, only the 5-th, 7-th and 11-th harmonics will be used to identify the possible harmonic source. For the 5-th and 11-th order harmonics, only the negative component will be used, and for 7-th harmonic, the positive component will be used. In order to illustrate this symmetrical component calculation method, a sample calculation for harmonic data listed in table 4.1 is presented as follows.

$$\begin{bmatrix} V_{5A}^{0} \\ V_{5A}^{+} \\ V_{5A}^{-} \end{bmatrix} = \frac{1}{3}\begin{bmatrix} 1 & 1 & 1 \\ 1 & \alpha & \alpha^{2} \\ 1 & \alpha^{2} & \alpha \end{bmatrix}\begin{bmatrix} V_{5A} \\ V_{5B} \\ V_{5C} \end{bmatrix} = \begin{bmatrix} 0.2513\angle 113.2337^{\circ} \\ 0.3096\angle 157.2365^{\circ} \\ 2.2494\angle 6.1584^{\circ} \end{bmatrix} kV$$

$$\begin{bmatrix} V_{7A}^{0} \\ V_{7A}^{+} \\ V_{7A}^{-} \end{bmatrix} = \frac{1}{3}\begin{bmatrix} 1 & 1 & 1 \\ 1 & \alpha & \alpha^{2} \\ 1 & \alpha^{2} & \alpha \end{bmatrix}\begin{bmatrix} V_{7A} \\ V_{7B} \\ V_{7C} \end{bmatrix} = \begin{bmatrix} 0.2106\angle -128.69^{\circ} \\ 1.4495\angle 172.1715^{\circ} \\ 0.1048\angle 65.6139^{\circ} \end{bmatrix} kV$$

$$\begin{bmatrix} V_{11A}^{0} \\ V_{11A}^{+} \\ V_{11A}^{-} \end{bmatrix} = \frac{1}{3}\begin{bmatrix} 1 & 1 & 1 \\ 1 & \alpha & \alpha^{2} \\ 1 & \alpha^{2} & \alpha \end{bmatrix}\begin{bmatrix} V_{11A} \\ V_{11B} \\ V_{11C} \end{bmatrix} = \begin{bmatrix} 0.058\angle -48.810^{\circ} \\ 0.098\angle 96.1728^{\circ} \\ 0.612\angle 114.822^{\circ} \end{bmatrix} kV$$

From above calculation, it appears that for the 5-th harmonic, the major component is the negative sequence part. For the 7-th harmonic, the major component is the positive sequence part. For the 11-th harmonic, the major component is the negative sequence part. Therefore, in this project, when measured raw data was applied, for the 5-th and 11-th harmonic, only the negative component will be used, and for 7-th harmonics, only the positive component will be used.

4.3 Harmonic Resonance Detection

The presence of capacitors, such as those used for power factor correction, can result in harmonic resonances, which lead in turn to excessive currents or voltages, and possibly subsequent damage to the equipments of power system [26-28]. Generally speaking, there are

two kinds of harmonic resonances in power system, Series Resonance and Parallel Resonance.

4.3.1 Series Resonance

Consider a system illustrated in figure 4.2, series resonance occurs when the following condition is met,

$$f_0 = \frac{1}{2\pi\sqrt{LC}} \tag{4.1}$$

In equation 4.1, f_0 is the series resonant frequency, L is the transformer inductance, and C is the capacitance of the capacitor bank.

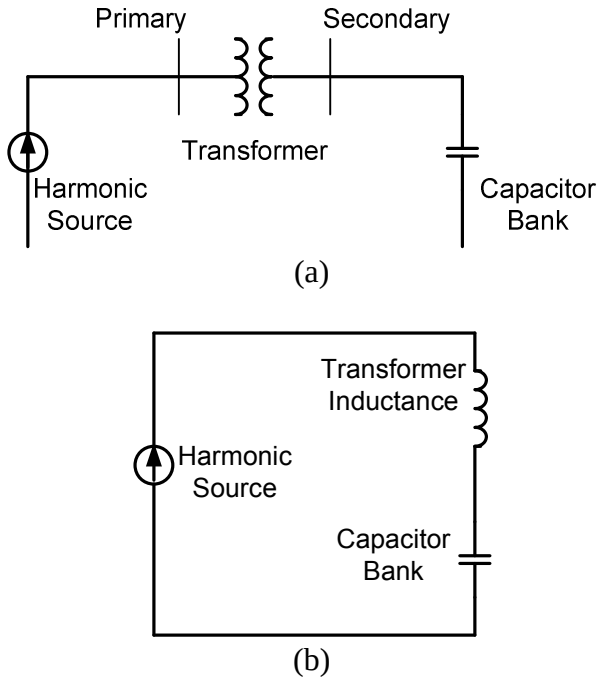

Figure 4.2 (a) One-Line Diagram of Series Resonance; (b) Equivalent Circuit

When series resonance happens, the circuit impedance will reach to its minimum value. The main concern with series resonance is that high harmonic current can flow with relatively small harmonic voltage, which will make the capacitor bank overload. The actual current that will flow depends upon the quality factor Q of the circuit.

4.3.2 Parallel Resonance

Consider a system illustrated in figure 4.2, a capacitor is connected to the same bus as the harmonic source. A parallel resonance can occur between the source impedance and the capacitor bank when the following condition is met.

$$f_0 = \sqrt{\frac{1}{LC} - \left(\frac{R}{L}\right)^2} \tag{4.2}$$

In equation 4.2, *C* is the capacitance of the capacitor bank, *L* is the source inductance, and *R* is the source resistance.

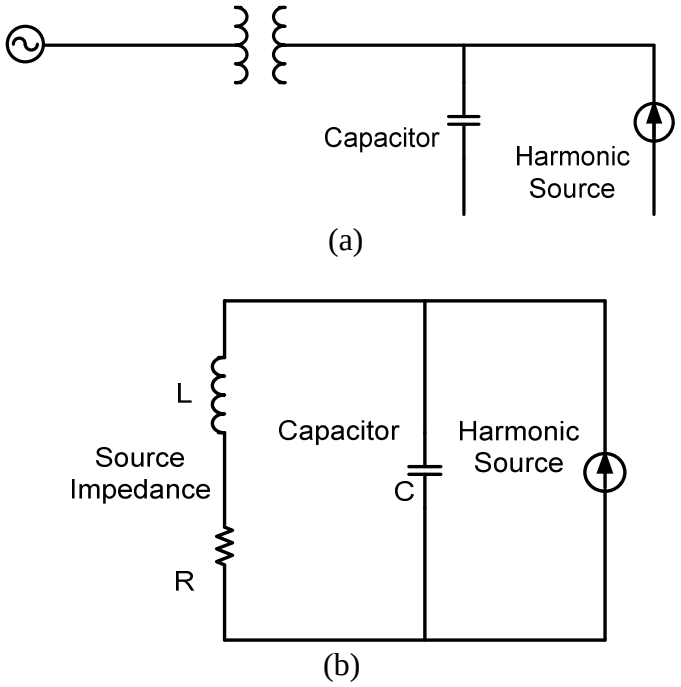

Figure 4.3 (a) One-Line Diagram of Parallel Resonance; (b) Equivalent Circuit

Parallel resonance may result in high impedance at the resonant frequency. This may cause excessive harmonic voltage and high harmonic currents in each leg of the parallel impedance.

4.3.3 Harmonic Resonance Detection Method

From the previous section, when series resonance happens, the circuit impedance will change and reach to its minimum value; when parallel resonance happens, the circuit impedance also will change and reach to its maximum value. Based on these facts, the circuit impedance gives a good indicator for harmonic resonance detection.

If the skin effect can be ignored, and the harmonic resonance does not occur, the circuit impedance should not change too much at different harmonic orders. For the n-th order and m-th order harmonics (n < m), if there is no harmonic resonance issue involved, the lower bound of the harmonic circuit impedance happens when the circuit is purely inductance, and the upper bond of the harmonic circuit impedance happens when the circuit is purely capacitance, which is illustrated in equation 4.3 and equation 4.4.

$$\frac{Z_n}{Z_m} \geq \frac{j \cdot 2 \cdot \pi \cdot f \cdot n \cdot L}{j \cdot 2 \cdot \pi \cdot f \cdot m \cdot L} = \frac{n}{m} \tag{4.3}$$

$$\frac{Z_n}{Z_m} \leq \frac{j \cdot 2 \cdot \pi \cdot f \cdot m \cdot L}{j \cdot 2 \cdot \pi \cdot f \cdot n \cdot L} = \frac{m}{n} \tag{4.4}$$

In equation 4.3 and 4.4, where,

Z_n is the harmonic impedance at n-th harmonic order,

Z_m is the harmonic impedance at m-th harmonic order,

j = $\sqrt{-1}$

f is the fundamental frequency, which is 60Hz in the North America power systems, and

L is the inductance of element

From the above analysis, if for a particular measurement point, the voltage and current at different harmonic order can be attained, then by calculating the *V/I* ratio at different harmonic orders, significant changes in the circuit impedance can be determined. If there is a big change in the circuit impedance, a harmonic resonance may exist at that location.

Since in this sample network, the observed dominant harmonics signals were the 5-th, 7-th, and 11-th harmonics, these three order harmonics will be employed to detect whether a harmonic resonance exists in the vicinity of measurement point.

(1) 5-th and 11-th harmonics

For 5-th and 11-th harmonics, ideally, the ratio of Z_{5th} / Z_{11th} should be in the range of,

$$\frac{5}{11} \leq \left(\frac{Z_{5th}}{Z_{11th}} \right) \leq \frac{11}{5} \tag{4.5}$$

If for a particular measurement point, the V/I ratio is smaller than 1/2.2 or larger than 2.2, a harmonic resonance may exist.

(2) 5-th and 7-th harmonics

Similarly, the ratio of Z_{5th} / Z_{7th} should be in the range of,

$$\frac{5}{7} \leq \left(\frac{Z_{5th}}{Z_{7th}} \right) \leq \frac{7}{5} \tag{4.6}$$

If for a particular measurement point, the ratio of V/I is smaller than 0.7134 or larger than 1.4, a harmonic resonance may exist.

(3) 7-th and 11-th harmonics

For 7-th and 11-th harmonics, ideally, the ratio of Z_{7th} / Z_{11th} should be

$$\frac{7}{11} \leq \left(\frac{Z_{7th}}{Z_{11th}} \right) \leq \frac{11}{7} \tag{4.7}$$

If for a particular measurement point, the ratio of V/I is smaller than 0.636 or larger than 1.571, a harmonic resonance may exist.

Table 4.4 and 4.5 gives a sample calculation on the detection of harmonic resonance. The data listed in table 4.4 and 4.5 is measured from a 345kV bus. From table 4.4 and 4.5, a parallel resonance may happen at the 5-th harmonic, and a series resonance may occur at the 7-th harmonic.

Table 4.4 Measured Harmonic Data of a 345kV Bus on Feb 8th 2008

	5-th	7-th	11-th
Phase A Current	0.47	1.41	0.31
Phase A Voltage	1.77	0.34	0.30
Phase B Current	0.30	1.31	0.26
Phase B Voltage	1.29	0.39	0.33
Phase C Current	0.23	1.28	0.48
Phase C Voltage	1.96	0.13	0.28

Table 4.5 Calculated V/I Ratio

	5-th	7-th	11-th
Phase A Voltage/Current Ratio	3.761	0.24	0.97
Phase B Voltage/Current Ratio	4.311	0.29	1.27
Phase C Voltage/Current Ratio	8.522	0.11	0.58

4.4 Subsystem Extraction

4.4.1 Why Perform Subsystem Extraction

Generally speaking, harmonic problems are localized issues. For a typical power system, the impedance matrix is dominated by series inductive or shunt capacitive. Harmonic signals are attenuated very fast if there is no harmonic resonance involved [29-30]. In a field test [31], the attenuation is so considerable that reliable measurements 30-50 km away from the harmonic source are impossible at the 11-th harmonic.

In high-voltage transmission systems, normally, there could not have too many large harmonic pollution contributors injecting three-phase balanced harmonic currents into the system. Besides, utility engineers have good knowledge and experiences on the studied system. With the help of utility engineers, several sub-transmission networks can be properly extracted from the whole transmission system to simplify the calculation.

Subsystem extraction can simplify the harmonic source identification problem. If the subsystem can be properly exacted from the whole transmission system, the harmonic source outside of this subsystem will have limited or negligible effect on harmonic measurements of the

internal buses. Without loss of generalization, in this research, it is assumed that there is only one harmonic source in each extracted subsystem.

4.4.2 Procedures for Subsystem Extraction

In order to simplify the complexity of harmonic sources identification problems, several sub-transmission networks were extracted from the original system. To build a sub-transmission network, a properly chosen bus is needed to be selected as the center-point bus. The main suspect of major harmonic source producer is selected as the central point of the sub-transmission system. This selection process relies upon the expertise of electric utility engineers. In this research work, a bus whose harmonic voltage THD exceeds the limit of IEEE recommended standard is chosen as the central point of sub-transmission system.

Using the selected central point bus as a starting point, five to seven layers of buses are extracted from the original transmission system to form a sub-transmission network. The reason of extracting only five to seven layers of buses is due to the geographic topology of the original transmission network. By studying the geographic topology of the example high voltage transmission system, it can be observed that by extracting five to seven layers of buses, the boundary buses are 50~70 km away from the central point bus. In that case, the harmonic sources outside the extracted sub-network system could have negligible or no effects on harmonic measurements inside the extracted sub-network. The flow chart of the sub-network extraction procedure is illustrated in figure 4.3.

In order to obtain better identification results, the driving-point impedance of the tie lines connecting the extracted sub-transmission network with the outside network should also be calculated. A power system simulation software package PSS/E Version 30.1 [32] is employed in this process. The calculation steps are listed as follows. [33]

a) Import the complete transmission system raw data into PSS/E.

b) Solve the power-flow problems using PSS/E.

c) Store the solved case as the initial condition for short circuit analysis.

d) Input the phase-sequence impedances of the studied transmission system.

e) Apply a three-phase fault to a tie line and then calculate the driving-point impedance.

f) Repeat step (e) until all tie lines have been calculated.

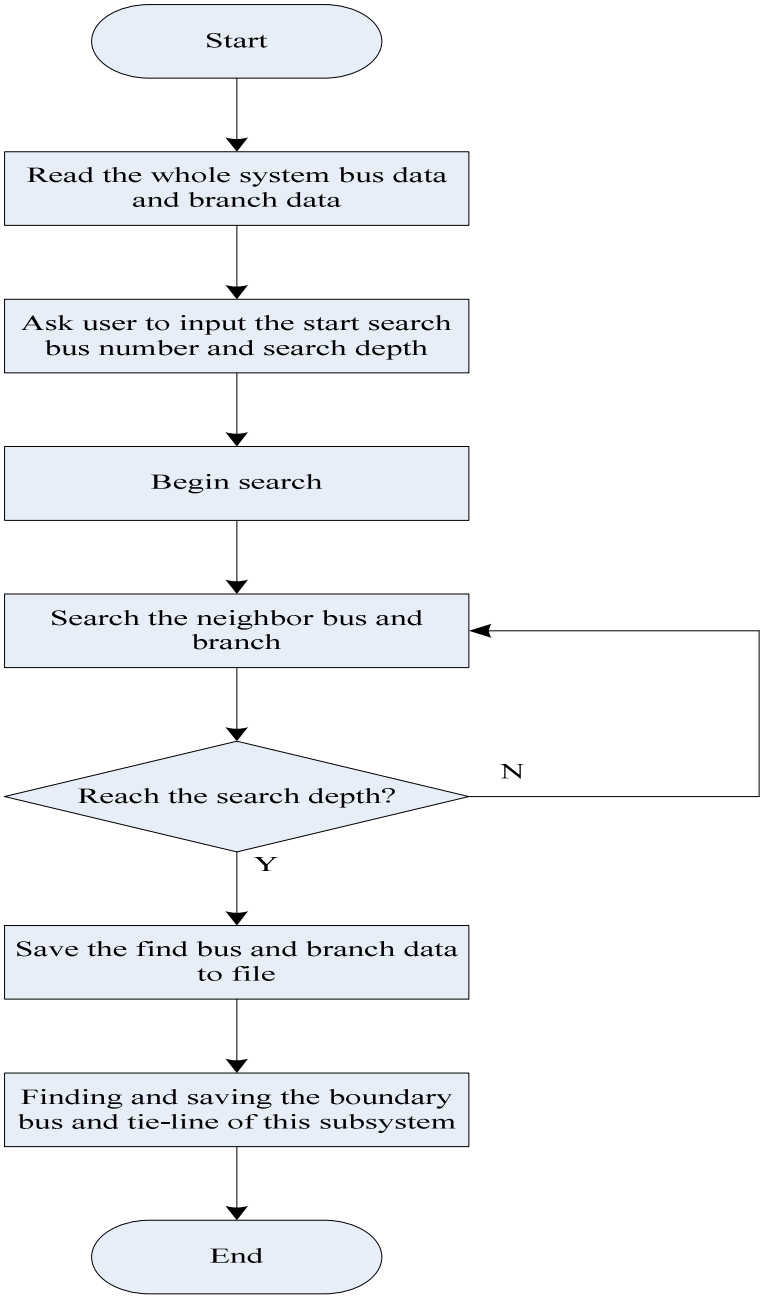

Figure 4.4 Flow Chart of Sub-system Extracting Process

4.5 Harmonic Source Identification Algorithm

Assume a sub-transmission network is already extracted from the original transmission network and only one three-phase balanced major harmonic source exists in this extracted network. Because the information of harmonic sources can not be known, the harmonic currents that the harmonic source injected into the studied power system can also be mysterious. However, we do know that, by harmonic-signal propagation, harmonic currents can lead to harmonic voltages at different buses. The harmonic measurement locations in an extracted sub network are illustrated in figure 4.4. Based on harmonic voltage measurements at different locations, a new method is proposed in this section to identify the possible harmonic sources.

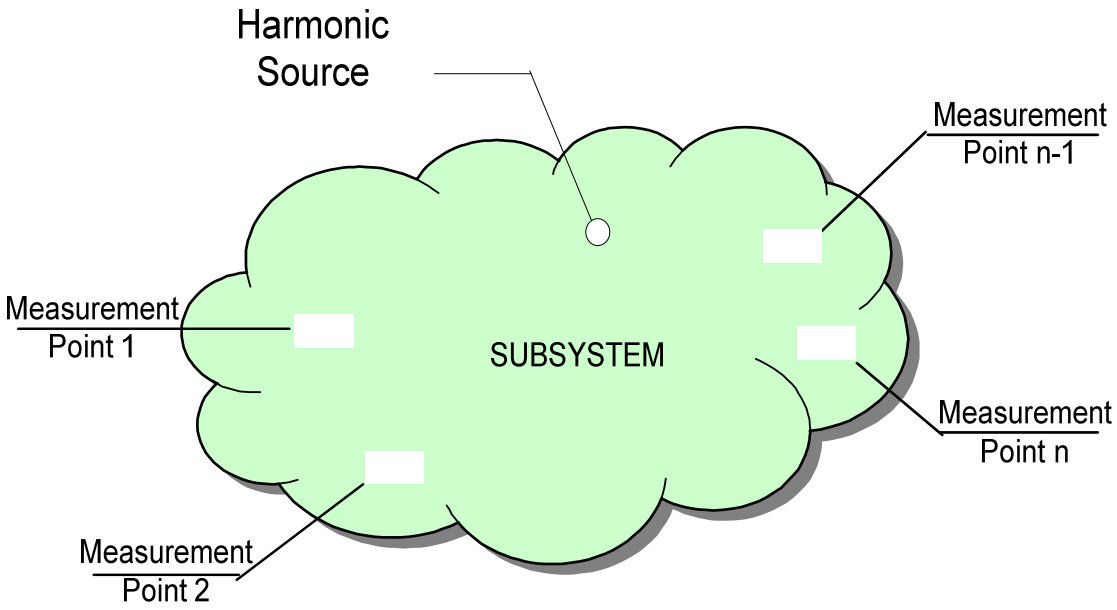

Figure 4.5 Illustration for Measurements of a Harmonic Source

Here, a two step harmonic source identification method is proposed.

Step 1: Preliminary Identification

A transmission subsystem can be extracted after subsystem extraction procedure, A triangularization method is employed to create a harmonic source suspect bus list.

Step 2: Refine Preliminary Results

Once the suspect list is created, more measurements should be taken at the vicinity of the suspect buses. Then, the least square error method can be employed to refine the preliminary identification results.

4.5.1 Preliminary Identification: Triangularization Method

Let V_{bus}^{h} and I_{bus}^{h} represent the bus voltages (referred to ground) and bus injection currents at harmonic number *h* for an *n* bus power system. The admittance matrix of the network at harmonic number *h* is shown below:

$$Y_h = \begin{bmatrix} Y_{11} & Y_{12} & \Lambda & Y_{1i} & \Lambda & Y_{1k} & \Lambda & Y_{1n} \\ Y_{21} & Y_{22} & \Lambda & Y_{1i} & \Lambda & Y_{2k} & \Lambda & Y_{2n} \\ \mathrm{M} & \mathrm{M} & \mathrm{O} & \mathrm{M} & \mathrm{O} & \mathrm{M} & \mathrm{O} & \mathrm{M} \\ Y_{i1} & Y_{i2} & \Lambda & Y_{ii} & \Lambda & Y_{ik} & \Lambda & Y_{in} \\ \mathrm{M} & \mathrm{M} & \mathrm{O} & \mathrm{M} & \mathrm{O} & \mathrm{M} & \mathrm{O} & \mathrm{M} \\ Y_{k1} & Y_{k2} & & Y_{ki} & & Y_{kk} & & Y_{kn} \\ \mathrm{M} & \mathrm{M} & \mathrm{O} & \mathrm{M} & \mathrm{O} & \mathrm{M} & \mathrm{O} & \mathrm{M} \\ Y_{n1} & Y_{n2} & \Lambda & Y_{ni} & \Lambda & Y_{nk} & \Lambda & Y_{nn} \end{bmatrix} \tag{4.8}$$

Where Y_{ki} is the mutual admittance between bus *k* and bus *i*, and Y_{ii} is the self admittance of bus *i* at harmonic number *h*.

The system harmonic current injection can be calculated through direct solution of the linear equation:

$$I_{bus}^{h} = Y_h \cdot V_{bus}^{h} \tag{4.9}$$

or

$$V_{bus}^{h} = Z_h \cdot I_{bus}^{h} \tag{4.10}$$

where $Z_h = \left(Y_h\right)^{-1}$, the system harmonic impedance matrix at harmonic *h* .

Rewriting equation 4.10, we can obtain,

$$\begin{bmatrix} V_1^h \\ \mathrm{M} \\ V_i^h \\ \mathrm{M} \\ V_k^h \\ \mathrm{M} \\ V_n^h \end{bmatrix} = \begin{bmatrix} Z_{11}^h & \Lambda & Z_{1i}^h & \Lambda & Z_{1k}^h & \Lambda & Z_{1n}^h \\ \mathrm{M} & \mathrm{O} & \mathrm{M} & \mathrm{O} & \mathrm{M} & \mathrm{O} & \mathrm{M} \\ Z_{i1}^h & \Lambda & Z_{ii}^h & \Lambda & Z_{ik}^h & \Lambda & Z_{in}^h \\ \mathrm{M} & \mathrm{O} & \mathrm{M} & \mathrm{O} & \mathrm{M} & \mathrm{O} & \mathrm{M} \\ Z_{k1}^h & \Lambda & Z_{ki}^h & \Lambda & Z_{kk}^h & \Lambda & Z_{kn}^h \\ \mathrm{M} & \mathrm{O} & \mathrm{M} & \mathrm{O} & \mathrm{M} & \mathrm{O} & \mathrm{M} \\ Z_{n1}^h & \Lambda & Z_{ni}^h & \Lambda & Z_{nk}^h & \Lambda & Z_{nn}^h \end{bmatrix} \begin{bmatrix} I_1^h \\ \mathrm{M} \\ I_i^h \\ \mathrm{M} \\ I_k^h \\ \mathrm{M} \\ I_n^h \end{bmatrix} \tag{4.11}$$

where:

V_i^h = the bus *i* voltages (referred to ground) at harmonic *h*

I_i^h = bus *i* injection currents at harmonic *h*

From equation 4.11,

$$\begin{aligned} &\Lambda \\ &V_i^h = Z_{i1}^h \cdot I_1^h + \Lambda + Z_{ii}^h \cdot I_i^h + \Lambda + Z_{ik}^h \cdot I_k^h + \Lambda + Z_{in}^h \cdot I_n^h \\ &\Lambda \\ &V_k^h = Z_{k1}^h \cdot I_1^h + \Lambda + Z_{ki}^h \cdot I_i^h + \Lambda + Z_{kk}^h \cdot I_k^h + \Lambda + Z_{kn}^h \cdot I_n^h \\ &\Lambda \end{aligned} \tag{4.12}$$

Assume there is only one major harmonic source exists in this extracted n-bus power system, and it is located at bus *m* (1≤*m*≤*n*). In other words, the harmonic current injection at bus *m* is much higher than other buses, i.e.

$$\begin{aligned} &I_i^h = 0, \quad 1 \le i \le n, \quad i \ne m \\ &I_m^h > 0 \end{aligned} \tag{4.13}$$

From equation 4.12 and equation 4.13, the following equation can be derived,

$$\frac{V_i^h}{V_k^h} = \frac{Z_{i1}^h \cdot I_1^h + \Lambda + Z_{ii}^h \cdot I_i^h + Z_{im}^h \cdot I_m^h + \Lambda + Z_{ik}^h \cdot I_k^h + \Lambda + Z_{in}^h \cdot I_n^h}{Z_{k1}^h \cdot I_1^h + \Lambda + Z_{ki}^h \cdot I_i^h + Z_{km}^h \cdot I_m^h + \Lambda + Z_{kk}^h \cdot I_k^h + \Lambda + Z_{kn}^h \cdot I_n^h} = \frac{Z_{im}^h \cdot I_m^h}{Z_{km}^h \cdot I_m^h}$$

$$\Rightarrow \frac{\left|V_i^h\right|}{\left|V_k^h\right|} = \frac{\left|Z_{im}^h\right|}{\left|Z_{km}^h\right|} \tag{4.14}$$

Equation 4.14 gives a good indicator for identifying single harmonic source in an n-bus power system. The possible candidates of the harmonic current injection sources can be identified if at least two bus harmonic voltages can be measured, and compared with the elements in equation 4.14.

According to equation 4.14 of the proposed algorithm, the harmonic voltage of at least two buses and the harmonic impedance matrix of the sub-system are required. Then, by comparing the ratio of $\left|V_i^h / V_k^h\right|$ and each ratio of $\left|Z_{im}^h / Z_{km}^h\right|$, the possible candidate of harmonic sources will be known. The whole process is described as follows.

Step 1:

Obtain the harmonic voltage of measurement points.

Step 2:

Calculate the ratio of $\left|V_i^h / V_k^h\right|$.

Step 3:

Calculate the harmonic impedance matrix at each order of harmonic.

Step 4:

Calculate the deviation of $\left|V_i^h / V_k^h\right| - \left|Z_{im}^h / Z_{km}^h\right|$. In order to show how close these two values are, the positive mean value and negative mean value are used. If the deviation falls into the area between positive mean value and negative mean value, then these two ratios are close. That bus will be marked as a possible candidate bus.

Step 5:

Repeat the above process until every bus is calculated. Then a suspect list can be generated.

4.5.2 Refine Preliminary Results: Least-Square Error Method

Once potential locations of harmonic source are identified, additional measurements can be taken at the vicinity of the suspect buses. Also, by using $V = ZI$, harmonic voltage at

each bus can be calculated. Ideally, if the suspect source is really the harmonic source bus, the calculated harmonic voltage should be equal to the actually measured harmonic voltage. In the presence of measurement noise, these two values may not be equal, but for each bus, the $\left(V_{mea} - V_{cal}\right)^2$ calculation should be minimal. Based on this theory, for each measured bus, $\left(V_{mea} - V_{cal}\right)^2$ can be calculated, and sum least-square error together. The bus that has the minimum least-square error sum is most likely to be the real harmonic source bus.

The calculation procedure for the least-square error method is listed as follows:

Step 1:

Choose a harmonic bus from the harmonic source suspect list. For instance, suppose there is a total of 300 buses in a subsystem, and 20 buses are marked as suspect buses, we can randomly choose one bus from that 20 suspect bus list.

Step 2:

For the selected suspect harmonic source bus, randomly give an initial bus injection current for the calculation process.

Using $V = ZI$, calculate the harmonic voltage at all harmonic voltage measure points.

Step 3:

Calculate the Least-square Error objective function of

$$\left(V_{1\_mea} - V_{1\_cal}\right)^2 + \left(V_{2\_mea} - V_{2\_cal}\right)^2 + \Lambda + \left(V_{N\_mea} - V_{N\_cal}\right)^2 \qquad (4.15)$$

where:

V_{N_mea} is the measurement value of the harmonic voltage at N-th measurement point, and,

V_{N_cal} is the calculated harmonic voltage at the N-th measurement point

Step 4:

Change the initial bus injection currents and repeat step 2 and step 3, until the objective function reaches its minimum value. Afterward, store this minimum value.

Step 5:

Repeat step 1 to 4 until every harmonic suspect is calculated.

Step 6:

Compare every stored objective function values. The bus that has minimum value is more likely to have a harmonic current injection source.

4.6 Model Representation of Transmission Network Elements

According to the above analysis, one task in the harmonic source identification process is to build the system harmonic frequency admittance matrices at each frequency of interest. In this task, the main difficulties are to determine which model best represents the various system components at each harmonic frequency and to obtain the appropriate parameters for them. With this information available, the admittance matrix of each harmonic order of our interest can be calculated.

4.6.1 Passive Elements

The following passive elements are considered to linearly vary with frequency changes. In terms of harmonic orders, the corresponding impedances of the inductors and capacitors are given in equation 4.16 and equation 4.17, where X_L and X_C are values at the fundamental frequency (60Hz). The resistance is assumed to be independent of frequency changes (i.e. the skin effect is ignored).

$$X_L^h = X_L \cdot h \tag{4.16}$$

$$X_C^h = \frac{X_C}{h} \tag{4.17}$$

4.6.2 Transmission Lines and Shunt Elements

Overhead lines and cables are modeled using multiple nominal sections, connected in series. According to [34], an error of less than 1.2% is achieved using three nominal sections for each line segment whose length is equal to 1/4 of the wavelength (1250 km at 60 Hz). Since in this study, the analysis is mainly focus on to the 5-th, 7-th and 11-th harmonic orders (1/4

wavelength = 250 km at 300 Hz, 1/4 wavelength = 179 km at 420 Hz, 1/4 wavelength = 113 km at 660 Hz), satisfactory results can be obtained by using one section for overhead lines and cables.

The harmonic impedance of a shunt capacitor is determined by equation 4.18.

$$X_C^h = \frac{V_L^2}{hQ_C} \tag{4.18}$$

Where V_L is the bus voltage in per unit. Q_C is the rated reactive power of the capacitor bank at the fundamental frequency.

4.6.3 Transformers

In the positive and negative sequence, transformers are modeled by their series harmonic impedance, which is illustrated in equation 4.19.

$$Z_T^h = R_T\left(C_0 + C_1 \cdot h^b + C_2 \cdot h^2\right) + j \cdot X_T \cdot h \tag{4.19}$$

In equation 4.19, R_T and X_T are the resistance and impedance of the transformer at the fundamental frequency (60Hz). Values for the parameters of equation 4.19 are given in [37], and summarized in table 4.6.

Table 4.6 Parameters Values for Transformer Model

	C_0	C_1	C_2	b
Small T/F	0.85~0.90	0.05~0.08	0.05~0.08	0.9~1.4
Large T/F	0.75~0.80	0.10~0.13	0.10~0.13	0.9~1.4

Note: C_0, C_1 and C_2 under the constraint $C_0 + C_1 + C_2 = 1$

4.6.4 System Load

In power systems, there are basically three types of loads: passive, motive, and power electronic. In practice, there is always a mix of three types of load, and therefore, no generally acceptable load equivalents for harmonics analysis. The derivation of accurate conductance and susceptance harmonic bandwidths from specified P (active) and Q (reactive) will need extra

information on the actual composition of the load. However, in this research work, it is infeasible to measure the accuracy of the harmonic conductance and susceptance on each load in the bulk power system. Without losing generality, some mathematical representation will be used to model the loads of the power system [34]–[38]. Three types of commonly used models are listed as follows.

Model 1

Predominantly passive loads can be represented approximately by series R and X impedance, i.e.

$$Z_{load}(\omega) = R_{load} \cdot \sqrt{h} + j \cdot X_{load} \cdot h \tag{4.20}$$

Where R_{load} is the load resistance at the fundamental frequency, X_{load} is the load reactance at the fundamental frequency, h is the harmonic order, and $\sqrt{h}$ is the weighting coefficient of harmonic numbers.

Model 2

The weighting coefficient of harmonic numbers, used in equation 4.20 depends upon the resistance component. They can be different in different models. For instance, reference [39] uses a factor of $0.6\sqrt{h}$ instead, i.e.

$$Z_{load}(\omega) = R_{load} \cdot 0.6 \cdot \sqrt{h} + j \cdot X_{load} \cdot h \tag{4.21}$$

Model 3

In studies concerning mainly the transmission network, the loads are usually equivalent parts of the distribution network, specified by the consumption of active and reactive power. A parallel model can be used, i.e.

$$R_{load} = \frac{V^2}{(0.1h + 0.9)P} \tag{4.22}$$

$$X_{load} = \frac{V^2}{(0.1h + 0.9)Q} \tag{4.23}$$

Where R_{load} is the load resistance at the fundamental frequency, X_{load} is the load reactance at the fundamental frequency. P and Q are the fundamental frequency active power and reactive power, and *h* is the harmonic order.

4.6.5 Generators

For the purpose of determining the network harmonic admittances, the generators are normally modeled as a series combination of resistance and inductive reactance, i.e.

$$Y_g^h = \frac{1}{R\sqrt{h} + j \cdot X_d^{''} \cdot h} \tag{4.24}$$

Where *R* is derived from the machine power loss at the fundamental frequency, $X_d^{''}$ is the generator sub-transient reactance at the fundamental frequency, and *h* is the harmonic order.

CHAPTER 5

NUMERICAL SIMULATION AND INTEGRATED SOFTWARE PACKAGE

5.1 Introduction of IEEE 300-Bus Test System

In this chapter, in order to verify the proposed harmonic source identification method, numerical simulations are carried out on the IEEE 300-bus test system. The IEEE 300-bus test case, which is a benchmark system for transmission-network studies, was developed by the IEEE Test Systems Task Force under the direction of Mike Adibi in 1993. The IEEE 300-bus test system is used in this dissertation to test the proposed method. Please refer to [40] for detailed information about IEEE 300-bus test system.

5.2 Preliminary Identification Process

5.2.1 Settings of Harmonic Sources

In this dissertation, the IEEE 300-bus test system and non-linear harmonic injection sources are modeled by using the harmonic analysis software named ‘PCFLOH” (courtesy of Dr. Mack Grady, UT Austin [41]). According to the harmonic information recorded in the real transmission network, the harmonic sources listed from table 5.1 to table 5.3 are chosen for the numerical simulation. Among various harmonic sources, only the 6-pulse power converters injecting three-phase balanced harmonic currents into each subsystem are assumed. The objective of this numerical simulation is to identify the possible location of this 6-pulse balanced harmonic current source. Single-phase power converters that inject three-phase unbalanced harmonic currents into the system are used to simulate the unbalanced harmonic sources in the studied system. The parameters and power ratings of different harmonic sources are listed from table 5.1 to table 5.3.

Table 5.1 Characteristics of the Simulated Harmonic Sources for Sub-system 1

Harmonic Source No.	1	2	3
Bus No.	27	87	9
Type of Harmonic Source	6-pulse current injection source	Single-phase electronic GY-GY	Single-phase electronic Δ-GY
Magnitude (pu)	0.12	0.03	0.02
Power Factor (lagging)	0.85	0.9	0.9

Table 5.2 Characteristics of the Simulated Harmonic Sources for Sub-system 2

Harmonic Source No.	1	2	3
Bus No.	135	128	174
Type of Harmonic Source	6-pulse current injection source	Single-phase electronic GY-GY	Single-phase electronic Δ-GY
Magnitude (pu)	0.10	0.02	0.02
Power Factor (lagging)	0.85	0.9	0.9

Table 5.3 Characteristics of the Simulated Harmonic Sources for Sub-system 3

Harmonic Source No.	1	2	3
Bus No.	235	246	189
Type of Harmonic Source	6-pulse current injection source	Single-phase electronic GY-GY	Single-phase electronic Δ-GY
Magnitude (pu)	0.08	0.02	0.01
Power Factor (lagging)	0.85	0.9	0.9

5.2.2 Sub-Transmission Network Extraction

In order to simplify the complexity of the harmonic sources identification process, the sub-transmission networks are extracted from the original 300-bus test system. To build a sub-transmission system, a bus is needed to be properly chosen as the center-point bus. The main suspect of major harmonic source producer is selected as the central point of the sub-transmission system. In an actual power system, this selection process needs to rely upon the expertise of utility engineers. Using this as a starting point, five layers of buses are extracted from the original transmission system to form a sub-transmission network. The reason for extracting only 5 layers of buses is due to the geographic topology of the IEEE 300-bus system. The flow chart of the proposed sub-network extraction process is illustrated in figure 5.1.

In order to obtain better identification results, the driving-point impedance of the tie lines between the extracted sub-transmission network and the outside network should also be calculated. The calculation process follows the driving-point impedance calculation steps listed in section 4.4.2.

Using the above steps, three sub-transmission networks are extracted from the test system. It should be pointed out that the extracted sub-transmission networks are different from the subsystems that are originally divided from the IEEE 300-bus system.

5.2.3 Placement of Meters

Since only a limited number of harmonic measurement devices are available in the actual power system, the measurement points of harmonic voltages are restricted to 12 buses in the numerical simulation. In each extracted sub-transmission network, four buses are randomly selected as the measurement buses. The detailed information on locating these meters is shown in figure 5.2.

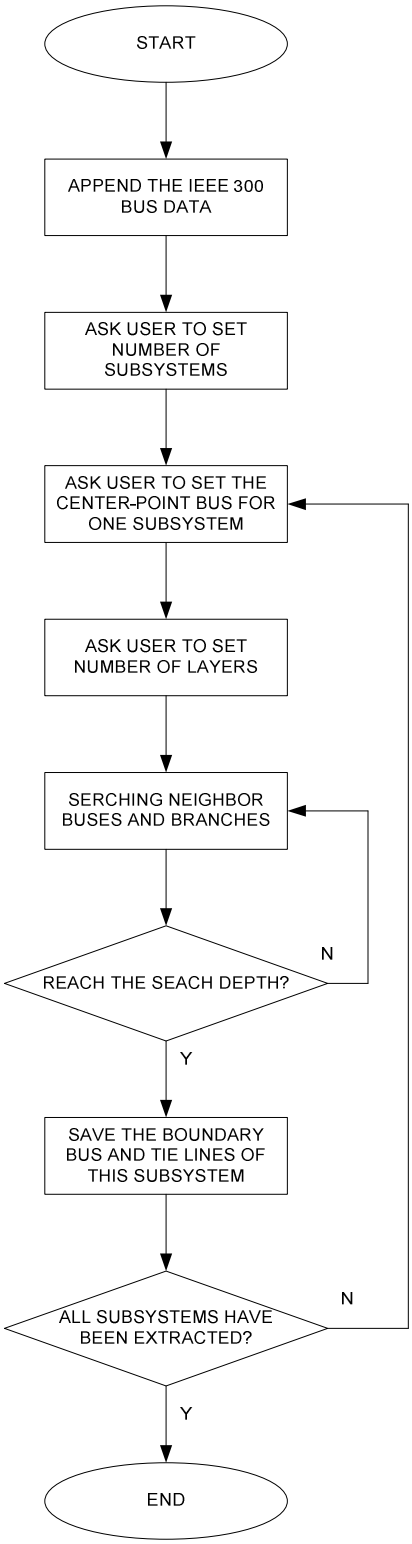

Figure 5.1 Flow chart of subsystem extracting process for IEEE 300-bus test system

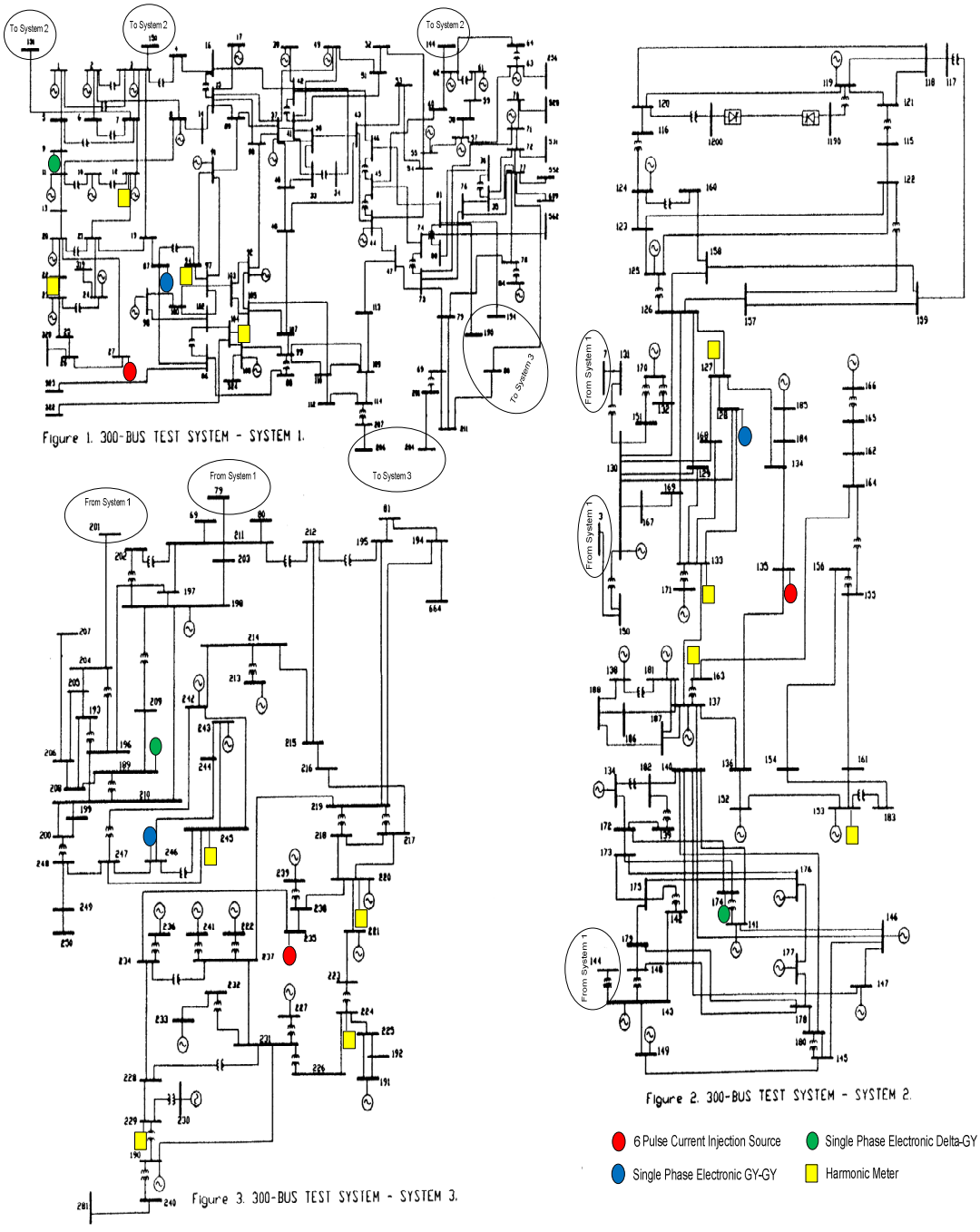

Figure 5.2 IEEE 300-bus test system with measurement meters

5.2.4 Identification Procedure

After the sub-transmission networks are extracted and the harmonic-voltage measurements are available, equation 4.14 can be employed to identify possible harmonic

sources. By comparing the value of $\left|V_i^{(k)} / V_k^{(k)}\right|$ to each value of $\left|Z_{im}^{(h)} / Z_{km}^{(h)}\right|$, the possible harmonic sources can be identified.

In building the impedance matrix at each harmonic order, the system load model should be included in the calculation process. However, in practice, there is no generally acceptable load equivalent for harmonics analysis, as stated in chapter 4. Therefore, three different harmonic load models described in section 4.6.4 are employed in the simulation process separately to test the validity of the proposed method. The identification process is described as follows.

Step 1: Read the harmonic voltages at each measurement point.

Step 2: Calculate of harmonic phase-sequence voltages, and get rid of the unbalanced harmonic components generated by the unbalanced sources.

Step 3: Calculate $|V_i^{(k)} / V_k^{(k)}|$. Because there are four harmonic-voltage measurement points in each extracted sub-network, only the ratios of the six harmonic voltages need to be calculated. In the numerical simulation cases, only the 5-th, 7-th and 11-th harmonic voltages are required.

Step 4: Import the raw data of the IEEE 300-bus system. Choose one system load model, and calculate the harmonic impedance matrix.

Step 5: Check whether $|V_i^{(k)} / V_k^{(k)}|$ and $|Z_{im}^{(k)} / Z_{km}^{(k)}|$ are close. Equation 5.1 is used to calculate the mismatch value.

$$\| V_i^{(k)} / V_k^{(k)} | - | Z_{im}^{(k)} / Z_{km}^{(k)} \| \tag{5.1}$$

where $Z_{im}^{(h)}$ and $Z_{km}^{(h)}$ are obtained from the harmonic impedance matrix, *m* is the bus number, and *i* and *k* are the bus numbers of the harmonic-voltage measurements.

Step 6: Sum all the mismatch values for all harmonic orders and check which bus has the smallest summed mismatch value. The possible candidates for the major harmonic source in the studied system can be identified.

Step 7: Repeat the whole process from step 4. Choose another system load model, until the all three load models are employed.

5.2.5 Preliminary Identification Simulations Results

Three numerical simulation cases are carried out to examine the effectiveness of the proposed method. The condition of each simulation case is the same except that the system load model is different. In order to test the robustness of the proposed algorithm in the presence of measurement noises, a measurement noise with zero-mean normal distribution of 3% standard deviation is added to the voltage measurement data in each case.

The simulation results of the three cases are listed from tables 5.4 to tables 5.12, respectively. In each table, only the five buses with the smallest summed mismatch values are listed. The listed buses are regarded as the suspect buses that contain harmonic sources. It can be observed from each table that buses 27, 135, and 235 have the smallest mismatch values and can be clearly identified as the suspect buses with the major balanced harmonic injection sources. The following tables show the effectiveness of the proposed approach.

Table 5.4 Calculated Mismatch Values of the Simulation Case with System Load Model 1 for Sub-Transmission Network 1

No.	Bus No.	Mismatch Value
1	27	6.13×10^{-4}
2	19	8.78×10^{-4}
3	21	2.12×10^{-3}
4	24	3.56×10^{-3}
5	90	4.98×10^{-3}

Table 5.5 Calculated Mismatch Values of the Simulation Case with System Load Model 1 for Sub-Transmission Network 2

No.	Bus No.	Mismatch Value
1	135	7.36×10^{-4}
2	154	1.95×10^{-3}
3	137	4.07×10^{-3}
4	152	5.15×10^{-3}
5	161	7.73×10^{-3}

Table 5.6 Calculated Mismatch Values of the Simulation Case with System Load Model 1 for Sub-Transmission Network 3

No.	Bus No.	Mismatch Value
1	235	5.54×10^{-5}
2	220	2.23×10^{-4}
3	223	4.76×10^{-4}
4	219	5.98×10^{-4}
5	239	7.12×10^{-4}

Table 5.7 Calculated mismatch values of the simulation case with system load model 2 for Sub-Transmission Network 1

No.	Bus No.	Mismatch Value
1	27	5.02×10^{-3}
2	20	8.64×10^{-3}
3	319	2.47×10^{-2}
4	90	2.89×10^{-2}
5	320	5.42×10^{-2}

Table 5.8 Calculated mismatch values of the simulation case with system load model 2 for Sub-Transmission Network 2

No.	Bus No.	Mismatch Value
1	135	8.19×10^{-3}
2	184	1.75×10^{-2}
3	137	3.67×10^{-2}
4	153	7.69×10^{-2}
5	152	8.97×10^{-2}

Table 5.9 Calculated mismatch values of the simulation case with system load model 2 for Sub-Transmission Network 3

No.	Bus No.	Mismatch Value
1	235	3.07×10^{-2}
2	237	6.89×10^{-2}
3	220	1.93×10^{-1}
4	234	3.52×10^{-1}
5	236	4.55×10^{-1}

Table 5.10 Calculated Mismatch Values of the Simulation Case with System Load Model 3 for Sub-Transmission Network 1

No.	Bus No.	Mismatch Value
1	27	7.34×10^{-4}
2	19	8.21×10^{-4}
3	21	1.45×10^{-3}
4	24	5.76×10^{-3}
5	90	8.87×10^{-4}

Table 5.11 Calculated Mismatch Values of the Simulation Case with System Load Model 3 for Sub-Transmission Network 2

No.	Bus No.	Mismatch Value
1	135	9.45×10^{-4}
2	154	3.21×10^{-3}
3	137	5.17×10^{-3}
4	152	6.25×10^{-3}
5	161	9.03×10^{-3}

Table 5.12 Calculated Mismatch Values of the Simulation Case with System Load Model 3 for Sub-Transmission Network 3

No.	Bus No.	Mismatch Value
1	235	8.54×10^{-5}
2	220	3.20×10^{-4}
3	223	4.16×10^{-4}
4	219	7.09×10^{-4}
5	239	9.04×10^{-4}

5.3 Refine Preliminary Results

After the list of harmonic source suspect buses is already obtained from the preliminary identification process, the next step is to refine the preliminary results. Additional measurements should be taken at the vicinity of the suspect buses. By using $V = ZI$, harmonic voltage at each bus can be calculated. Ideally, if a suspect source is really the harmonic injection source bus, the calculated harmonic voltage should be equal to the actual measured harmonic voltage. In the presence of measurement noise, these two values may not be equal, but for each bus, the $(V_{mea} - V_{cal})^2$ should be minimum. Based on this, for each measured bus, $(V_{mea} - V_{cal})^2$ can be calculated, and sum the least square error together. The bus that has minimum least square error sum is more likely to be the real harmonic source bus. The calculation procedure for the least-square error method follows the steps listed in section 4.5.2.

Three numerical simulation cases were carried out to examine the effectiveness of the least square error method. In each simulation case, 12 buses, which are in the vicinity of primary harmonic source suspect, are chosen as harmonic measurement points. The measurement points are illustrated in figure 5.3 and also listed from table 5.13 to table 5.15.

The conditions of each simulation case are the same except that the system load model is different. In order to test the robustness of the proposed algorithm in the presence of measurement noises, measurement noise of zero-mean normal distribution with 3% standard deviation is added to the voltage measurement data.

Table 5.13 Harmonic Measurement Points Arrangement for the Least Square Method Test for Sub-Transmission Network 1

No.	Bus No.
1	19
2	20
3	24
4	220

Table 5.14 Harmonic Measurement Points Arrangement for the Least Square Method Test for Sub-Transmission Network 2

No.	Bus No.
1	134
2	140
3	152
4	154

Table 5.15 Harmonic Measurement Points Arrangement for the Least Square Method Test for Sub-Transmission Network 3

No.	Bus No.
1	217
2	236
3	237
4	239

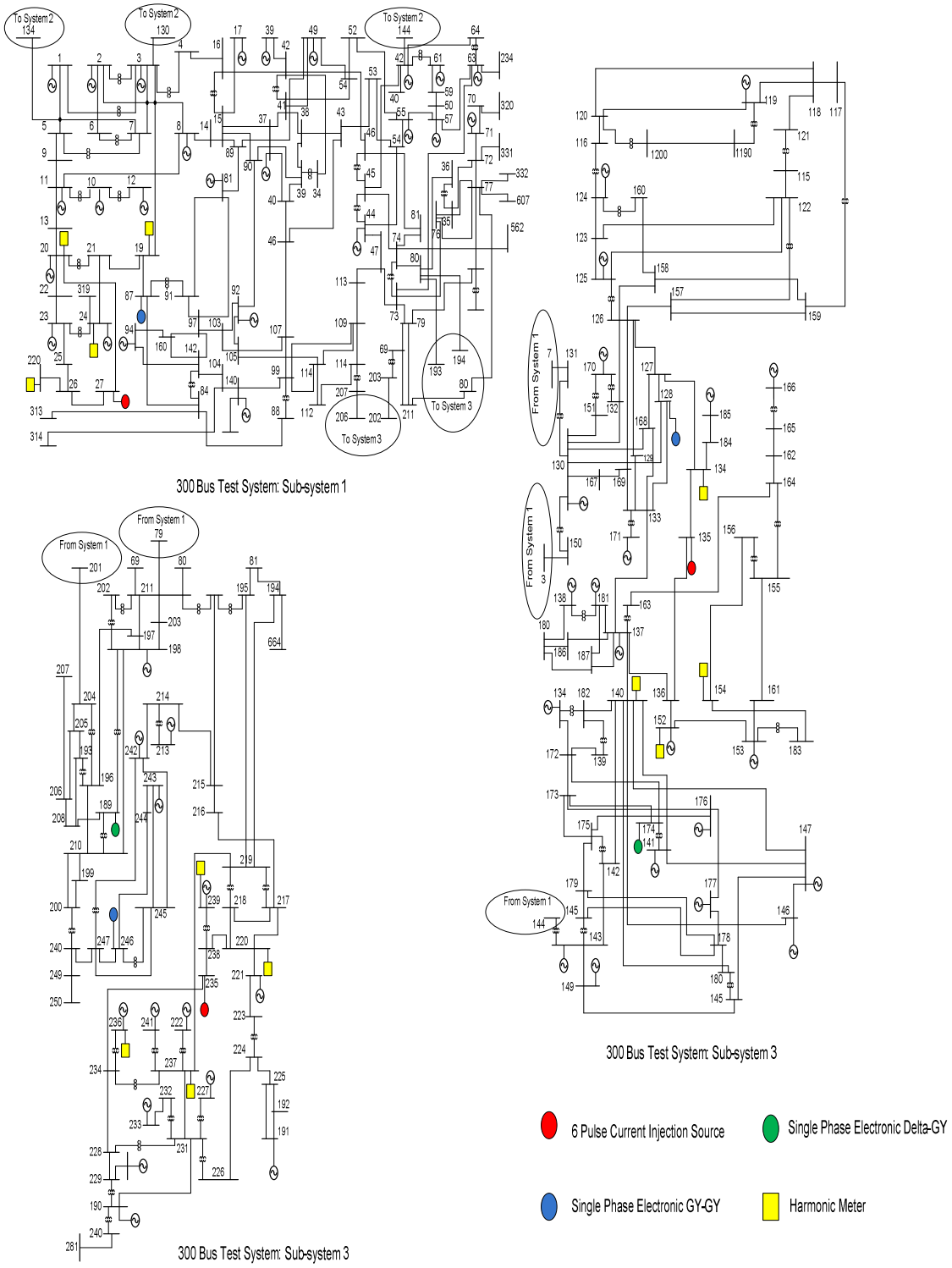

Figure 5.3 Measurement Meters Setup for Least Square Method

The simulation results of the three different cases are listed from tables 5.16 to tables 5.24. In these tables, only five buses which are marked as harmonic suspect buses in the preliminary identification process are listed. It can be observed from these tables that buses 27, 135, and 235 have the smallest values and they can be clearly identified as the suspect buses with the major balanced harmonic injection sources. These tables show the effectiveness of the least square error identification algorithm.

Table 5.16 Calculated Sum of Least Square Error Values with System Load Model 1 for Sub-Transmission Network 1

No.	Bus No.	Mismatch Value
1	27	2.56×10^{-3}
2	19	4.38×10^{-2}
3	21	7.29×10^{-2}
4	24	9.81×10^{-2}
5	90	2.01×10^{-1}

Table 5.17 Calculated Sum of Least Square Error Values with System Load Model 1 for Sub-Transmission Network 2

No.	Bus No.	Mismatch Value
1	135	3.74×10^{-3}
2	154	4.67×10^{-3}
3	137	1.17×10^{-2}
4	152	3.15×10^{-2}
5	161	4.38×10^{-1}

Table 5.18 Calculated Sum of Least Square Error Values with System Load Model 1 for Sub-Transmission Network 3

No.	Bus No.	Mismatch Value
1	235	2.14×10^{-4}
2	220	5.64×10^{-4}
3	223	1.26×10^{-3}
4	219	3.68×10^{-2}
5	239	4.92×10^{-2}

Table 5.19 Calculated Sum of Least Square Error Values with System Load Model 2 for Sub-Transmission Network 1

No.	Bus No.	Mismatch Value
1	27	3.72×10^{-3}
2	20	5.09×10^{-3}
3	319	2.03×10^{-2}
4	90	7.58×10^{-2}
5	320	9.91×10^{-2}

Table 5.20 Calculated Sum of Least Square Error Values with System Load Model 2 for Sub-Transmission Network 2

No.	Bus No.	Mismatch Value
1	135	1.99×10^{-3}
2	184	2.71×10^{-3}
3	137	3.87×10^{-2}
4	153	6.63×10^{-2}
5	152	9.17×10^{-2}

Table 5.21 Calculated Sum of Least Square Error Values with System Load Model 2 for Sub-Transmission Network 3

No.	Bus No.	Mismatch Value
1	235	2.17×10^{-3}
2	237	5.11×10^{-2}
3	220	7.23×10^{-2}
4	234	9.25×10^{-1}
5	236	3.45×10^{-1}

Table 5.22 Calculated sum of least square error values with system load model 3 for Sub-Transmission Network 1

No.	Bus No.	Mismatch Value
1	27	5.23×10^{-2}
2	19	7.81×10^{-2}
3	21	3.77×10^{-1}
4	24	5.91×10^{-1}
5	90	8.78×10^{-1}

Table 5.23 Calculated sum of least square error values with system load model 3 for Sub-Transmission Network 2

No.	Bus No.	Mismatch Value
1	135	2.65×10^{-2}
2	154	3.57×10^{-2}
3	137	7.87×10^{-2}
4	152	2.15×10^{-1}
5	161	4.13×10^{-1}

Table 5.24 Calculated sum of least square error values with system load model 3 for Sub-Transmission Network 3

No.	Bus No.	Mismatch Value
1	235	2.14×10^{-2}
2	220	4.71×10^{-2}
3	223	5.32×10^{-1}
4	219	7.11×10^{-1}
5	239	8.14×10^{-1}

5.4 Integrated Software Package

Based on the proposed harmonic source identification method, an integrated software package was programmed, which is named Harmonic Source Identification Software (HSIS). HSIS performs harmonic source identification for high voltage transmission systems. It reads Microsoft Excel files as prepared input data, and calculates possible harmonic sources. The identified possible harmonic sources are stored in an output file. The flow chart of the whole identification process of HSIS is illustrated in figure 5.4. For detailed information about HSIS, please refer to Appendix B.

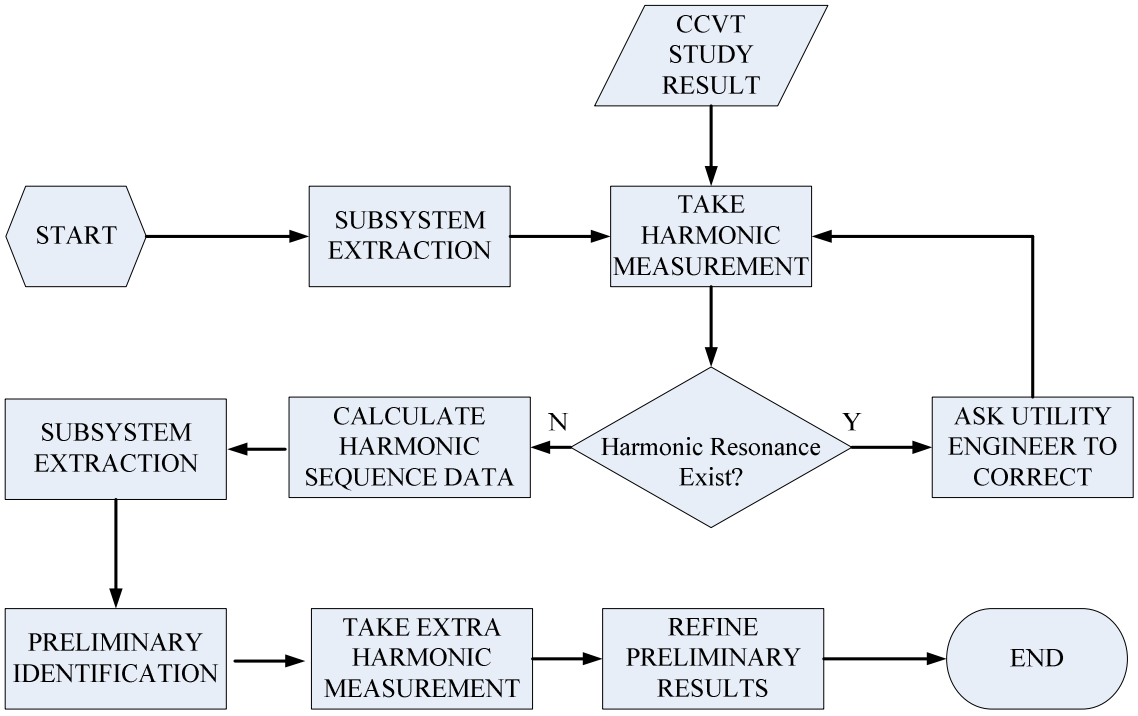

Figure 5.4 Flow chart of harmonic source identification procedure

CHAPTER 6

SUMMARY, CONTRIBUTIONS AND RECOMMENDATIONS

6.1 Summary

Recently, a utility company in Texas observed that harmonic levels on some of its 138 kV, 161kV, and 345 kV transmission systems may exceed the recommended levels of IEEE Std. 519-1992. In order to maintain good power quality within its service territory, it is important to find the harmonic sources and then some correction procedure on harmonic problems can be taken, so that the requirement of IEEE Std. 519-1992 can be met.

Since the harmonic problem in this high voltage transmission system emerged and exceeded the IEEE Std. 519-1992 recommended standard, based on knowledge and experience of engineers of this utility company, two field investigations were conducted. The purpose of these investigations was trying to find the possible harmonic sources in this high voltage transmission system. One field investigation was carried out in the west Texas area, where many wind farms were built at that area in recent years. The other was carried out at a High Voltage Direct Current (HVDC) back-to-back transmission system. Neither of these two field investigations led to conclusive results. Since there is no suitable algorithm that can be utilized for the desired application, a new method is developed to identify the harmonic sources in this high voltage transmission system.

Ensuring data accuracy is the most important step in any computer simulation. In this research work, before applying any harmonic sources identification algorithms, one important task is to verify the accuracy of the harmonic component measurement equipments used in this transmission network. As conventional substation monitoring equipments had already been installed in the sample transmission system, it was decided to take the harmonic measurements based on the existing instruments. The harmonic current waveform is measured through a

Current Transformer (CT). If the bus voltage is below 345-kV, for example 138-kV or 161-kV, a Potential Transformer (PT) is used. For the 345kV system, the voltage waveform is measured through a Coupling Capacitor Voltage Transformer (CCVT). Due to the frequency response and available bandwidth of the measurement devices, measurement errors may exist when measuring different order of harmonic components. Unlike Potential Transformer and Current Transformer, CCVT may cause either errors or distortions when measuring harmonic signals. Therefore, it is necessary to provide adjustments for the measured data by studying the frequency response of the CCVT to obtain true picture of the harmonic voltage signal contents at the primary side.

Frequency-domain studies are conducted on two types of 345kV CCVTs. Since in real world substations from the sample transmission network, there is no GPS unit to synchronize phase measurement, this study effort focuses on harmonic magnitude measurements. In order to validate the digital simulation results, field tests are carried out at two substations in the sample transmission network. In substation 1, the potential transformer was used to measure the harmonic voltage component at a 138kV bus, and a type 1 CCVT was employed to measure the harmonic voltage component of a nearby 345kV bus. In substation 2, the potential transformer was used to measure the harmonic voltage component of a 161kV bus, and a type 2 CCVT was employed to measure the harmonic voltage component of a 345kV bus. Since in both case, the MV bus and HV bus are located in the same substation, the harmonic components should be identical.

From field tests results, one can observe that after adjustment, the measurement result from the PT and CCVT are very close, which indicates that the CCVT frequency study results are suitable for harmonic measurement adjustment.

After the accuracy of measurement instruments is verified, a series of additional harmonic measurement efforts were taken inside of the sample high voltage network. From the

measurement results, the characteristics of harmonics existing in the sample transmission network can be summed up as follows:

- Harmonic levels are time variant.
- The major components of harmonics signals are the 5-th, 7-th, and 11-th harmonics, and the 5-th harmonic signal is the dominant one.
- The measured harmonic voltages are not balanced almost at every measurement points.
- In some parts of the sample high voltage transmission system, the harmonic resonance problems may be present.

According to the observed harmonic characteristics, a new harmonic source identification method is developed in this research work, which is described as follows.

(1) The proposed method first examines whether there is a harmonic resonance within the transmission system. If a harmonic resonance is observed, it will inform the electric utility engineer to deal with the harmonic resonance problem. If no harmonic resonance is reported, the process will continue.

(2) Since the harmonic voltages in the studied transmission system are not balanced, the sequence components calculation will be used to deal with the unbalance harmonic voltages.

(3) In the next step, the subsystem extraction method is employed to simplify the identification process.

(4) Once the sub transmission networks are extracted from the original network, the triangular method is employed to obtain the harmonic source suspect buses list.

(5) After the suspect buses list is generated, additional measurements should be taken in the vicinity of suspect buses. The additional measurement results can be used to refine the preliminary results.

In order to verify the proposed method, the proposed approach was applied to the IEEE 300-bus test system. The results of the simulation cases have shown that the proposed approach can identify the major harmonic sources in power systems when harmonic signals are unbalanced and measurement noises exist.

6.2 Contributions

The major contribution of this research work is that it proposes and develops a novel approach to identify harmonic sources in power systems. Comparing to other methods, the proposed approach only requires very few synchronized measurement points and it can still perform the desired functions even if the harmonic voltages are unbalanced and measurement noises exist. Based on this proposed method, numerical simulations on the IEEE 300-bus system demonstrated the effectiveness of the proposed approach. A harmonic source identification software package was coded according to proposed method, and can be used to identification the harmonic sources in high voltage transmission system.

6.3 Recommendations for Future Studies

For future studies and extension of this work, the author suggests the following:

(1) Conduct further research on power system load models in the presence on harmonics. The dissertation emphasized a simplified model of the high voltage transmission system with the system load components represented by straightforward models. Load buses where distribution systems are connected may need more detailed modeling which could improve accuracy to the overall transmission system analysis.

(2) Use PMU to synchronize harmonic measurement. In this dissertation work, since there is no PMU to synchronize harmonic measurement, only the magnitudes of harmonic voltage are employed to identify the possible harmonic sources. If PMUs are available, the harmonic phase can also be used in the identification process. Therefore, the overall identification accuracy can be improved.

APPENDIX A

MEASURED HARMONIC INFORMATION

A.1 Description of Harmonic Measurement Information

Four different sets of harmonic measurements were taken within the example high voltage transmission system. The detailed information about the measurement efforts is listed in the following tables.

Table A.1 Information of Time and Total Number of Measurement Points

Number	Measurement Time	Number of Measurement Points
1	February 2, 2007	6
2	July 27, 2007	5
3	September 19, 2007	5
4	February 8, 2008	5

It should be pointed out that, as described in chapter 3, if a bus voltage is below 345 kV, for example 138 kV or 161 kV, a Potential Transformer (PT) is used; for the 345 kV system, the voltage is measured through a Coupling Capacitor Voltage Transformer (CCVT). Therefore, if a bus voltage is 138kV or 161kV, the measured harmonic information presented in this dissertation is considered to be the actual value. For a 345 kV system, the measured harmonic information presented in this dissertation is after adjustment of the value by using the CCVT frequency response study results presented in chapter 3.

A.2 Harmonic Information Measured from Feb 2nd 2007 Data

On February 2, 2007, a harmonic measurement effort was carried out at six measurement points. The description of these six measurement points and the detailed information on the harmonic problems at each measurement point are listed in the following tables.

Table A.2 Information of February 2, 2007 Measurement

Number	Bus Name	Bus Voltage (kV)	Sample Rate (second/sample)
1	Bus 1692	138	2.60×10^{-4}
2	Bus 1816	345	3.86×10^{-4}
3	Bus 2461	345	3.86×10^{-4}
4	Bus 1697	138	2.60×10^{-4}
5	Bus 1694	138	2.60×10^{-4}
6	Bus 2373	345	2.60×10^{-4}

Table A.3 Measured Voltage Harmonic Results of Bus 1692 for Phase A. Measurement

Harmonic No.	DFT Peak (V)	DFT RMS (V)	Percent of Fundamental	Angle (Degree)
0	615.171	434.991	0.389	90.000
1	158080	111781	100.000	113.460
2	15.396	10.886	0.010	244.670
3	2021.800	1429.600	1.279	114.950
4	49.837	35.240	0.032	-34.305
5	463.460	327.720	0.293	214.180
6	21.162	14.964	0.013	-58.665
7	138.380	97.848	0.088	45.400
8	27.145	19.194	0.017	266.310
9	29.330	20.739	0.019	264.610
10	4.588	3.244	0.003	223.970
11	69.851	49.392	0.044	138.360
12	11.930	8.436	0.008	120.930
13	49.246	34.822	0.031	-5.765
14	12.567	8.886	0.008	139.550
15	51.785	36.618	0.033	141.050
16	5.973	4.223	0.004	180.000
17	35.368	25.009	0.022	246.460
18	17.180	12.148	0.011	170.340
19	25.354	17.928	0.016	248.860
20	15.686	11.091	0.010	241.100
21	40.656	28.748	0.026	23.432
22	21.152	14.957	0.013	21.513
23	34.842	24.637	0.022	185.860
24	18.256	12.909	0.012	56.049
25	24.365	17.229	0.015	226.130
26	16.861	11.922	0.011	53.218
27	32.058	22.669	0.020	37.800
28	11.145	7.881	0.007	136.320
29	10.887	7.699	0.007	-88.546
30	10.338	7.310	0.007	16.173
31	12.094	8.552	0.389	125.870
THD	1.37%			

Table A.4 Measured Voltage Harmonic Results of Bus 1692 for Phase B. Measurement

Harmonic No.	DFT Peak (V)	DFT RMS (V)	Percent of Fundamental	Angle (Degree)
0	111.410	78.776	0.070	270.000
1	158230.000	111880.000	100.000	-10.421
2	17.133	12.115	0.011	-70.456
3	1281.200	905.920	0.810	55.450
4	31.209	22.068	0.020	215.150
5	175.910	124.390	0.111	-24.754
6	11.568	8.180	0.007	174.080
7	87.789	62.076	0.055	1.543
8	19.447	13.751	0.012	199.760
9	32.190	22.762	0.020	-76.083
10	26.394	18.663	0.017	246.960
11	144.340	102.070	0.091	232.570
12	21.423	15.149	0.014	231.390
13	65.056	46.002	0.041	223.350
14	15.965	11.289	0.010	24.964
15	43.925	31.060	0.028	241.380
16	13.111	9.271	0.008	63.435
17	34.436	24.350	0.022	101.840
18	19.051	13.471	0.012	227.200
19	25.878	18.299	0.016	239.240
20	11.967	8.462	0.008	-15.898
21	21.412	15.141	0.014	-63.236
22	22.492	15.904	0.014	175.590
23	29.423	20.805	0.019	-67.373
24	19.447	13.751	0.012	109.760
25	32.098	22.696	0.020	149.770
26	9.791	6.923	0.006	-12.302
27	0.621	0.439	0.000	214.690
28	14.548	10.287	0.009	92.521
29	23.575	16.670	0.015	141.170
30	11.482	8.119	0.007	-0.343
31	9.857	6.970	0.070	36.765
THD	0.83%			

Table A.5 Measured Voltage Harmonic Results of Bus 1692 for Phase C. Measurement

Harmonic No.	DFT Peak (V)	DFT RMS (V)	Percent of Fundamental	Angle (Degree)
0	166.560	117.770	0.105	270.000
1	158910.000	112360.000	100.000	233.680
2	69.382	49.061	0.044	59.942
3	1809.400	1279.400	1.139	54.856
4	34.008	24.047	0.021	69.568
5	512.050	362.080	0.322	72.341
6	8.093	5.723	0.005	187.600
7	140.450	99.313	0.088	175.350
8	12.738	9.007	0.008	52.861
9	45.143	31.921	0.028	-28.201
10	8.926	6.311	0.006	-65.414
11	86.792	61.371	0.055	32.450
12	42.937	30.361	0.027	65.387
13	55.843	39.487	0.035	135.610
14	12.726	8.999	0.008	-54.179
15	58.557	41.406	0.037	11.572
16	34.685	24.526	0.022	149.040
17	53.854	38.080	0.034	-50.973
18	13.927	9.848	0.009	134.540
19	11.390	8.054	0.007	-45.135
20	26.074	18.437	0.016	76.728
21	7.670	5.423	0.005	-63.521
22	8.406	5.944	0.005	-69.846
23	39.567	27.978	0.025	79.493
24	16.197	11.453	0.010	173.820
25	42.091	29.763	0.026	64.892
26	9.783	6.918	0.006	258.980
27	39.414	27.870	0.025	71.174
28	23.795	16.825	0.015	-2.663
29	12.118	8.569	0.008	118.430
30	27.319	19.317	0.017	147.670
31	17.875	12.640	0.105	-6.112
THD	1.19%			

Table A.6 Measured Voltage Harmonic Results of Bus 1816 for Phase A. Measurement

Harmonic No.	DFT Peak (kV)	DFT RMS (kV)	% of Fundamental	Angle (Degree)
0	2.582	1.826	0.861	180.000
1	299.800	211.990	100.000	27.363
2	1.453	1.027	0.485	50.651
3	1.558	1.102	0.520	68.622
4	0.636	0.449	0.212	101.910
5	5.074	3.588	1.692	-74.306
6	0.243	0.171	0.081	-163.790
7	0.512	0.362	0.171	-49.341
8	0.287	0.203	0.096	163.070
9	0.187	0.132	0.062	123.850
10	0.373	0.264	0.124	139.040
11	0.649	0.459	0.217	28.286
12	0.235	0.166	0.078	-31.115
13	0.774	0.547	0.258	86.662
14	0.046	0.032	0.015	-111.110
15	0.082	0.058	0.027	-169.730
16	0.158	0.112	0.053	49.324
17	0.071	0.050	0.024	-78.669
18	0.080	0.057	0.027	54.060
19	0.101	0.071	0.034	95.795
THD	1.89%			

Table A.7 Measured Voltage Harmonic Results of Bus 1816 for Phase B. Measurement

Harmonic No.	DFT Peak (kV)	DFT RMS (kV)	% of Fundamental	Angle (Degree)
0	0.534	0.378	0.177	0.000
1	301.990	213.540	100.000	-92.642
2	1.733	1.226	0.574	-85.154
3	0.618	0.437	0.205	11.602
4	0.934	0.660	0.309	-86.777
5	5.544	3.920	1.836	36.988
6	0.605	0.428	0.200	-44.025
7	0.241	0.170	0.080	-153.410
8	0.303	0.214	0.100	-58.045
9	0.582	0.412	0.193	-85.763
10	0.348	0.246	0.115	-22.931
11	0.309	0.218	0.102	113.230
12	0.125	0.088	0.041	-36.636
13	0.802	0.567	0.265	-60.793
14	0.256	0.181	0.085	-37.965
15	0.283	0.200	0.094	-17.504
16	0.313	0.222	0.104	-46.605
17	0.229	0.162	0.076	-40.974
18	0.336	0.238	0.111	-14.864
19	0.166	0.117	0.055	-9.430
THD	2.02%			

Table A.8 Measured Voltage Harmonic Results of Bus 1816 for Phase C. Measurement

Harmonic No.	DFT Peak (kV)	DFT RMS (kV)	% of Fundamental	Angle (Degree)
0	2.582	1.826	0.862	0.000
1	299.500	211.780	100.000	146.850
2	1.572	1.111	0.525	131.600
3	1.892	1.338	0.632	96.370
4	0.514	0.364	0.172	128.380
5	6.018	4.255	2.009	157.100
6	0.268	0.190	0.090	122.110
7	0.575	0.407	0.192	104.570
8	0.474	0.335	0.158	152.180
9	0.088	0.062	0.029	142.160
10	0.318	0.225	0.106	173.480
11	0.558	0.395	0.186	-151.390
12	0.230	0.163	0.077	157.500
13	0.935	0.661	0.312	-179.710
14	0.221	0.156	0.074	-173.560
15	0.371	0.263	0.124	138.540
16	0.277	0.196	0.092	130.900
17	0.141	0.100	0.047	164.490
18	0.227	0.161	0.076	171.260
19	0.246	0.174	0.082	-67.951
THD	2.24%			

Table A.9 Measured Voltage Harmonic Results of Bus 2461 for Phase A. Measurement

Harmonic No.	DFT Peak (kV)	DFT RMS (kV)	% of Fundamental	Angle (Degree)
0	0.122	0.086	0.043	0.000
1	284.790	201.380	100.000	76.041
2	1.760	1.244	0.618	86.107
3	2.562	1.812	0.900	125.470
4	0.802	0.567	0.282	91.526
5	1.067	0.754	0.375	127.190
6	0.452	0.319	0.159	107.100
7	0.498	0.352	0.175	-159.460
8	0.388	0.274	0.136	132.340
9	0.262	0.185	0.092	-178.630
10	0.341	0.241	0.120	116.460
11	0.493	0.348	0.173	-136.670
12	0.302	0.214	0.106	-170.350
13	0.234	0.166	0.082	110.110
14	0.370	0.261	0.130	144.880
15	0.366	0.259	0.128	147.200
16	0.171	0.121	0.060	124.420
17	0.160	0.113	0.056	131.660
18	0.253	0.179	0.089	136.950
19	0.258	0.182	0.091	159.670
THD	1.28%			

Table A.10 Measured Voltage Harmonic Results of Bus 2461 for Phase B. Measurement

Harmonic No.	DFT Peak (kV)	DFT RMS (kV)	% of Fundamental	Angle (Degree)
0	0.974	0.689	0.343	180.000
1	284.200	200.960	100.000	-43.820
2	1.676	1.185	0.590	-58.938
3	3.364	2.379	1.184	-157.370
4	0.456	0.322	0.160	-90.294
5	1.632	1.154	0.574	-52.086
6	0.466	0.330	0.164	-51.002
7	0.147	0.104	0.052	-74.823
8	0.197	0.140	0.069	-69.345
9	0.390	0.276	0.137	-27.189
10	0.291	0.206	0.102	-38.489
11	0.780	0.551	0.274	-25.191
12	0.285	0.201	0.100	-54.995
13	0.240	0.170	0.084	-40.073
14	0.221	0.156	0.078	-19.595
15	0.090	0.063	0.032	-43.112
16	0.224	0.158	0.079	-27.692
17	0.112	0.079	0.039	-87.901
18	0.183	0.130	0.065	-17.456
19	0.260	0.184	0.092	-8.627
THD	1.51%			

Table A.11 Measured Voltage Harmonic Results of Bus 2461 for Phase C. Measurement

Harmonic No.	DFT Peak (kV)	DFT RMS (kV)	% of Fundamental	Angle (Degree)
0	3.135	2.217	1.107	0.000
1	283.290	200.310	100.000	-164.170
2	0.871	0.616	0.308	-154.700
3	1.587	1.122	0.560	-177.310
4	0.380	0.269	0.134	-111.620
5	0.855	0.605	0.302	-32.607
6	0.206	0.146	0.073	-98.911
7	0.256	0.181	0.090	-25.113
8	0.190	0.134	0.067	-15.435
9	0.236	0.167	0.083	-93.580
10	0.158	0.112	0.056	-68.586
11	0.658	0.465	0.232	137.910
12	0.043	0.031	0.015	-117.520
13	0.072	0.051	0.025	-65.619
14	0.197	0.139	0.069	-99.252
15	0.230	0.162	0.081	10.922
16	0.125	0.088	0.044	-59.555
17	0.046	0.032	0.016	-117.230
18	0.189	0.133	0.067	178.610
19	0.066	0.047	0.023	152.270
THD	0.79%			

Table A.12 Measured Voltage Harmonic Results of Bus 1697 for Phase A. Measurement

Harmonic No.	DFT Peak (V)	DFT RMS (V)	Percent of Fundamental	Angle (Degree)
0	91.227	64.507	0.140	0.000
1	65125.000	46050.000	100.000	20.196
2	11.984	8.474	0.018	145.480
3	410.850	290.520	0.631	-49.583
4	10.380	7.340	0.016	-164.790
5	266.490	188.440	0.409	74.710
6	17.766	12.562	0.027	35.048
7	229.210	162.080	0.352	28.155
8	22.928	16.213	0.035	-131.790
9	20.822	14.723	0.032	-94.440
10	16.374	11.578	0.025	-22.396
11	73.327	51.850	0.113	144.450
12	7.250	5.127	0.011	170.920
13	151.310	106.990	0.232	-13.109
14	9.109	6.441	0.014	-83.577
15	11.277	7.974	0.017	-26.541
16	13.998	9.898	0.021	-59.036
17	18.289	12.932	0.028	24.022
18	7.298	5.161	0.011	-66.587
19	21.076	14.903	0.032	-59.882
20	11.892	8.409	0.018	-85.411
21	0.977	0.691	0.002	-5.733
22	9.418	6.659	0.014	165.310
23	106.920	75.604	0.164	-63.891
24	16.768	11.857	0.026	24.339
25	36.370	25.718	0.056	88.445
26	8.744	6.183	0.013	143.100
27	16.605	11.742	0.025	156.030
28	4.586	3.243	0.007	130.560
29	20.527	14.515	0.032	-179.230
30	8.822	6.238	0.014	-149.820
31	8.596	6.078	0.140	-32.428
THD	0.90%			

Table A.13 Measured Voltage Harmonic Results of Bus 1697 for Phase B. Measurement

Harmonic No.	DFT Peak (V)	DFT RMS (V)	Percent of Fundamental	Angle (Degree)
0	188.160	133.050	0.290	180.000
1	64788.000	45812.000	100.000	-98.780
2	13.144	9.294	0.020	14.308
3	413.810	292.610	0.639	-50.297
4	3.762	2.660	0.006	40.538
5	232.200	164.190	0.358	-177.910
6	2.639	1.866	0.004	-62.686
7	242.620	171.560	0.374	-74.754
8	2.611	1.846	0.004	67.500
9	4.728	3.343	0.007	-27.911
10	11.821	8.359	0.018	140.810
11	121.210	85.708	0.187	-93.071
12	10.198	7.211	0.016	32.129
13	135.770	96.003	0.210	-134.280
14	7.662	5.418	0.012	-155.770
15	10.412	7.363	0.016	141.960
16	4.825	3.412	0.007	90.000
17	14.636	10.349	0.023	162.550
18	7.471	5.283	0.012	-140.920
19	21.481	15.189	0.033	-168.540
20	11.594	8.198	0.018	-14.039
21	16.243	11.486	0.025	53.952
22	18.356	12.980	0.028	152.360
23	107.590	76.077	0.166	57.529
24	6.304	4.457	0.010	-157.500
25	56.993	40.300	0.088	-48.408
26	16.507	11.673	0.025	160.450
27	5.948	4.206	0.009	-161.590
28	5.172	3.657	0.008	131.760
29	13.261	9.377	0.020	108.820
30	8.593	6.076	0.013	81.831
31	4.393	3.107	0.290	150.480
THD	0.94%			

Table A.14 Measured Voltage Harmonic Results of Bus 1697 for Phase C. Measurement

Harmonic No.	DFT Peak (V)	DFT RMS (V)	Percent of Fundamental	Angle (Degree)
0	252.340	178.430	0.389	180.000
1	64829.000	45841.000	100.000	140.440
2	18.604	13.155	0.029	-50.999
3	441.470	312.170	0.681	-58.266
4	4.608	3.259	0.007	126.670
5	303.420	214.550	0.468	-45.571
6	17.134	12.116	0.026	-71.178
7	237.820	168.170	0.367	150.300
8	6.607	4.672	0.010	173.820
9	27.715	19.598	0.043	-101.940
10	11.177	7.903	0.017	146.160
11	126.650	89.552	0.195	26.809
12	1.763	1.247	0.003	-130.990
13	115.670	81.788	0.178	107.510
14	7.151	5.056	0.011	-86.573
15	7.323	5.178	0.011	-84.278
16	12.372	8.748	0.019	-101.310
17	8.660	6.123	0.013	-51.060
18	6.187	4.375	0.010	30.748
19	18.641	13.181	0.029	112.820
20	12.163	8.600	0.019	170.060
21	15.960	11.286	0.025	-4.933
22	13.186	9.324	0.020	12.071
23	120.790	85.410	0.186	-175.070
24	5.196	3.674	0.008	-127.140
25	33.852	23.937	0.052	-154.140
26	6.889	4.871	0.011	-120.100
27	15.100	10.677	0.023	-60.550
28	7.950	5.621	0.012	116.290
29	13.187	9.325	0.020	-71.894
30	18.372	12.991	0.028	31.388
31	16.643	11.768	0.389	-124.670
THD	0.92%			

Table A.15 Measured Voltage Harmonic Results of Bus 1694 for Phase A. Measurement

Harmonic No.	DFT Peak (V)	DFT RMS (V)	Percent of Fundamental	Angle (Degree)
0	396.740	280.540	0.598	0.000
1	66319.000	46895.000	100.000	16.755
2	13.039	9.220	0.020	-177.500
3	170.500	120.560	0.257	-44.646
4	8.488	6.002	0.013	-174.280
5	194.250	137.360	0.293	101.550
6	19.589	13.851	0.030	82.988
7	226.240	159.980	0.341	32.348
8	13.647	9.650	0.021	-119.500
9	25.177	17.802	0.038	-105.240
10	8.932	6.316	0.013	-10.530
11	77.770	54.992	0.117	142.070
12	3.934	2.782	0.006	-129.720
13	149.250	105.540	0.225	-13.488
14	9.434	6.671	0.014	151.660
15	9.568	6.766	0.014	-18.397
16	2.376	1.680	0.004	0.000
17	2.975	2.104	0.004	-135.160
18	7.161	5.064	0.011	-43.608
19	15.309	10.825	0.023	-73.772
20	11.858	8.385	0.018	84.568
21	2.908	2.057	0.004	138.010
22	9.337	6.602	0.014	-2.961
23	119.970	84.832	0.181	-67.866
24	13.647	9.650	0.021	60.504
25	42.971	30.385	0.065	69.583
26	4.383	3.099	0.007	94.429
27	15.477	10.944	0.023	147.040
28	4.495	3.178	0.007	85.736
29	19.481	13.775	0.029	-150.830
30	8.247	5.832	0.012	-119.120
31	5.133	3.629	0.598	52.515
THD	0.86%			

Table A.16 Measured Voltage Harmonic Results of Bus 1694 for Phase B. Measurement

Harmonic No.	DFT Peak (V)	DFT RMS (V)	Percent of Fundamental	Angle (Degree)
0	147.730	104.460	0.220	0.000
1	67076.000	47430.000	100.000	-102.190
2	13.240	9.362	0.020	117.360
3	186.600	131.950	0.278	-54.353
4	10.046	7.103	0.015	56.512
5	193.020	136.480	0.288	-174.200
6	3.853	2.725	0.006	-137.480
7	264.190	186.810	0.394	-77.503
8	11.315	8.001	0.017	76.113
9	14.507	10.258	0.022	45.890
10	11.054	7.816	0.016	25.649
11	133.400	94.326	0.199	-101.530
12	10.538	7.452	0.016	107.370
13	131.290	92.838	0.196	-131.050
14	4.189	2.962	0.006	-179.310
15	14.388	10.174	0.021	87.330
16	8.732	6.174	0.013	123.690
17	9.467	6.694	0.014	117.010
18	12.271	8.677	0.018	-177.730
19	22.554	15.948	0.034	-172.350
20	13.603	9.619	0.020	-61.114
21	9.274	6.558	0.014	121.610
22	9.040	6.392	0.013	-118.310
23	122.420	86.566	0.183	55.752
24	9.739	6.887	0.015	140.910
25	56.868	40.212	0.085	-39.851
26	5.798	4.100	0.009	168.160
27	14.005	9.903	0.021	-174.770
28	9.780	6.916	0.015	-156.480
29	12.705	8.984	0.019	138.280
30	10.393	7.349	0.015	54.752
31	10.384	7.342	0.220	-11.019
THD	0.76%			

Table A.17 Measured Voltage Harmonic Results of Bus 1694 for Phase C. Measurement

Harmonic No.	DFT Peak (V)	DFT RMS (V)	Percent of Fundamental	Angle (Degree)
0	12.132	8.578	0.018	0.000
1	65612.000	46395.000	100.000	139.960
2	20.576	14.550	0.031	-61.635
3	441.620	312.270	0.673	-56.583
4	5.332	3.770	0.008	157.690
5	329.140	232.740	0.502	-38.450
6	12.833	9.074	0.020	-45.211
7	231.670	163.820	0.353	152.920
8	7.303	5.164	0.011	-61.974
9	26.684	18.868	0.041	-131.530
10	4.614	3.262	0.007	2.816
11	129.920	91.868	0.198	25.623
12	10.925	7.725	0.017	-137.990
13	130.320	92.152	0.199	117.990
14	0.294	0.208	0.000	-85.961
15	5.996	4.240	0.009	-76.207
16	5.425	3.836	0.008	-116.570
17	16.752	11.845	0.026	-72.848
18	2.860	2.022	0.004	51.764
19	8.126	5.746	0.012	85.421
20	7.096	5.018	0.011	172.130
21	4.694	3.319	0.007	-26.288
22	7.096	5.018	0.011	19.916
23	132.790	93.895	0.202	-178.050
24	21.283	15.049	0.032	-99.278
25	35.209	24.897	0.054	-165.640
26	11.432	8.084	0.017	-58.620
27	10.532	7.447	0.016	-21.237
28	10.391	7.348	0.016	3.324
29	11.201	7.920	0.017	-58.192
30	1.402	0.992	0.002	45.581
31	2.826	1.998	0.018	-51.397
THD	1.03%			

Table A.18 Measured Voltage Harmonic Results of Bus 2373 for Phase A. Measurement

Harmonic No.	DFT Peak (V)	DFT RMS (V)	Percent of Fundamental	Angle (Degree)
0	549.440	388.520	0.188	270.000
1	291620.000	206200.000	100.000	59.684
2	260.640	184.300	0.089	44.249
3	1678.500	1186.900	0.576	-62.214
4	66.771	47.214	0.023	38.399
5	1406.900	994.810	0.482	-33.944
6	73.782	52.172	0.025	39.389
7	246.080	174.000	0.084	88.900
8	63.513	44.910	0.022	52.559
9	37.536	26.542	0.013	51.140
10	61.661	43.601	0.021	39.179
11	126.520	89.460	0.043	-84.396
12	28.197	19.938	0.010	84.117
13	31.994	22.623	0.011	65.829
14	13.877	9.812	0.005	135.070
15	65.419	46.258	0.022	-11.962
16	13.211	9.341	0.005	243.430
17	20.929	14.799	0.007	67.012
18	12.073	8.537	0.004	60.974
19	21.549	15.238	0.007	54.066
20	18.192	12.864	0.006	-3.011
21	5.831	4.124	0.002	-6.422
22	33.579	23.744	0.012	76.613
23	56.166	39.716	0.019	60.941
24	9.212	6.514	0.003	69.913
25	46.254	32.706	0.016	8.944
26	17.630	12.467	0.006	50.285
27	25.334	17.914	0.009	36.071
28	20.474	14.478	0.007	6.533
29	30.224	21.371	0.010	15.076
30	8.309	5.875	0.003	-24.006
31	549.440	388.520	0.188	270.000
THD	0.79%			

Table A.19 Measured Voltage Harmonic Results of Bus 2373 for Phase B. Measurement

Harmonic No.	DFT Peak (V)	DFT RMS (V)	Percent of Fundamental	Angle (Degree)
0	360.000	254.560	0.125	270.000
1	288830.000	204230.000	100.000	-58.714
2	220.540	155.940	0.076	-50.555
3	3975.100	2810.800	1.376	12.283
4	137.180	97.002	0.047	-5.953
5	1272.400	899.720	0.441	55.537
6	40.053	28.322	0.014	-8.073
7	494.040	349.340	0.171	5.672
8	47.704	33.732	0.017	44.126
9	40.881	28.907	0.014	168.370
10	78.302	55.368	0.027	-2.712
11	160.230	113.300	0.055	64.658
12	31.921	22.571	0.011	-3.383
13	10.605	7.499	0.004	-67.254
14	15.745	11.134	0.005	167.910
15	39.224	27.735	0.014	198.450
16	8.485	6.000	0.003	225.000
17	16.228	11.475	0.006	-76.366
18	5.272	3.728	0.002	106.090
19	24.228	17.132	0.008	31.597
20	16.411	11.604	0.006	19.205
21	14.695	10.391	0.005	-34.670
22	24.161	17.085	0.008	56.308
23	44.427	31.414	0.015	89.066
24	27.356	19.343	0.009	199.680
25	54.456	38.506	0.019	-45.207
26	14.161	10.013	0.005	171.560
27	47.252	33.412	0.016	153.960
28	34.712	24.545	0.012	89.877
29	29.822	21.088	0.010	134.400
30	27.280	19.290	0.009	169.250
31	360.000	254.560	0.125	270.000
THD	1.47%			

Table A.20 Measured Voltage Harmonic Results of Bus 2373 for Phase C. Measurement

Harmonic No.	DFT Peak (V)	DFT RMS (V)	Percent of Fundamental	Angle (Degree)
0	847.010	598.930	0.293	270.000
1	288990.000	204350.000	100.000	180.310
2	271.120	191.710	0.094	182.660
3	5272.800	3728.500	1.825	239.660
4	153.970	108.870	0.053	221.030
5	2196.100	1552.900	0.760	193.160
6	105.560	74.642	0.037	195.860
7	565.630	399.960	0.196	221.240
8	116.610	82.455	0.040	209.150
9	103.650	73.291	0.036	258.620
10	84.244	59.570	0.029	219.610
11	176.350	124.700	0.061	217.110
12	86.716	61.317	0.030	211.610
13	54.913	38.829	0.019	227.150
14	7.100	5.021	0.002	224.520
15	60.488	42.771	0.021	247.220
16	68.595	48.504	0.024	239.040
17	30.962	21.893	0.011	251.540
18	42.190	29.833	0.015	209.180
19	31.523	22.290	0.011	265.030
20	57.334	40.541	0.020	255.670
21	51.409	36.352	0.018	218.700
22	39.130	27.669	0.014	258.810
23	106.980	75.649	0.037	254.610
24	32.739	23.150	0.011	162.680
25	32.239	22.796	0.011	213.780
26	63.402	44.832	0.022	-85.932
27	55.707	39.391	0.019	247.700
28	34.531	24.417	0.012	254.130
29	29.859	21.113	0.010	173.110
30	22.677	16.035	0.008	214.910
31	847.010	598.930	0.293	270.000
THD	2.01%			

A.3 Harmonic Information Measured from July 27 2007 Data

Table A.21 Information of July 27 2007 Measurement

Number	Bus Name	Bus Voltage (kV)	Sample Rate (second/sample)
1	Bus 1692	138	2.60×10^{-4}
2	Bus 2461	345	3.86×10^{-4}
3	Bus 1697	138	2.60×10^{-4}
4	Bus 1694	138	2.60×10^{-4}
5	Bus 2373	345	2.60×10^{-4}

Table A.22 Measured Voltage Harmonic Results of Bus 1692 for Phase A. Measurement

Harmonic No.	DFT Peak (V)	DFT RMS (V)	Percent of Fundamental	Angle (Degree)
0	69.251	48.967	0.024	0.000
1	284140.000	200920.000	100.000	102.080
2	224.020	158.410	0.079	86.401
3	135.410	95.750	0.048	163.170
4	86.611	61.244	0.030	81.288
5	2625.400	1856.400	0.924	4.024
6	48.619	34.379	0.017	123.150
7	721.130	509.920	0.254	175.180
8	62.666	44.311	0.022	59.036
9	152.590	107.900	0.054	98.139
10	19.438	13.745	0.007	-44.966
11	326.470	230.850	0.115	32.075
12	83.332	58.925	0.029	-60.843
13	138.950	98.251	0.049	58.883
14	37.012	26.171	0.013	-113.030
15	69.792	49.350	0.025	55.614
16	22.699	16.050	0.008	-123.690
17	37.011	26.171	0.013	91.304
18	62.098	43.910	0.022	-135.120
19	42.352	29.947	0.015	139.760
20	29.077	20.560	0.010	-55.409
21	18.322	12.955	0.006	-90.936
22	47.402	33.518	0.017	97.932
23	85.252	60.282	0.030	-77.675
24	10.752	7.603	0.004	-59.036
25	104.770	74.085	0.037	121.270
26	39.756	28.112	0.014	-41.435
27	85.985	60.800	0.030	5.626
28	48.020	33.956	0.017	-159.720
29	57.106	40.380	0.020	-13.768
30	21.939	15.513	0.008	-138.280
31	57.226	40.465	0.020	4.924
THD	0.97%			

Table A.23 Measured Voltage Harmonic Results of Bus 1692 for Phase B. Measurement

Harmonic No.	DFT Peak (V)	DFT RMS (V)	Percent of Fundamental	Angle (Degree)
0	320.100	226.350	0.113	180.000
1	284420.000	201110.000	100.000	-17.836
2	96.451	68.201	0.034	-24.025
3	25.710	18.180	0.009	153.360
4	86.504	61.167	0.030	-57.032
5	3011.300	2129.300	1.059	123.650
6	84.695	59.889	0.030	177.540
7	661.560	467.790	0.233	56.058
8	32.146	22.730	0.011	135.560
9	46.188	32.660	0.016	-116.480
10	69.467	49.121	0.024	-167.010
11	395.960	279.990	0.139	115.390
12	23.011	16.271	0.008	-146.340
13	199.510	141.070	0.070	-40.698
14	39.775	28.125	0.014	-44.497
15	103.090	72.894	0.036	-47.767
16	33.800	23.900	0.012	-158.200
17	75.674	53.509	0.027	118.230
18	14.958	10.577	0.005	-151.090
19	30.585	21.627	0.011	12.810
20	17.649	12.480	0.006	-2.704
21	75.036	53.058	0.026	161.240
22	97.862	69.199	0.034	162.620
23	103.650	73.292	0.036	152.840
24	62.693	44.330	0.022	-39.953
25	35.001	24.749	0.012	-6.228
26	41.344	29.234	0.015	-64.249
27	11.653	8.240	0.004	-145.630
28	40.044	28.315	0.014	83.314
29	77.585	54.861	0.027	-76.366
30	24.260	17.154	0.009	-9.290
31	97.623	69.030	0.034	-84.324
THD	1.10%			

Table A.24 Measured Voltage Harmonic Results of Bus 1692 for Phase C. Measurement

Harmonic No.	DFT Peak (V)	DFT RMS (V)	Percent of Fundamental	Angle (Degree)
0	269.820	190.800	0.094	0.000
1	285680.000	202010.000	100.000	-137.780
2	201.270	142.320	0.070	-110.620
3	214.250	151.500	0.075	-153.180
4	44.999	31.819	0.016	150.100
5	2798.700	1979.000	0.980	-110.480
6	141.340	99.941	0.049	-58.421
7	587.500	415.420	0.206	-73.344
8	87.658	61.983	0.031	-100.670
9	50.901	35.992	0.018	-70.510
10	16.739	11.836	0.006	52.026
11	241.590	170.830	0.085	154.080
12	85.551	60.493	0.030	-24.492
13	187.260	132.410	0.066	-158.250
14	20.923	14.795	0.007	108.070
15	65.461	46.288	0.023	60.136
16	22.625	15.998	0.008	-33.690
17	90.773	64.186	0.032	-99.073
18	36.194	25.593	0.013	29.711
19	93.663	66.229	0.033	-124.780
20	95.473	67.509	0.033	170.200
21	79.588	56.277	0.028	2.810
22	95.964	67.857	0.034	-18.212
23	172.050	121.660	0.060	-64.116
24	81.056	57.315	0.028	-114.780
25	137.720	97.385	0.048	45.607
26	34.352	24.290	0.012	23.846
27	31.208	22.068	0.011	144.950
28	24.475	17.306	0.009	78.123
29	34.050	24.077	0.012	140.000
30	41.863	29.602	0.015	-17.870
31	117.430	83.036	0.041	70.984
THD	1.01%			

Table A.25 Measured Voltage Harmonic Results of Bus 2461 for Phase A. Measurement

Harmonic No.	DFT Peak (V)	DFT RMS (V)	% of Fundamental	Angle (Degree)
0	151.890	107.400	0.131	0.000
1	116270.000	82214.000	100.000	-140.810
2	85.921	60.755	0.074	-130.970
3	120.181	84.982	0.103	-81.481
4	24.391	17.247	0.021	-3.341
5	1762.573	1246.316	1.516	-117.890
6	47.961	33.913	0.041	-70.954
7	212.853	150.504	0.183	-80.670
8	24.688	17.458	0.021	-82.139
9	41.108	29.068	0.035	143.680
10	70.297	49.708	0.060	-61.017
11	3031.856	2143.832	2.608	-152.300
12	29.066	20.553	0.025	-74.451
13	142.721	100.920	0.123	27.165
14	49.381	34.917	0.042	-83.116
15	20.122	14.229	0.017	-136.780
16	30.693	21.703	0.026	-78.690
17	37.258	26.346	0.032	-74.101
18	19.006	13.439	0.016	-52.846
19	12.801	9.052	0.011	168.960
THD	3.03%			

Table A.26 Measured Voltage Harmonic Results of Bus 2461 for Phase B. Measurement

Harmonic No.	DFT Peak (V)	DFT RMS (V)	% of Fundamental	Angle (Degree)
0	51.485	36.405	0.045	0.000
1	115560.000	81711.000	100.000	99.032
2	85.107	60.179	0.074	112.870
3	177.097	125.229	0.153	-70.868
4	42.502	30.054	0.037	88.640
5	1746.550	1234.971	1.511	-2.787
6	23.707	16.763	0.021	96.202
7	248.196	175.511	0.215	169.260
8	52.257	36.951	0.045	69.506
9	67.911	48.020	0.059	124.240
10	77.203	54.593	0.067	111.920
11	3604.132	2548.503	3.119	-38.698
12	48.000	33.940	0.042	89.181
13	152.954	108.155	0.132	-129.300
14	25.801	18.244	0.022	109.370
15	34.406	24.329	0.030	162.960
16	24.835	17.562	0.021	104.040
17	11.557	8.172	0.010	111.520
18	19.583	13.847	0.017	113.400
19	41.917	29.641	0.036	169.960
THD	3.48%			

Table A.27 Measured Voltage Harmonic Results of Bus 2461 for Phase C. Measurement

Harmonic No.	DFT Peak (V)	DFT RMS (V)	% of Fundamental	Angle (Degree)
0	46.457	32.850	0.040	180.000
1	115830.000	81902.000	100.000	-20.953
2	49.336	34.886	0.043	-62.738
3	136.995	96.873	0.118	-28.029
4	33.421	23.633	0.029	-19.105
5	1885.848	1333.567	1.628	117.250
6	34.168	24.161	0.029	-76.403
7	196.825	139.172	0.170	44.578
8	22.094	15.622	0.019	-27.236
9	58.944	41.679	0.051	-101.530
10	32.991	23.328	0.028	-21.931
11	3725.269	2634.132	3.216	90.826
12	21.107	14.925	0.018	56.104
13	88.463	62.552	0.076	167.820
14	14.744	10.425	0.013	-31.559
15	34.005	24.045	0.029	11.990
16	13.433	9.499	0.012	153.430
17	30.668	21.685	0.026	112.180
18	40.776	28.833	0.035	13.148
19	20.412	14.433	0.018	2.363
THD	3.61%			

Table A.28 Measured Voltage Harmonic Results of Bus 1697 for Phase A. Measurement

Harmonic No.	DFT Peak (V)	DFT RMS (V)	% of Fundamental	Angle (Degree)
0	5.826	4.120	2.073	0.000
1	281.060	198.740	100.000	-77.258
2	1.583	1.119	0.563	-72.887
3	0.342	0.242	0.122	-44.636
4	0.802	0.567	0.286	-68.956
5	2.562	1.811	0.911	-156.580
6	0.521	0.369	0.186	-92.142
7	0.736	0.521	0.262	6.078
8	1.259	0.890	0.448	-55.395
9	0.728	0.515	0.259	-82.092
10	1.464	1.035	0.521	-39.418
11	5.037	3.561	1.792	-56.319
12	1.491	1.054	0.530	-24.031
13	0.576	0.407	0.205	123.880
14	1.360	0.962	0.484	-70.938
15	0.479	0.338	0.170	-128.740
16	0.898	0.635	0.320	-41.883
17	0.924	0.653	0.329	1.308
18	0.142	0.100	0.050	14.425
19	0.281	0.199	0.100	96.221
THD	2.44%			

Table A.29 Measured Voltage Harmonic Results of Bus 1697 for Phase B. Measurement

Harmonic No.	DFT Peak (V)	DFT RMS (V)	% of Fundamental	Angle (Degree)
0	7.783	5.503	2.771	0.000
1	280.920	198.640	100.000	162.760
2	0.485	0.343	0.173	128.460
3	0.468	0.331	0.167	141.710
4	0.202	0.143	0.072	-178.300
5	2.381	1.684	0.848	-47.295
6	0.464	0.328	0.165	160.640
7	0.563	0.398	0.201	-57.571
8	0.170	0.120	0.060	87.189
9	0.628	0.444	0.224	-177.510
10	0.413	0.292	0.147	119.510
11	1.756	1.241	0.625	88.699
12	0.413	0.292	0.147	-177.490
13	0.394	0.278	0.140	50.182
14	0.246	0.174	0.087	162.010
15	0.577	0.408	0.206	-110.030
16	1.113	0.787	0.396	-87.326
17	0.690	0.488	0.246	151.040
18	0.472	0.334	0.168	91.688
19	0.237	0.167	0.084	-176.630
THD	1.31%			

Table A.30 Measured Voltage Harmonic Results of Bus 1697 for Phase C. Measurement

Harmonic No.	DFT Peak (V)	DFT RMS (V)	% of Fundamental	Angle (Degree)
0	3.7359	2.6416	1.3302	0
1	280.85	198.59	100	43.095
2	1.077988	0.762234	0.383823	46.378
3	1.227198	0.867764	0.436956	80.27
4	0.638981	0.45183	0.227517	125.41
5	3.073684	2.17345	1.094409	77.073
6	0.707159	0.500038	0.251796	138.1
7	0.720531	0.509497	0.256545	164.09
8	0.476491	0.33692	0.169657	113.59
9	0.904885	0.639869	0.3222	55.799
10	2.337161	1.652627	0.832161	117.84
11	4.770838	3.373473	1.698743	-178.83
12	1.352646	0.956459	0.481634	109.38
13	0.294425	0.208184	0.10483	131.3
14	0.816053	0.57704	0.29056	66.226
15	0.996015	0.704286	0.354637	-157.97
16	0.686192	0.485209	0.244327	-142.32
17	0.426897	0.301862	0.152	172.38
18	0.888141	0.628	0.316235	169.39
19	0.787742	0.557028	0.280484	120.6
THD	2.49%			

Table A.31 Measured Voltage Harmonic Results of Bus 1694 for Phase A. Measurement

Harmonic No.	DFT Peak (V)	DFT RMS (V)	% of Fundamental	Angle (Degree)
0	1.403	0.992	1.227	0.000
1	114.290	80.814	100.000	-158.380
2	0.419	0.297	0.367	-137.070
3	0.502	0.355	0.439	-133.440
4	0.123	0.087	0.108	-109.670
5	1.274	0.901	1.114	116.080
6	0.062	0.044	0.054	-116.180
7	0.258	0.182	0.225	-95.976
8	0.080	0.056	0.070	-66.718
9	0.107	0.076	0.094	-120.610
10	0.126	0.089	0.111	-87.310
11	1.303	0.921	1.140	82.845
12	0.088	0.063	0.077	70.099
13	0.063	0.044	0.055	14.387
14	0.038	0.027	0.034	95.344
15	0.002	0.001	0.002	-10.854
16	0.045	0.032	0.039	-27.861
17	0.097	0.068	0.084	66.454
18	0.028	0.020	0.025	-144.250
19	0.049	0.034	0.043	-82.865
THD	1.72%			

Table A.32 Measured Voltage Harmonic Results of Bus 1694 for Phase B. Measurement

Harmonic No.	DFT Peak (V)	DFT RMS (V)	% of Fundamental	Angle (Degree)
0	0.221	0.157	0.192	0.000
1	115.280	81.517	100.000	81.735
2	0.677	0.478	0.587	91.096
3	0.389	0.275	0.338	119.280
4	0.303	0.214	0.263	105.590
5	1.185	0.838	1.028	-135.980
6	0.174	0.123	0.151	113.400
7	0.398	0.281	0.345	140.810
8	0.177	0.125	0.153	136.240
9	0.205	0.145	0.178	124.060
10	0.116	0.082	0.100	116.110
11	1.325	0.937	1.149	-153.680
12	0.150	0.106	0.130	168.950
13	0.148	0.105	0.129	-158.140
14	0.116	0.082	0.101	126.270
15	0.100	0.071	0.087	149.650
16	0.090	0.064	0.078	-158.270
17	0.128	0.090	0.111	170.630
18	0.118	0.084	0.103	147.320
19	0.137	0.097	0.119	-173.510
THD	1.77%			

Table A.33 Measured Voltage Harmonic Results of Bus 1694 for Phase C. Measurement

Harmonic No.	DFT Peak (V)	DFT RMS (V)	% of Fundamental	Angle (Degree)
0	0.529	0.374	0.460	180.000
1	115.000	81.319	100.000	-38.329
2	0.526	0.372	0.457	-61.443
3	0.291	0.206	0.253	-88.231
4	0.230	0.163	0.200	-56.017
5	1.297	0.917	1.128	-9.314
6	0.105	0.074	0.091	-12.987
7	0.282	0.200	0.246	11.552
8	0.147	0.104	0.128	-44.779
9	0.045	0.032	0.039	-70.117
10	0.074	0.052	0.064	-108.960
11	1.479	1.046	1.286	-35.011
12	0.142	0.101	0.124	-44.290
13	0.099	0.070	0.086	13.051
14	0.069	0.049	0.060	-50.014
15	0.123	0.087	0.107	-12.463
16	0.065	0.046	0.057	-52.074
17	0.118	0.083	0.102	-22.689
18	0.088	0.062	0.076	-12.237
19	0.156	0.110	0.136	-27.836
THD	1.83%			

Table A.34 Measured Voltage Harmonic Results of Bus 2373 for Phase A. Measurement

Harmonic No.	DFT Peak (V)	DFT RMS (V)	% of Fundamental	Angle (Degree)
0	3.195	2.260	1.123	0.000
1	284.540	201.200	100.000	-145.320
2	1.127	0.797	0.396	-108.140
3	2.392	1.692	0.841	-141.840
4	0.399	0.282	0.140	-73.129
5	3.992	2.823	1.403	156.990
6	0.243	0.172	0.086	170.980
7	0.480	0.340	0.169	-1.965
8	0.444	0.314	0.156	-95.481
9	0.266	0.188	0.094	127.360
10	0.326	0.231	0.115	11.537
11	1.866	1.320	0.656	165.860
12	0.119	0.084	0.042	-82.191
13	0.456	0.323	0.160	52.016
14	0.348	0.246	0.122	-58.450
15	0.171	0.121	0.060	-72.156
16	0.029	0.020	0.010	-2.732
17	0.294	0.208	0.103	-32.366
18	0.048	0.034	0.017	173.100
19	0.086	0.060	0.030	49.729
THD	1.84%			

Table A.35 Measured Voltage Harmonic Results of Bus 2373 for Phase B. Measurement

Harmonic No.	DFT Peak (V)	DFT RMS (V)	% of Fundamental	Angle (Degree)
0	0.700	0.495	0.245	0.000
1	285.250	201.700	100.000	94.944
2	1.897	1.342	0.665	95.901
3	3.143	2.223	1.102	-125.510
4	0.783	0.554	0.275	104.940
5	4.143	2.929	1.452	-85.765
6	0.298	0.211	0.105	113.390
7	0.305	0.216	0.107	133.830
8	0.390	0.276	0.137	125.570
9	0.622	0.440	0.218	137.990
10	0.375	0.265	0.131	142.820
11	1.858	1.314	0.651	-68.238
12	0.060	0.043	0.021	114.560
13	0.366	0.259	0.128	-92.669
14	0.227	0.160	0.079	157.370
15	0.335	0.237	0.117	134.560
16	0.141	0.100	0.049	148.520
17	0.213	0.151	0.075	146.340
18	0.228	0.161	0.080	131.700
19	0.168	0.119	0.059	-170.490
THD	2.10%			

Table A.36 Measured Voltage Harmonic Results of Bus 2373 for Phase C. Measurement

Harmonic No.	DFT Peak (V)	DFT RMS (V)	% of Fundamental	Angle (Degree)
0	2.252	1.592	0.793	180.000
1	284.140	200.920	100.000	-25.766
2	1.042	0.737	0.367	-35.992
3	1.255	0.888	0.442	-117.270
4	0.431	0.305	0.152	-85.486
5	3.741	2.645	1.317	17.165
6	0.309	0.219	0.109	-37.958
7	0.168	0.118	0.059	133.560
8	0.314	0.222	0.110	-63.886
9	0.178	0.126	0.063	-9.156
10	0.122	0.086	0.043	-101.790
11	2.192	1.550	0.772	38.335
12	0.144	0.102	0.051	-28.028
13	0.034	0.024	0.012	-64.402
14	0.187	0.132	0.066	-56.197
15	0.249	0.176	0.088	22.684
16	0.233	0.165	0.082	-70.378
17	0.126	0.089	0.044	-98.708
18	0.161	0.114	0.057	-3.719
19	0.251	0.177	0.088	-51.472
THD	1.65%			

A.4 Harmonic Information Measured from September 19 2007 Data

Table A.37 Information of September 19 2007 Measurement

Number	Bus Name	Bus Voltage (kV)	Sample Rate (second/sample)
1	Bus 1692	345	5.00×10^{-4}
2	Bus 1816	138	5.00×10^{-4}
3	Bus 1758	138	5.00×10^{-4}
4	Bus 1694	138	5.00×10^{-4}
5	Bus 2373	345	5.00×10^{-4}

Table A.38 Measured Voltage Harmonic Results of Bus 1692 for Phase A. Measurement

Harmonic No.	Frequency	DFT Peak (kV)	% of Fundamental
1	60	286.7930	100.0000
2	120	0.1552	0.0540
3	180	0.2654	0.0927
4	240	0.0539	0.0190
5	300	4.1404	1.4433
6	360	0.0713	0.0242
7	420	2.2168	0.7734
8	480	0.0585	0.0214
9	540	0.2820	0.0984
10	600	0.1695	0.0593
11	660	3.5928	1.2515
12	720	0.0973	0.0350
13	780	0.3534	0.1236
14	840	0.0667	0.0240
15	900	0.0802	0.0276
16	960	0.0344	0.0123
THD	2.07%		

Table A.39 Measured Voltage Harmonic Results of Bus 1692 for Phase B. Measurement

Harmonic No.	Frequency	DFT Peak (kV)	% of Fundamental
1	60	288.0400	100.0000
2	120	0.1355	0.0471
3	180	0.0579	0.0203
4	240	0.0465	0.0159
5	300	4.3942	1.5251
6	360	0.0803	0.0280
7	420	2.0490	0.7119
8	480	0.0273	0.0097
9	540	0.1115	0.0393
10	600	0.1229	0.0424
11	660	5.4192	1.8802
12	720	0.0700	0.0233
13	780	0.2931	0.1006
14	840	0.0480	0.0160
15	900	0.0902	0.0326
16	960	0.0491	0.0172
THD	2.53%		

Table A.40 Measured Voltage Harmonic Results of Bus 1692 for Phase c. Measurement

Harmonic No.	Frequency	DFT Peak (kV)	% of Fundamental
1	60	288.4740	100.0000
2	120	0.1051	0.0363
3	180	0.2008	0.0695
4	240	0.0148	0.0053
5	300	4.3076	1.4936
6	360	0.0127	0.0038
7	420	1.8238	0.6322
8	480	0.0565	0.0195
9	540	0.2557	0.0885
10	600	0.0381	0.0127
11	660	0.9581	0.3353
12	720	0.0156	0.0078
13	780	0.3506	0.1207
14	840	0.0293	0.0107
15	900	0.0100	0.0050
16	960	0.0123	0.0049
THD	1.66%		

Table A.41 Measured Voltage Harmonic Results of Bus 1816 for Phase A. Measurement

Harmonic No.	Frequency	DFT Peak (kV)	% of Fundamental
1	60	114.9770	100.0000
2	120	0.0442	0.0383
3	180	0.0936	0.0820
4	240	0.0095	0.0085
5	300	1.6901	1.4702
6	360	0.0178	0.0153
7	420	0.2098	0.1818
8	480	0.0117	0.0097
9	540	0.0885	0.0754
10	600	0.0254	0.0254
11	660	1.9880	1.7246
12	720	0.0117	0.0078
13	780	0.0920	0.0805
14	840	0.0107	0.0107
15	900	0.0125	0.0125
16	960	0.0098	0.0098
THD	2.28%		

Table A.42 Measured Voltage Harmonic Results of Bus 1816 for Phase B. Measurement

Harmonic No.	Frequency	DFT Peak (kV)	% of Fundamental
1	60	115.6130	100.0000
2	120	0.0678	0.0580
3	180	0.1255	0.1091
4	240	0.0307	0.0264
5	300	1.7392	1.5041
6	360	0.0191	0.0166
7	420	0.1035	0.0895
8	480	0.0234	0.0195
9	540	0.0721	0.0623
10	600	0.0466	0.0381
11	660	2.4910	2.1557
12	720	0.0428	0.0350
13	780	0.0948	0.0805
14	840	0.0267	0.0240
15	900	0.0251	0.0226
16	960	0.0295	0.0246
THD	2.64%		

Table A.43 Measured Voltage Harmonic Results of Bus 1816 for Phase C. Measurement

Harmonic No.	Frequency	DFT Peak (kV)	% of Fundamental
1	60	115.4910	100.0000
2	120	0.0393	0.0344
3	180	0.0627	0.0540
4	240	0.0254	0.0222
5	300	1.7099	1.4807
6	360	0.0102	0.0089
7	420	0.0769	0.0657
8	480	0.0195	0.0175
9	540	0.0262	0.0230
10	600	0.0169	0.0169
11	660	2.5689	2.2275
12	720	0.0156	0.0156
13	780	0.0718	0.0603
14	840	0.0133	0.0107
15	900	0.0150	0.0125
16	960	0.0221	0.0197
THD	2.68%		

Table A.44 Measured Voltage Harmonic Results of Bus 1758 for Phase A. Measurement

Harmonic No.	Frequency	DFT Peak (kV)	% of Fundamental
1	60	114.7280	100.0000
2	120	0.0344	0.0304
3	180	0.1013	0.0888
4	240	0.0011	0.0011
5	300	1.9988	1.7427
6	360	0.0127	0.0102
7	420	0.9483	0.8266
8	480	0.0058	0.0039
9	540	0.0820	0.0721
10	600	0.0085	0.0085
11	660	1.8802	1.6407
12	720	0.0311	0.0272
13	780	0.2299	0.2011
14	840	0.0107	0.0080
15	900	0.0175	0.0150
16	960	0.0049	0.0049
THD	2.54%		

Table A.45 Measured Voltage Harmonic Results of Bus 1758 for Phase B. Measurement

Harmonic No.	Frequency	DFT Peak (kV)	% of Fundamental
1	60	115.1990	100.0000
2	120	0.0737	0.0638
3	180	0.0251	0.0212
4	240	0.0349	0.0307
5	300	2.0795	1.8047
6	360	0.0115	0.0102
7	420	0.8937	0.7762
8	480	0.0331	0.0292
9	540	0.0590	0.0492
10	600	0.0297	0.0254
11	660	0.3653	0.3174
12	720	0.0467	0.0389
13	780	0.2787	0.2414
14	840	0.0320	0.0267
15	900	0.0301	0.0251
16	960	0.0246	0.0197
THD	2.01%		

Table A.46 Measured Voltage Harmonic Results of Bus 1758 for Phase C. Measurement

Harmonic No.	Frequency	DFT Peak (kV)	% of Fundamental
1	60	115.4640	100.0000
2	120	0.0481	0.0413
3	180	0.0637	0.0560
4	240	0.0307	0.0264
5	300	2.0830	1.8035
6	360	0.0153	0.0127
7	420	0.8098	0.7021
8	480	0.0370	0.0331
9	540	0.1148	0.0984
10	600	0.0297	0.0254
11	660	0.2695	0.2335
12	720	0.0195	0.0156
13	780	0.3362	0.2931
14	840	0.0320	0.0267
15	900	0.0125	0.0100
16	960	0.0147	0.0147
THD	1.98%		

Table A.47 Measured Voltage Harmonic Results of Bus 1694 for Phase A. Measurement

Harmonic No.	Frequency	DFT Peak (kV)	% of Fundamental
1	60	113.5580	100.0000
2	120	0.0678	0.0599
3	180	0.1139	0.1004
4	240	0.0180	0.0159
5	300	1.6246	1.4304
6	360	0.0204	0.0178
7	420	0.4517	0.3972
8	480	0.0292	0.0253
9	540	0.2525	0.2230
10	600	0.0381	0.0339
11	660	1.7725	1.5569
12	720	0.0272	0.0272
13	780	0.2759	0.2443
14	840	0.0187	0.0160
15	900	0.0802	0.0702
16	960	0.0172	0.0147
THD	2.18%		

Table A.48 Measured Voltage Harmonic Results of Bus 1694 for Phase B. Measurement

Harmonic No.	Frequency	DFT Peak (kV)	% of Fundamental
1	60	114.1490	100.0000
2	120	0.1051	0.0913
3	180	0.1023	0.0888
4	240	0.0465	0.0402
5	300	1.6000	1.3988
6	360	0.0280	0.0242
7	420	0.2951	0.2573
8	480	0.0448	0.0390
9	540	0.1705	0.1508
10	600	0.0763	0.0678
11	660	2.3952	2.0958
12	720	0.0584	0.0506
13	780	0.2126	0.1868
14	840	0.0373	0.0320
15	900	0.0727	0.0652
16	960	0.0319	0.0295
THD	2.55%		

Table A.49 Measured Voltage Harmonic Results of Bus 1694 for Phase C. Measurement

Harmonic No.	Frequency	DFT Peak (kV)	% of Fundamental
1	60	114.3070	100.0000
2	120	0.0727	0.0638
3	180	0.1187	0.1042
4	240	0.0317	0.0286
5	300	1.6327	1.4292
6	360	0.0204	0.0178
7	420	0.2643	0.2322
8	480	0.0351	0.0312
9	540	0.0852	0.0754
10	600	0.0254	0.0254
11	660	2.1257	1.8623
12	720	0.0467	0.0389
13	780	0.2500	0.2184
14	840	0.0080	0.0080
15	900	0.0426	0.0351
16	960	0.0172	0.0147
THD	2.37%		

Table A.50 Measured Voltage Harmonic Results of Bus 2373 for Phase A. Measurement

Harmonic No.	Frequency	DFT Peak (kV)	% of Fundamental
1	60	285.2300	100.0000
2	120	0.0481	0.0167
3	180	0.9121	0.3195
4	240	0.0370	0.0127
5	300	4.4374	1.5556
6	360	0.0229	0.0076
7	420	2.5762	0.9035
8	480	0.0429	0.0156
9	540	0.4754	0.1672
10	600	0.0763	0.0254
11	660	0.4491	0.1557
12	720	0.0389	0.0156
13	780	0.1925	0.0661
14	840	0.0240	0.0080
15	900	0.1153	0.0401
16	960	0.0197	0.0074
THD	1.84%		

Table A.51 Measured Voltage Harmonic Results of Bus 2373 for Phase B. Measurement

Harmonic No.	Frequency	DFT Peak (kV)	% of Fundamental
1	60	286.2670	100.0000
2	120	0.0953	0.0334
3	180	0.6795	0.2374
4	240	0.0624	0.0222
5	300	4.5357	1.5848
6	360	0.0306	0.0102
7	420	2.4951	0.8713
8	480	0.0234	0.0078
9	540	0.3279	0.1148
10	600	0.0127	0.0042
11	660	0.4371	0.1497
12	720	0.0156	0.0078
13	780	0.1810	0.0632
14	840	0.0160	0.0053
15	900	0.1253	0.0426
16	960	0.0270	0.0098
THD	1.84%		

Table A.52 Measured Voltage Harmonic Results of Bus 2373 for Phase C. Measurement

Harmonic No.	Frequency	DFT Peak (kV)	% of Fundamental
1	60	287.0630	100.0000
2	120	0.0216	0.0079
3	180	0.7026	0.2452
4	240	0.0518	0.0180
5	300	4.4561	1.5520
6	360	0.0484	0.0166
7	420	2.1455	0.7483
8	480	0.0585	0.0195
9	540	0.5311	0.1836
10	600	0.0424	0.0127
11	660	0.5749	0.1976
12	720	0.0428	0.0156
13	780	0.1782	0.0632
14	840	0.0373	0.0133
15	900	0.1028	0.0351
16	960	0.0221	0.0074
THD	1.76%		

A.5 Harmonic Information Measured from February 8 2008 Data

Table A.53 Information of February 8 2008 Measurement

Number	Bus Name	Bus Voltage (kV)	Sample Rate (second/sample)
1	Bus 1816	138	5.00×10^{-4}
2	Bus 1758	138	5.00×10^{-4}
3	Bus 2373	345	5.00×10^{-4}
4	Bus 1692	345	5.00×10^{-4}
5	Bus 2462	345	5.00×10^{-4}

Table A.54 Measured Voltage Harmonic Results of Bus 1816 for Phase C. Measurement

Harmonic No.	Frequency	DFT Peak (kV)	% of Fundamental
1	60	113.5660	100.0000
2	120	0.0265	0.0236
3	180	0.0338	0.0299
4	240	0.0127	0.0106
5	300	0.7345	0.6468
6	360	0.0140	0.0127
7	420	0.3874	0.3399
8	480	0.0175	0.0117
9	540	0.0787	0.0689
10	600	0.0508	0.0424
11	660	1.2515	1.1018
12	720	0.0039	0.0039
13	780	0.2155	0.1897
14	840	0.0160	0.0133
15	900	0.0175	0.0150
16	960	0.0344	0.0295
THD	1.34%		

Table A.55 Measured Voltage Harmonic Results of Bus 1816 for Phase C. Measurement

Harmonic No.	Frequency	DFT Peak (kV)	% of Fundamental
1	60	114.2620	100.0000
2	120	0.0540	0.0471
3	180	0.0521	0.0454
4	240	0.0180	0.0159
5	300	0.7099	0.6211
6	360	0.0255	0.0217
7	420	0.5133	0.4503
8	480	0.0214	0.0195
9	540	0.0918	0.0820
10	600	0.0424	0.0381
11	660	1.4491	1.2695
12	720	0.0156	0.0117
13	780	0.1580	0.1379
14	840	0.0053	0.0053
15	900	0.0075	0.0075
16	960	0.0319	0.0270
THD	1.49%		

Table A.56 Measured Voltage Harmonic Results of Bus 1816 for Phase C. Measurement

Harmonic No.	Frequency	DFT Peak (kV)	% of Fundamental
1	60	114.6320	100.0000
2	120	0.0422	0.0373
3	180	0.0270	0.0232
4	240	0.0127	0.0116
5	300	0.6784	0.5918
6	360	0.0127	0.0115
7	420	0.4098	0.3566
8	480	0.0136	0.0117
9	540	0.0689	0.0590
10	600	0.0254	0.0212
11	660	1.2575	1.1018
12	720	0.0117	0.0078
13	780	0.1264	0.1092
14	840	0.0187	0.0160
15	900	0.0100	0.0075
16	960	0.0270	0.0221
THD	1.31%		

Table A.57 Measured Voltage Harmonic Results of Bus 1758 for Phase A. Measurement

Harmonic No.	Frequency	DFT Peak (kV)	% of Fundamental
1	60	113.7950	100.0000
2	120	0.0540	0.0471
3	180	0.0589	0.0512
4	240	0.0201	0.0169
5	300	0.7076	0.8257
6	360	0.0166	0.0153
7	420	0.4587	0.3720
8	480	0.0214	0.0175
9	540	0.0754	0.0656
10	600	0.0424	0.0381
11	660	0.8862	0.7784
12	720	0.0233	0.0272
13	780	0.1667	0.1466
14	840	0.0240	0.0160
15	900	0.0351	0.0301
16	960	0.0147	0.0172
THD	1.21%		

Table A.58 Measured Voltage Harmonic Results of Bus 1758 for Phase B. Measurement

Harmonic No.	Frequency	DFT Peak (kV)	% of Fundamental
1	60	114.5860	100.0000
2	120	0.0521	0.0452
3	180	0.0608	0.0695
4	240	0.0116	0.0106
5	300	0.8620	0.7520
6	360	0.0229	0.0204
7	420	0.6112	0.5049
8	480	0.0175	0.0117
9	540	0.0721	0.0623
10	600	0.0212	0.0169
11	660	0.8323	0.7246
12	720	0.0233	0.0272
13	780	0.1580	0.1379
14	840	0.0240	0.0160
15	900	0.0326	0.0301
16	960	0.0098	0.0074
THD	1.17%		

Table A.59 Measured Voltage Harmonic Results of Bus 1758 for Phase C. Measurement

Harmonic No.	Frequency	DFT Peak (kV)	% of Fundamental
1	60	114.8040	100.0000
2	120	0.0403	0.0354
3	180	0.0357	0.0319
4	240	0.0063	0.0063
5	300	0.8608	0.7497
6	360	0.0013	0.0013
7	420	0.4839	0.4224
8	480	0.0097	0.0097
9	540	0.0393	0.0361
10	600	0.0254	0.0212
11	660	1.1976	1.0419
12	720	0.0117	0.0078
13	780	0.1293	0.1149
14	840	0.0107	0.0080
15	900	0.0150	0.0175
16	960	0.0049	0.0049
THD	1.36%		

Table A.60 Measured Voltage Harmonic Results of Bus 2373 for Phase A. Measurement

Harmonic No.	Frequency	DFT Peak (kV)	% of Fundamental
1	60	282.7950	100.0000
2	120	0.0147	0.0049
3	180	0.8464	0.2992
4	240	0.0571	0.0201
5	300	1.6807	0.5942
6	360	0.0624	0.0217
7	420	1.1147	0.3944
8	480	0.0195	0.0078
9	540	0.3967	0.1410
10	600	0.0212	0.0085
11	660	0.2994	0.1078
12	720	0.0389	0.0156
13	780	0.1897	0.0661
14	840	0.0107	0.0027
15	900	0.0727	0.0251
16	960	0.0147	0.0049
THD	0.8%		

Table A.61 Measured Voltage Harmonic Results of Bus 2373 for Phase B. Measurement

Harmonic No.	Frequency	DFT Peak (kV)	% of Fundamental
1	60	283.6170	100.0000
2	120	0.0835	0.0295
3	180	0.6573	0.2316
4	240	0.0571	0.0243
5	300	1.7345	0.6117
6	360	0.0854	0.0306
7	420	1.0783	0.3804
8	480	0.0253	0.0097
9	540	0.1705	0.0590
10	600	0.0466	0.0169
11	660	0.3293	0.1377
12	720	0.0467	0.0156
13	780	0.1494	0.0517
14	840	0.0160	0.0053
15	900	0.0125	0.0050
16	960	0.0270	0.0098
THD	0.78%		

Table A.62 Measured Voltage Harmonic Results of Bus 2373 for Phase C. Measurement

Harmonic No.	Frequency	DFT Peak (kV)	% of Fundamental
1	60	284.5030	100.0000
2	120	0.0766	0.0265
3	180	0.7432	0.2616
4	240	0.0783	0.0275
5	300	1.6784	0.5895
6	360	0.0318	0.0115
7	420	0.8601	0.3021
8	480	0.0487	0.0175
9	540	0.3574	0.1246
10	600	0.0169	0.0042
11	660	0.3772	0.1317
12	720	0.0195	0.0078
13	780	0.1609	0.0575
14	840	0.0133	0.0053
15	900	0.0476	0.0175
16	960	0.0074	0.0025
THD	0.74%		

Table A.63 Measured Voltage Harmonic Results of Bus 1692 for Phase A. Measurement

Harmonic No.	Frequency	DFT Peak (kV)	% of Fundamental
1	60	288.1990	100.0000
2	120	0.0992	0.0344
3	180	0.2529	0.0878
4	240	0.0169	0.0063
5	300	0.9509	0.3298
6	360	0.0229	0.0076
7	420	1.7049	0.5916
8	480	0.0234	0.0078
9	540	0.3148	0.1082
10	600	0.0339	0.0127
11	660	3.0599	1.0599
12	720	0.0389	0.0117
13	780	0.1466	0.0517
14	840	0.0267	0.0080
15	900	0.0977	0.0326
16	960	0.0565	0.0197
THD	1.27%		

Table A.64 Measured Voltage Harmonic Results of Bus 1692 for Phase B. Measurement

Harmonic No.	Frequency	DFT Peak (kV)	% of Fundamental
1	60	288.9580	100.0000
2	120	0.1287	0.0442
3	180	0.1206	0.0415
4	240	0.0497	0.0169
5	300	0.8468	0.2924
6	360	0.0688	0.0242
7	420	1.7608	0.6098
8	480	0.0487	0.0175
9	540	0.1115	0.0393
10	600	0.1102	0.0381
11	660	3.4551	1.1976
12	720	0.0739	0.0272
13	780	0.1466	0.0517
14	840	0.0587	0.0213
15	900	0.0702	0.0251
16	960	0.0663	0.0221
THD	1.38%		

Table A.65 Measured Voltage Harmonic Results of Bus 1692 for Phase C. Measurement

Harmonic No.	Frequency	DFT Peak (kV)	% of Fundamental
1	60	288.4520	100.0000
2	120	0.0619	0.0216
3	180	0.2519	0.0878
4	240	0.0317	0.0106
5	300	0.9146	0.3170
6	360	0.0153	0.0051
7	420	1.4280	0.4951
8	480	0.0643	0.0234
9	540	0.2230	0.0787
10	600	0.0678	0.0254
11	660	0.6228	0.2156
12	720	0.0428	0.0156
13	780	0.1609	0.0546
14	840	0.0267	0.0080
15	900	0.0451	0.0150
16	960	0.0467	0.0147
THD	0.64%		

Table A.66 Measured Voltage Harmonic Results of Bus 2462 for Phase A. Measurement

Harmonic No.	Frequency	DFT Peak (kV)	% of Fundamental
1	60	280.1930	100.0000
2	120	0.0083	0.0295
3	180	0.8648	0.3098
4	240	0.0603	0.0212
5	300	2.1696	0.7743
6	360	0.0357	0.0127
7	420	2.0923	0.7483
8	480	0.0331	0.0117
9	540	0.2590	0.0918
10	600	0.0932	0.0254
11	660	0.2874	0.1018
12	720	0.0739	0.0272
13	780	0.1782	0.0632
14	840	0.0400	0.0133
15	900	0.0226	0.0075
16	960	0.0246	0.0074
THD	1.13%		

Table A.67 Measured Voltage Harmonic Results of Bus 2462 for Phase B. Measurement

Harmonic No.	Frequency	DFT Peak (kV)	% of Fundamental
1	60	281.4210	100.0000
2	120	0.0933	0.0334
3	180	0.6360	0.2258
4	240	0.0624	0.0222
5	300	2.1778	0.7743
6	360	0.0191	0.0064
7	420	1.5343	0.5455
8	480	0.0448	0.0117
9	540	0.0623	0.0230
10	600	0.0636	0.0212
11	660	0.3114	0.1138
12	720	0.0700	0.0233
13	780	0.1408	0.0489
14	840	0.0320	0.0107
15	900	0.0100	0.0050
16	960	0.0369	0.0123
THD	0.98%		

Table A.68 Measured Voltage Harmonic Results of Bus 2462 for Phase C. Measurement

Harmonic No.	Frequency	DFT Peak (kV)	% of Fundamental
1	60	282.7760	100.0000
2	120	0.0923	0.0324
3	180	0.6187	0.2191
4	240	0.0127	0.0042
5	300	2.0643	0.7298
6	360	0.0586	0.0204
7	420	1.5245	0.5399
8	480	0.0429	0.0156
9	540	0.3607	0.1279
10	600	0.1102	0.0381
11	660	0.2874	0.1018
12	720	0.1089	0.0389
13	780	0.2098	0.0747
14	840	0.0693	0.0240
15	900	0.1003	0.0351
16	960	0.0614	0.0221
THD	0.95%		

APPENDIX B

HARMONIC SOURCE IDENTIFICATION SOFTWARE PACKAGE

B.1 Introduction

The Harmonic Source Identification Software (HSIS) package performs harmonic source identification for high voltage transmission systems. It reads Microsoft Excel files as prepared input data, and calculates possible harmonic sources. The identified possible harmonic sources are stored in an output file.

B.2 Setup Instructions

1) Establish a new directory named C:\HSIS,
2) Copy HSIS.ZIP into it,
3) Unzip HSIS.ZIP to C:\HSIS.

B.3 Two Step Identification Process

In the HSIS package, a two steps identification process is employed to identify potential harmonic source. The first step is a preliminary identification. In this step, a harmonic source suspect bus list is generated by using the triangularization method.

Once the suspect list is produced, more measurements can be taken at the vicinity of the suspect buses. Then, the least square error method is employed to refine the preliminary identification results in the second step.

B.4 Preparation of Measurement Data File

In order to assure the accuracy of the identification process, it is recommended that at least five measurement points should be taken in a field measurement activity. Also, it is recommended that at least two of these measurement points come from 345kV buses, and two of measurement points taken from 138 kV buses.

After the field measurement process is completed, the measured data should be transferred into a Microsoft Excel File. Although this Microsoft Excel file can be named randomly, for easy comprehension, it is recommended that the user include the measurement time to the name of the Microsoft Excel File. For example, a measurement activity was taken on 01/01/2008, so this measurement file can be named as ‘Mea_Jan_01_2008.xls’.

For a measurement data file, there should be eleven worksheets in this excel file. The name of each worksheet is listed in the table B.1.

Table B.1 Worksheets Name

No.	Worksheets Name
1	measurement_information
2	mea_1_data
3	mea_2_data
4	mea_3_data
5	mea_4_data
6	mea_5_data
7	mea_6_data
8	mea_7_data
9	mea_8_data
10	mea_9_data
11	mea_10_data

Here, an example is used to illustrate how to prepare the measurement data file. Assume a measurement activity was taken on 01/01/2008. Then, a file named 'Mea_Jan_01_2008.xls' should be built to store the measured information.

Suppose on January 1, 2008, five harmonic measurements were taken at the following locations:

- Bus # 1758, 138 kV
- Bus # 2373, 345 kV
- Bus # 1816, 138 kV
- Bus # 1692, 345 kV
- Bus # 1694, 138 kV

The first worksheet 'measurement_information' is used to store the field measurement information of each measurement point. The first column is the measurement number, the second column is the measurement bus name, the third column is the measurement bus number, the fourth column is measurement bus voltage, and the fifth column is the sampling rate in Hz. An example is shown in the table B.2. In this example, because there are only five

measurement points, the contents of the remaining measurements, six, seven, eight, nine, ten are left blank.

Table B.2 A Sample of Worksheet 'Measurement_Information'

	bus number	bus voltage (kV)	sampling frequency (Hz)
measurement bus 1	1758	138	2000
measurement bus 2	2373	345	2000
measurement bus 3	1816	138	2000
measurement bus 4	1692	345	2000
measurement bus 5	1694	138	2000
measurement bus 6			
measurement bus 7			
measurement bus 8			
measurement bus 9			
measurement bus 10			

In worksheet 'mea_*_data', the measured information of each location is stored. For this particular case, because there are only five measurement points, only 'mea_1_data', 'mea_2_data', 'mea_3_data', 'mea_4_data', 'mea_5_data' have stored data. The content of 'mea_6_data', 'mea_7_data', 'mea_8_data', 'mea_9_data', 'mea_10_data' are left blank.

In worksheet 'mea_1_data', the raw data of the measurement bus No.1 is stored. In worksheet 'mea_2_data', the raw data of the measurement bus No.2 is stored. In worksheet 'mea_3_data', the raw data of the measurement bus No.3 is stored. In worksheet 'mea_4_data', the raw data of the measurement bus No.4 is stored. In worksheet 'mea_5_data', the raw data of the measurement bus No.5 is stored.

Also, in every worksheet 'mea_*_data', the first column stores the current raw data of phase A in amperes. The second column stores the current raw data of phase B in amperes, and the third column stores the current raw data of phase C in amperes. The fourth column stores the voltage raw data of phase A in kilovolts, the fifth column stores the voltage raw data of phase B in kilovolts, and The sixth column stores the voltage raw data of phase C in kilovolts.

After preparation, please move the prepared measurement file to directory 'C:\HSIS\Measured Data'. Also, the sample measurement file can be found in this directory.

B.5 Extracted Subsystem

Three subsystems are pre-defined in the sample high voltage transmission system, and they are 'East Texas Subsystem', 'West Texas Subsystem', 'Central area subsystem'. The basic description of these subsystems are listed as follows. Also, user can view description of each subsystem by click 'View -> Existing Subsystem', and select a subsystem from the dialog.

Table B.3 Subsystem Description

	East Texas	West Texas	Central area
Central bus	bus 1695	bus 1122	bus 2009
Number of layers	7	7	7
Total buses	446	284	172
Total branches	517	332	192
Total generator	44	42	11
Total load buses	220	104	72

B.6 Run HSIS

Here, a sample case is used to illustrate how to run HSIS. Please follow these instructions after unzipping HSIS.ZIP into directory C:\HSIS. To run HSIS, you need to run MATLAB first, because HSIS is a MATLAB based program. Version 7.0 or greater of MATLAB 7.0 is required.

1) In MATLAB, OPEN 'C:\HSIS\MainForm.m', which is illustrated on figure B.1.
2) In the MATLAB Editor window, RUN 'C:\HSIS\MainForm.m', which is illustrated on figure B.2.
3) The HSIS program main interface will appear on the screen, which is illustrated on figure B.3.
4) On the HSIS program interface, move the mouse pointer to the menu 'Harmonic _Source_Identification', then click 'Preliminary_identification', which is illustrate in figure B.4.
5) The 'New_Preliminary_IDENTIFICATION' dialog will appear, which is shown in figure B.5.

6) Click the subsystem selection button, and select ‘C:\HSIS\ East_Texas_subsystem.xls’, which is shown in figure B.6.

7) Click the pop-up menu of the measurement points selection, a pop-up menu will appear, and select the number of measurement points in the identification process. In this example case, because the sample data has five measurement points, ‘5’ was selected. This procedure is illustrated in figure B.7.

8) Click the measurement point file selection button, and a measurement data selection dialog will appear. In this example, select ‘C:\HSIS\MeasuredData\Sep19,2007\Mea_09_19_2007.xls’, which is shown in figure B.8.

9) Click the continue button, and the program will begin the preliminary identification process. At the same time, a waiting dialog will also appear which is illustrated in figure B.9.

10) Sometimes, harmonic resonance may present in the example high voltage transmission system. The HSIS has the ability to detect harmonic resonance. When a harmonic resonance is detected, a warning message will pop up and ask the user whether this process should continue. If the user clicks the ‘No’ button, the program will terminate current identification process. If the user chooses the ‘Yes’ button, the program will continue the identification process. However, the accuracy of the results can not be guaranteed.

11) If no error occurred during this identification process, a success dialog will appear after identification process finished. This is shown in figure B.11.

12) In the main dialog, click ‘View -> Result File’, then an open file dialog will appear. In this dialog, select ‘preliminary_result.out’, which will allow user to check the preliminary result file. This process is illustrated in figure B.12. The preliminary result file is illustrated in figure B.13.

13) Once the suspect list is produced, more measurements should be taken at the vicinity of the suspect buses. Then, in the second step, the extra measurement data will be used to refine the preliminary identification results. Since this is a basic example, we do not have this kind of information, so the original measurement data is used twice to illustrate the refine process. In main menu, select 'Harmonic_Source_Identification -> Refine Preliminary Results'. A 'Refine Preliminary Results' dialog will appear, which is shown in figure B.14.

14) In the 'Refine Preliminary Results' dialog, first, the user needs to select the subsystem file. Here the user can select 'C:\HSIS\East_Texas_subsystem.xls'. Then, the user can select 'C:\HSIS\MeasuredData\Sep19,2007\ Mea_09_19_2007.xls' as the measurement data. Finally, the user should select 'C:\HSIS\preliminary_result.out' as the preliminary result file. By clicking continue, the refine process begins, and result will be stored in file 'refined_preliminary_result.out'.

15) Again, harmonic resonance may present in the example high voltage transmission system. And this software package has the ability to detect harmonic resonance. During this refine process, if a harmonic resonance is detected, a warning message will pop up and ask user whether this process should continue. If the user clicks the 'No' button, the program will exit present identification process. If the user chooses the 'Yes' button, the program will continue the present identification process. However, the accuracy of the results can not be guaranteed.

16) After the refine process is finished, the user can use 'View -> Result File' to check the refined result file, which is illustrated in Figure B.15. In the refined results, the bus with the smaller rank value is more likely to be our suspect bus. In figure B.15, it can be observed that bus 2034 has rank 1, which means that bus 2034 is our No.1 suspect. It may also be observed that bus 645 has the highest rank value, which means that bus 645 has smallest possibility to be our suspect bus.

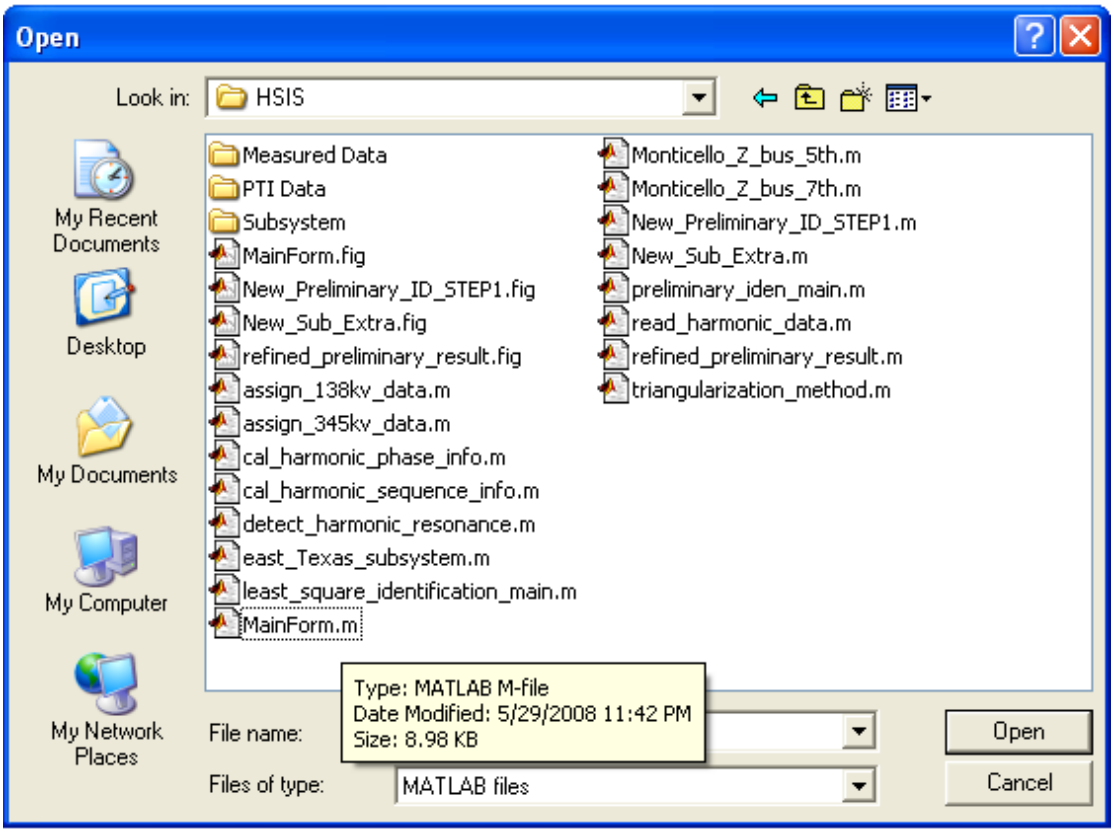

Figure B.1 OPEN 'C:\HSIS\MainForm.m'

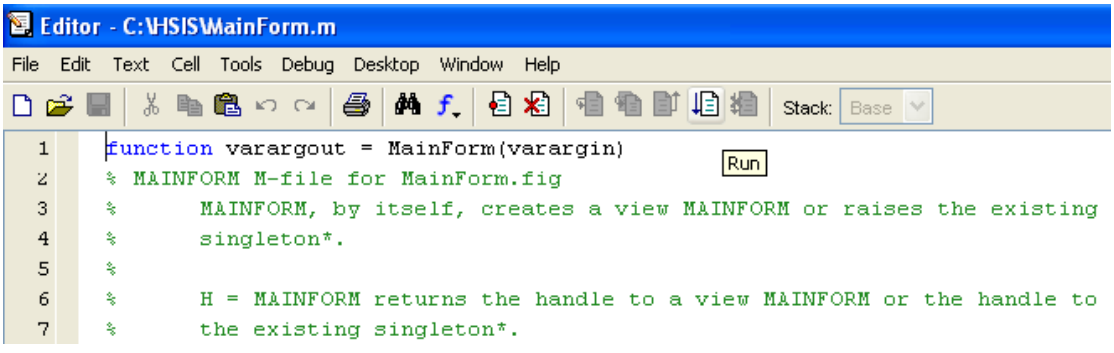

Figure B.2 RUN 'C:\HSIS\MainForm.m'

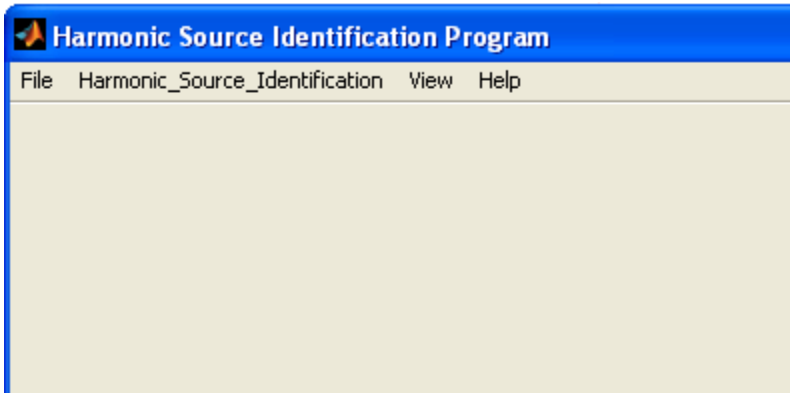

Figure B.3 HSIS Program Main Interface

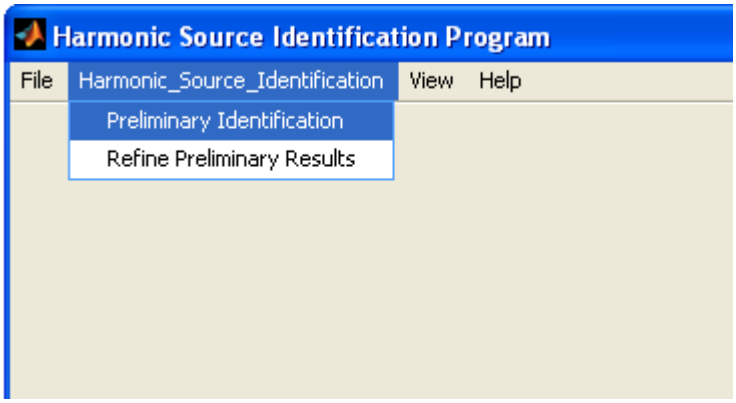

Figure B.4 Run Preliminary Identification

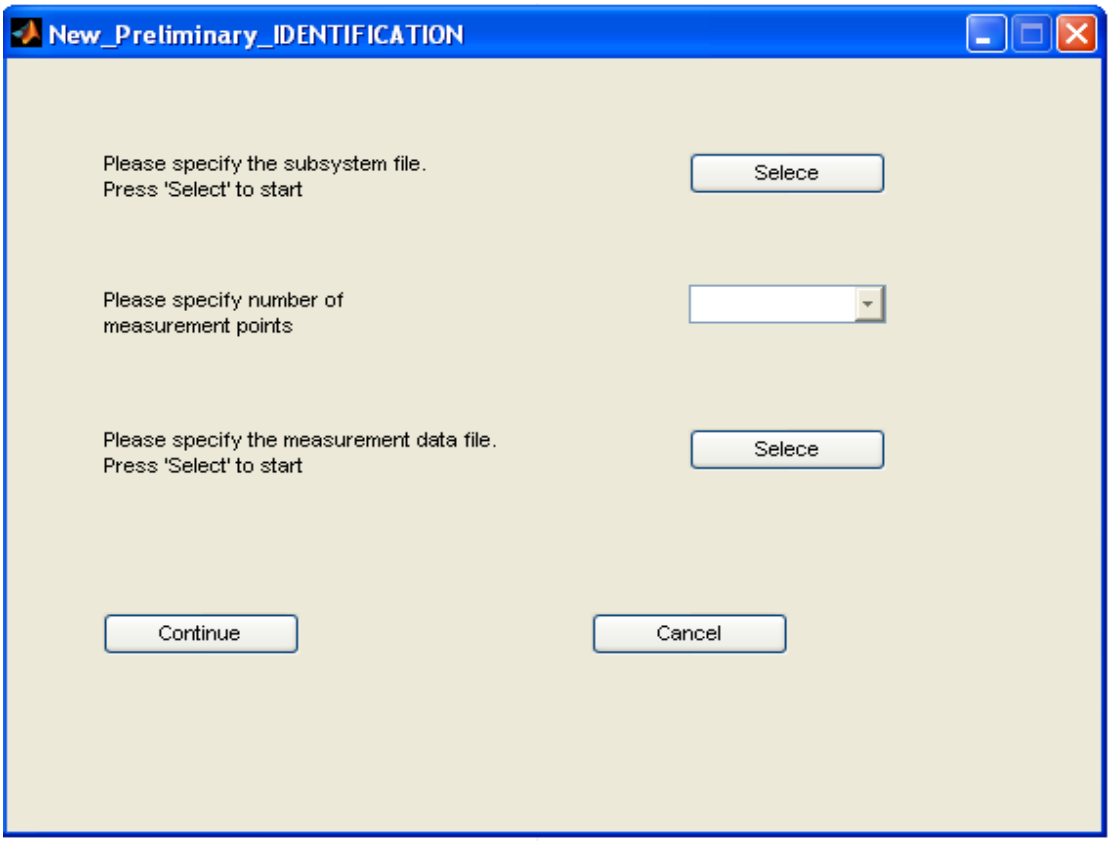

Figure B.5 “New_Preliminary_IDENTIFICATION” Dialog

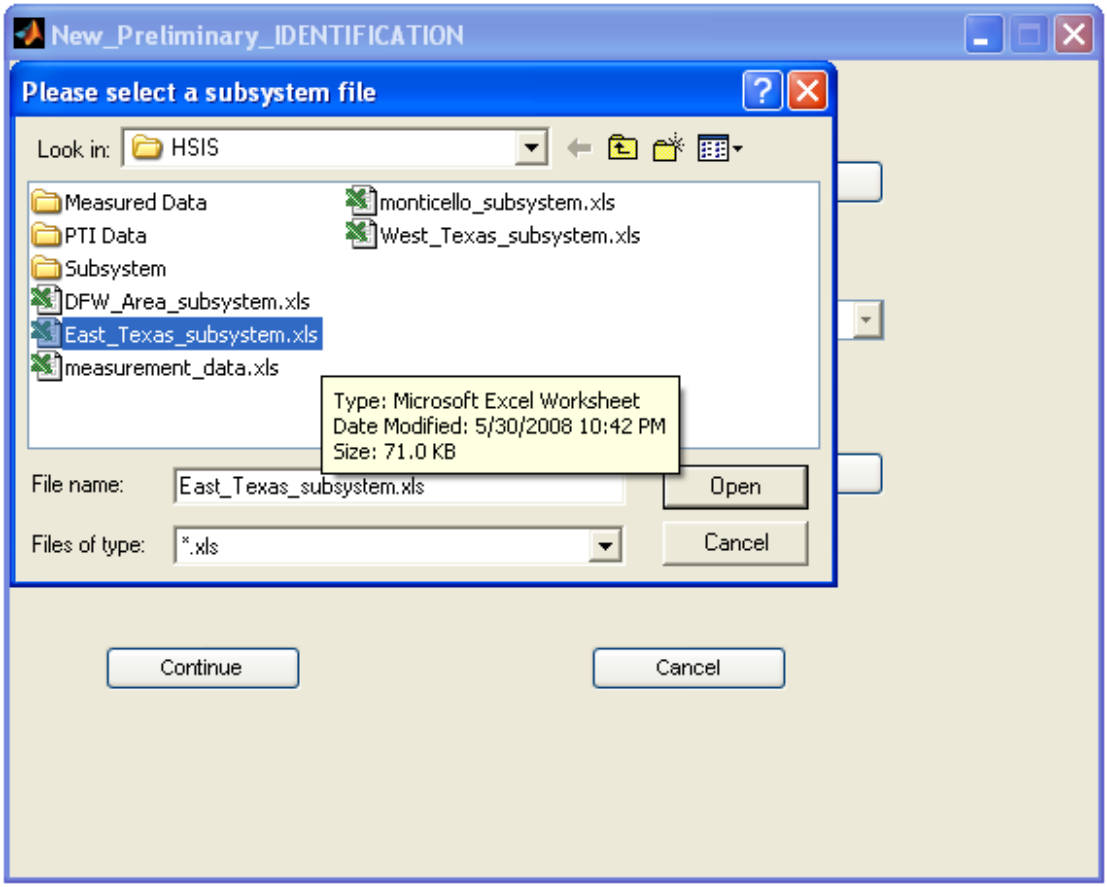

Figure B.6 Subsystem File Selection

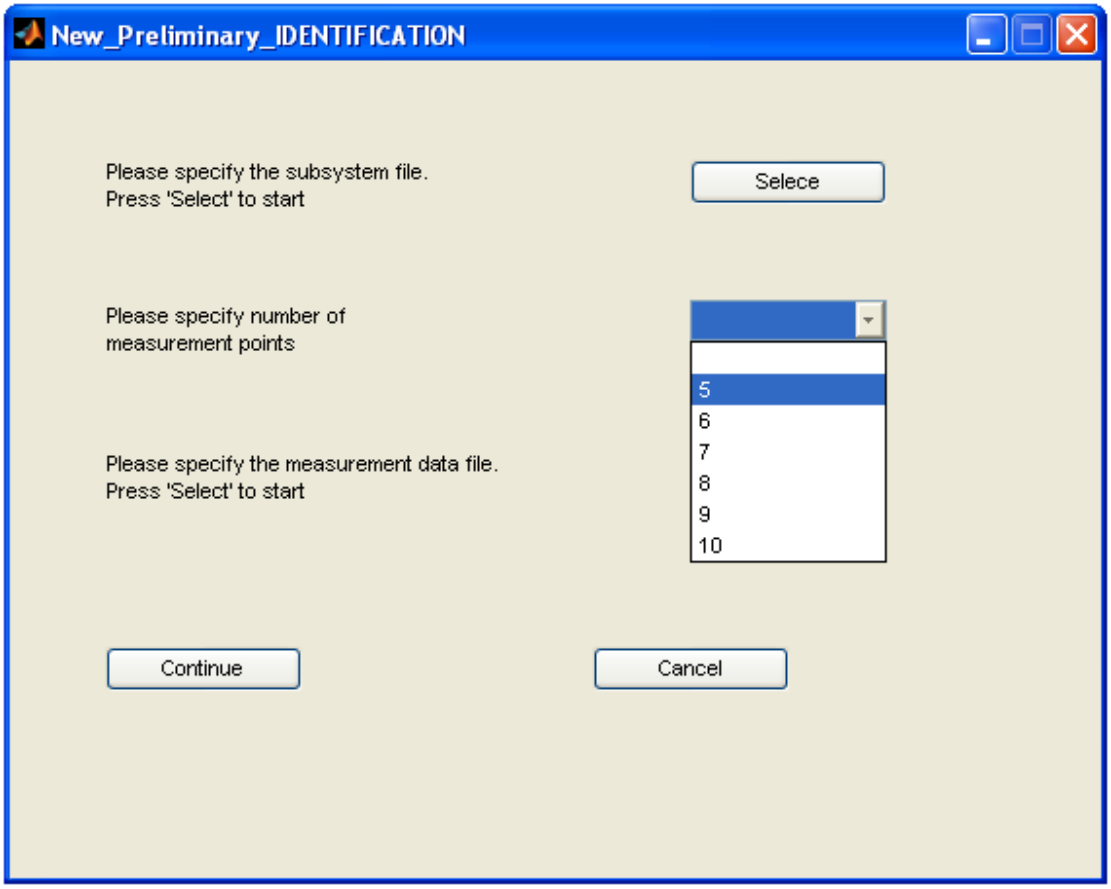

Figure B.7 Number of Measurement Points Selection

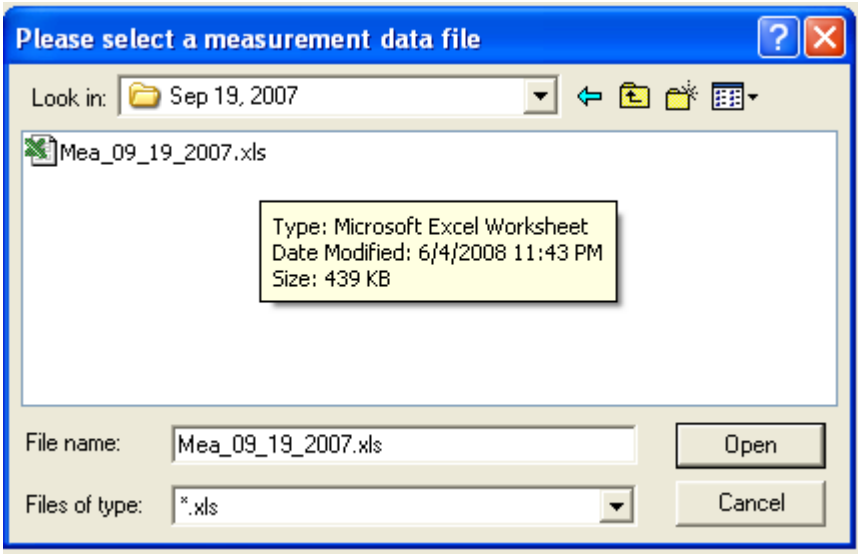

Figure B.8 Measurement Data Selection Dialog

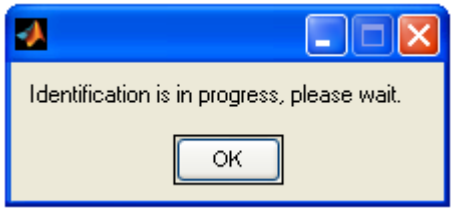

Figure B.9 Waiting Dialog

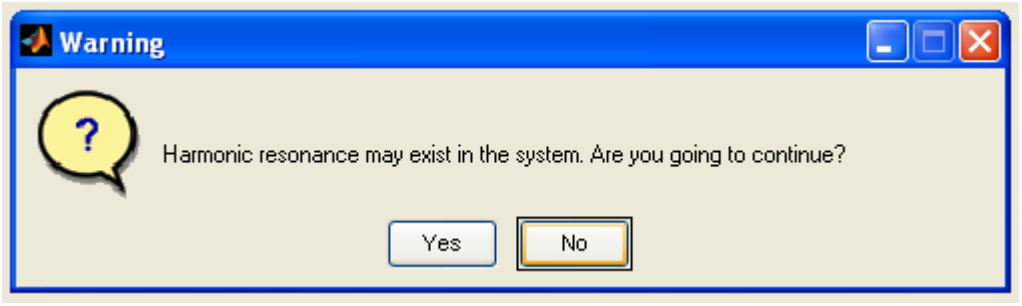

Figure B.10 Harmonic Resonance Selection Dialog

Figure B.11 Identification Success Dialog

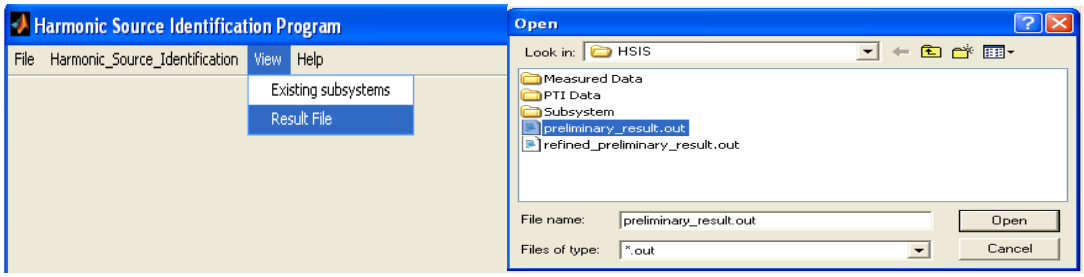

Figure B.12 Preliminary Result File Selection

```
/* Preliminary results */

This file stores the preliminary identification results, which generated on 04-Jun-2008 22:33.


  2441
  2460
  2461
  2462
  2463
  2471
  2472
  2473
  2474
  2514
  2701
  2702
  2707
  2713
  2715
  2718
  2722
  2733
  6868
  6888
 37260
```

Figure B.13 A Sample Preliminary Results Which Was Generated

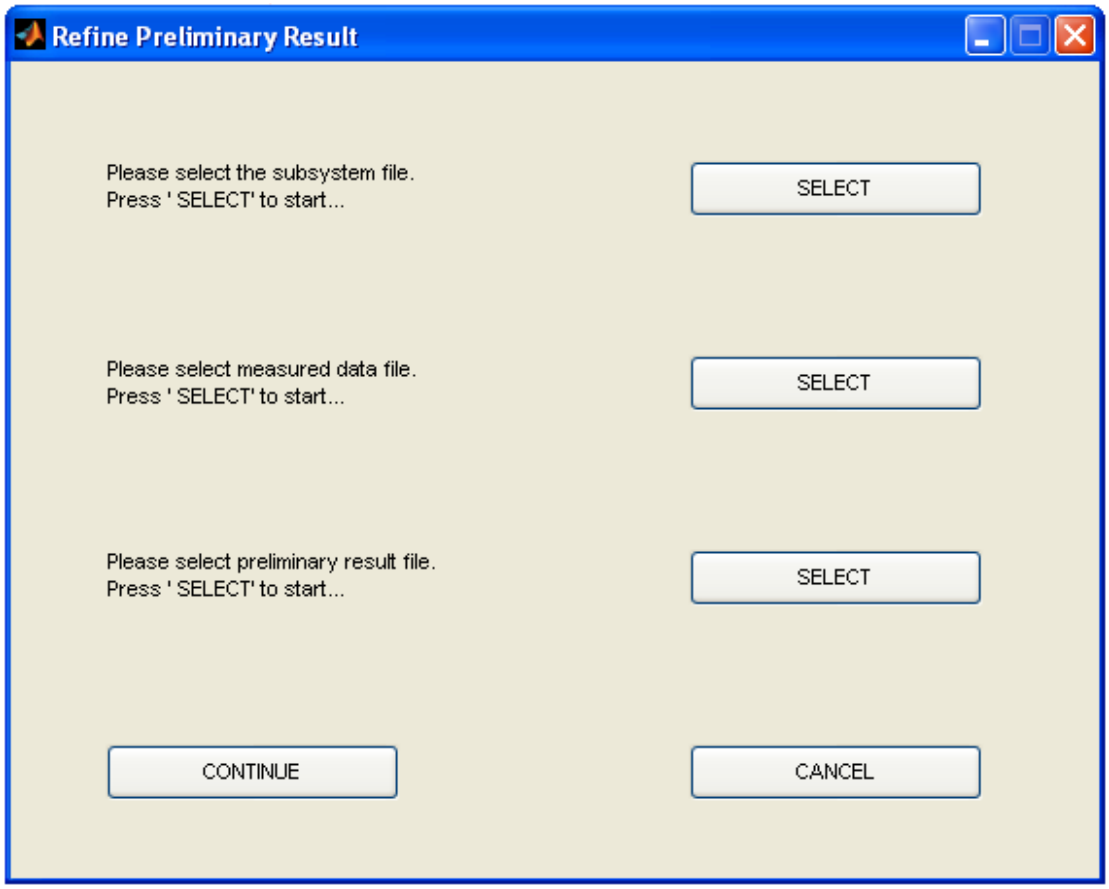

Figure B.14 Refine Preliminary Results Dialog

This file stores the refined preliminary identification results, which generated on 03-Jun-2008 23:39.

Bus	Rank
555	26
556	27
645	30
648	24
656	28
657	17
658	25
660	29
1957	12
2014	18
2015	23
2016	10
2018	22
2019	15
2020	14
2023	17
2024	19
2025	21
2026	11
2027	7
2031	20
2034	1
2038	13
2040	4
2041	5
2044	3
2045	2
2047	6
2050	8
2051	9

Figure B.15 A Sample of Refined Results Which Was Generated

REFERENCES

[1] J. Meeuwsen and W. Kling, “The influence of different network structures on power supply reliability,” in Proc. Quality of Power Supply, ETG-Conf., Nov. 1997, pp. 9–14.

[2] R. Billington and R. N. Allan, Reliability Assessment of Large Electric Power Systems. Norwell, MA: Kluwer, 1988.

[3] A. Moreno-Muñoz, Power Quality: Mitigation Technology in a Distributed Environment, Springer, 2007.

[4] V.E. Wagner, J.C. Balda, D.C. Griffith, A. McEachern, T.M. Barnes, D.P. Hartmann, D.J. Phileggi, A.E. Emannuel, W.F. Horton, W.E. Reid, R.J. Ferraro, and W.T. Jewell, “Effects of harmonics on equipment,” IEEE Trans. Power Delivery, vol. 8, no. 2, pp. 672-680, April 1993.

[5] IEEE 519-1992, IEEE Recommended Practices and Requirements for Harmonic Control in Electrical Power Systems (ANSI), New York: IEEE, 1992.

[6] Cohen, J., Cohen P., West, S.G., Aiken, L.S. Applied multiple regression/correlation analysis for the behavioral sciences. (3rd Ed.) Hillsdale, NJ: Lawrence Erlbaum Associates, 2003.

[7] G.T. Heydt, “Identification of harmonic sources by a state estimation technique,” IEEE Trans. Power Delivery, vol. 4, no. 1, pp. 569-576, January 1989.

[8] J. Arrillaga, M.H.J. Bollen, and N.R. Watson, “Power quality following deregulation,” Proc. IEEE, vol. 88, no. 2, pp. 246-261, February 2000.

[9] Hartana, R.K.; Richards, G.G.; “Harmonic source monitoring and identification using neural networks”, IEEE Tran. Power System, Volume 5, Issue 4, pp. 1098-1104, Nov, 1990.

[10] Z.P. Du, J. Arrillaga, and N. Watson, “Continuous harmonic state estimation of power systems,” IEE Proc.-Gen., Transm., Distrib., vol. 143, no. 4, pp. 329-336, July 1996.

[11] Z.P. Du, J. Arrillaga, N.R. Watson, and S. Chen, “Identification of harmonic sources of power systems using state estimation,” IEE Proc.-Gen., Transm., Distrib., vol. 146, no. 1, pp. 7-12, January 1999.

[12] N. R. Watson, J. Arrillaga, and Z. P. Du, “Modified symbolic observability for harmonic state estimation,” Proc. Inst. Elect. Eng., Gen., Transm., Distrib., vol. 147, no. 2, pp. 105–111, Mar. 2000.

[13] H. Liao, “Power system harmonic state estimation and observability analysis via sparsity maximization,” IEEE Trans. Power Systems, vol. 22, no. 1, pp. 15-23, February 2007.

[14] A. Kumar, B. Das, and J. Sharma, “Genetic algorithm-based meter placement for static estimation of harmonic sources,” IEEE Trans. Power Delivery, vol. 20, no. 2, pp. 1088-1096, April 2005.

[15] C. Madtharad, S. Premrudeepreechacharn, N. R. Watson, and R. Saeng-Udom, “An optimal measurement placement method for power system harmonic state estimation,” IEEE Trans. Power Delivery, vol. 20, no. 2, pp. 1514-1521, April 2005.

[16] N. Kanao, M. Yamashita, H. Yanagida, M. Mizukami, Y. Hayashi, and J. Matsuki, “Power system harmonic analysis using state-estimation method for Japanese field data,” IEEE Trans. Power Delivery, vol. 20, no. 2, pp. 970-977, April 2005.

[17] H. Ma and A.A. Grigis, “Identification and tracking of harmonic source in a power system using a Kalman filter,” IEEE Trans. Power Delivery, vol. 11, no. 3, pp. 1659-1665, July 1996.

[18] K.K.C. Yu, N.R. Watson, and J. Arrillaga, “An adaptive Kalman filter for dynamic harmonic state estimation and harmonic injection tracking,” IEEE Trans. Power Delivery, vol. 20, no. 2, pp. 1577-1584, April 2005.

[19] W.-M. Lin, C.-H. Lin, K.-P. Tu, and C.-H. Wu, “Multiple harmonic source detection and equipment identification with cascade correlation network,” IEEE Trans. Power Delivery, vol. 20, no. 3, pp. 2166-2173, July 2005.

[20] “Harmonic, characteristic parameters, methods of study, estimates of existing values in the network,” CIGRE Working group 36-05, Electra 77, 1981.

[21] D. A. Tziouvaras, P. McLaren, G. Alexander, D. Dawson, J. Ezstergalyos, C. Fromen, M. Glinkowski, I. Hasenwinkle, M. Kezunovic, Lj. Kojovic, B. Kotheimer, R. Kuffel, J. Nordstrom, and S. Zocholl, "Mathematical Models for Current, Voltage and Coupling Capacitor Voltage Transformers," IEEE Trans. Power Delivery, vol. 15, no. 1, pp. 62-72, Jan 2000.

[22] L. Kojovic, M. Kezunovic, and C. W. Fromen, “A new method for the CCVT performance analysis using field measurements, signal processing and EMTP modeling,” IEEE Trans. Power Delivery, vol. 9, pp. 1907–1915, Oct. 1994.

[23] H.J. Vermulen, L.R. Dann, J. van Rooijen, “Equivalent Circuit Modeling of a Capacitive Voltage Transformer for Power System Harmonics”, IEEE Trans. Power Delivery, vol. 10, No.4, pp. 1743–1749, Oct. 1995

[24] M. R. Iravani, X. Wang, I. Polishchuk, J. Riberio, and A. Sarshar, “Digital time-domain investigation of transient behavior of coupling capacitor voltage transformer,” IEEE Trans. Power Delivery, vol. 13, pp. 622–629, Apr. 1998.

[25] M. Graovac, R. Iravani, X. Wang, R. D. McTaggart, “Fast Ferroresonance Suppression of Coupling Capacitor Voltage Transformers,” IEEE Tran. Power Delivery, Vol. 18, No.1, pp. 158–163, Jan. 2003.

[26] Ross, N. W. “Harmonic and ripple control carrier series resonance with P.F. correction capacitors,” Trans. Electr. Supply Authority, Vol. 52, 48-6, 1982.

[27] Lemieux, G, “Power System Harmonic Resonance: A Document Case,” Pulp and Paper Industry Technical Conference, Conference Record of 1988 Annual 6-10, Page(s): 38-42, June 1988.

[28] Zhenyu Huang; Wilsun Xu; Dinavahi, V.R.; “A practical harmonic resonance guideline for shunt capacitor applications”, IEEE Transaction on Power Delivery, Volume 16, Issue 6, Page(s):821 – 827, Nov. 2001.

[29] R. Bernadelli, R. Shmidt, and S. Ihara, “Harmonic resonance– Occurrence and prevention,” Op. Cit., pp. 214-221, 1986.

[30] L. Kraft and G. Heydt, “An improved prediction technique for voltage resonance studies”, Proc. Second International Conference On Harmonics in Power System, Manitoba HVDC Research Center, Winnipeg, MB, October 1996.

[31] D. Carlson, L. Crane, C. Fedora, and G. Heydt, “The analysis and measurement of harmonics in the vicinity of an HVDC inverter,” Electric Machines and Power Systems vol. 11, no. 6, pp. 499-510, 1986.

[32] Shaw Power Technologies Inc., PSS/E 30.1 User Manual, August 2004.

[33] Ming-Tse Kuo, “Dynamic stability analysis of large-scale power systems using a fast investigation method,” Ph. D dissertation, Department of Electrical Engineering, University of Texas at Arlington, December 2006.

[34] J. Arrillaga, B. C. Smith, N. R. Watson, and A. R. Wood, Power System Harmonic Analysis. New York: Wiley, 1998.

[35] Harmonics, Characteristic Parameters, Methods of Study, Estimates of Existing Values in the Network 1981, CIGRE WG 36-05.

[36] Guide for Assessing the Network Harmonic Impedance 1996, CIGRE WG CC02.

[37] AC System Modeling for ac Filter Design—An Overview of Impedance Modeling 1996, CIGRE JTF 36.05.02/14.03.03.

[38] “Modeling and simulation of the propagation of harmonics in electric power networks—Part I: Concepts, models and simulation techniques,” IEEE Trans. Power Del., vol. 11, no. 1, pp. 452–465, Jan. 1996.

[39] Pesonen, “Harmonics, characteristic parameters, method of study, estimates of existing values in the network”, Electra, 77, 35-36, 1981

[40] D.C. Richard. (1999). IEEE 300 bus Test Case. [Online]. Available: http://www.ee.washington.edu/research/pstca/pf300/pg_tca300bus.htm

[41] W. Mack Grady. (2001). PCFLO Version 5.5. [Online]. Available: http://users.ece.utexas.edu/~grady/

BIOGRAPHICAL INFORMATION

Shun Liang received Bachelor's and Master's degrees in electrical engineering from University of Science and Technology Beijing, CHINA, in 1999 and 2003. His employment experience includes being a system integration engineer in Intelligent Transportation Research Center, Beijing, China from 2003 to 2005. At present, his interests include renewable energy, deregulation for utility companies, and power quality assessment in electric power systems.